THE EFFECTS OF FREE SURFACES AND MOLECULAR CONFINEMENT ON RELAXATION PROCESSES IN THIN POLYMER FILMS

By

Haidong Yang, MSc.

SUBMITTED IN PARTIAL FULFILLMENT OF THE
REQUIREMENTS FOR THE DEGREE OF
DOCTOR OF PHILOSOPHY
AT
UNIVERSITY OF NOTTINGHAM
UNIVERSITY PARK, NOTTINGHAM, NG7 2RD
JULY 2008

To my wife

Table of Contents

Abstract

Glass transition, physical aging and dielectric relaxation in ultra-thin polymer films ($<$ 100 nm) were investigated using complementary techniques (ellipsometry and dielectric spectroscopy).

PtBMA films of different thicknesses were prepared and the thickness dependence of the glass transition temperature ($Tg(h)$) was investigated with ellipsometry. The uncapped films thinner than 40nm showed significant depression of Tg and this was explained using the enhanced molecular mobility near the free surfaces. Several sets of PtBMA film samples were then prepared and capped by Al layers; the coating procedure is different for each set. The $Tg(h)$ in PtBMA films with evaporated Al capping layers was essentially the same as that of the uncapped PtBMA films, and this suggests evaporated Al capping layers can not remove the free surface effect. Another set of samples was capped with Al layers using a novel '$2(h/2)$' sample preparation procedure, and was expected to have no free surface effect. These samples exhibit no apparent thickness dependence. These results suggest that the effect of free surfaces are responsible for the altered dynamics in thin polymer films. However great care has to be taken in attempt to remove the free surface effects caused by solid capping layers.

The frequency dependence of the thickness dependence of α relaxation temperature ($T_\alpha(h)$) in ultra-thin PVAc films was measured using dielectric spectroscopy. Films thinner than 80nm exhibit smaller T_α's than the bulk values at a measurement frequency lower than 10Hz, but there is no significant thickness dependence of T_α at measurement frequencies higher than 10Hz. The results demonstrated that the

$T_\alpha(h)$ has an intrinsic dependence on measurement frequency. We also measured the cooling rate dependence of the $T_g(h)$ using the same samples, and compared $T_g(h)$ with $T_\alpha(h)$ for different cooling rates/measurement frequencies. The results help to address the existing controversial reports about the apparent discrepancies observed between measurements that are performed using different techniques.

Dielectric spectroscopy in the temperature domain $\epsilon''(T)$ was measured on thin (<486nm) PVAc films. The data were plotted against $\ln\tau$ and the parameters describing the widening and distortion of the α relaxation peaks are constant for all measurement frequencies. The observed symmetry of the α relaxation peaks in $\epsilon''(T)$ were related to the constant shape parameters of the asymmetric α relaxation peaks in $\epsilon''(\ln\tau)$. An explanation is given to the observed widening of the α relaxation peaks with increasing measurement frequency in $\epsilon''(T)$. At a lower measurement frequency (<1Hz), the data obtained from thinner PVAc films showed wider α relaxation peaks (in $\epsilon''(T)$) than the data obtained from thicker films, and at a higher frequency (>1Hz) this thickness dependence doesn't exist. This was explained using the existence of the liquid-like surface layer with enhanced molecular mobility, and using the measurement frequency effects.

PS films of different thickness were prepared and physical aging process in these samples was investigated using ellipsometry. On each sample the measurements were performed at different aging temperatures, and a trend of a decreasing aging rate with decreasing aging temperature is found for all samples. In ultra-thin PS films (<100nm thick) a maximum aging rate at ∼17K below $T_{g,\mathrm{film}}$ is observed, and these observations were explained using the competition of the two factors that affect the aging, that is, the distance to the equilibrium and the fraction of the free volume. A comparison between the thickness dependence of aging rate and the thickness dependence of T_g suggests that the aging rate serves as a more sensitive probe in the study of polymer molecular dynamics than T_g does.

Acknowledgements

Finally it's done. The writing up experience is like waiting for the end of an endless physical aging experiment, and I hope the next challenge to be less time consuming.

I would like to thank my supervisor Dr. James Sharp for every effort he put into this research project. He came up with the ideas, and built, or restored some instruments which were used in the experiments. His research experience in this area was the essential factor of this project, and his constant advice kept the process going. I am also very grateful to his support in preparing posters, papers, reports and this thesis.

Prof. Steve Howdle kindly donated the dielectric spectrometry to us, and the Engineering and Physical Sciences Research Council (EPSRC, U.K.) sponsored this project.

I would like to thank my parents for their spiritual support. They are the most reliable strength source that I always resort to in my life. I am grateful to my wife. Thank you for your staying with me, and thank you for the happiness you bring to me.

Dr. Mike Smith showed me the operation of many instruments in the early years. I am very glad to have this nice guy to chat with in the noisy lab. Thanks to my Chinese mate Dr. Yan, Mr. Xiong and all others who give me friendship during these years.

Haidong Yang

Chapter 1

Introduction

1.1 Polymers

A large variety of natural and synthetic materials are polymers. Natural polymers such as proteins, nucleic acids and cellulose serve us as food, clothes, medicine and many other useful materials [1]. In 1909 the first wholly synthetic polymer bakelite was invented by Dr. Leo Baekeland [2]. Ever since a huge variety of synthetic polymers have been manufactured and find application in almost every area of the modern world.

Despite the importance of polymers, details of their molecular structure remained a mystery until 1922, when Hermann Staudinger proposed the correct structure model of polymer molecules [3]. He was awarded the Nobel Prize for this discovery. Ever since polymer science has experienced a rapidly accelerating development and six Nobel prizes have been awarded in this area.

Polymer molecules are composed of many repeating units (sometimes hundreds of thousands of them), called monomers, which link together with covalent bonds and

form long molecular chains. The term 'polymer' is the combination of the Greek roots poly (many), and meros (part). Polymers are also often referred to as 'macromolecules' because of their large size.

Fig. 1.1 shows an example, the chemical structure of polyethylene, which has one of the simplest polymer structures. From left to right in turn shown are ethylene, polyethylene and the condensed formula of polyethylene.

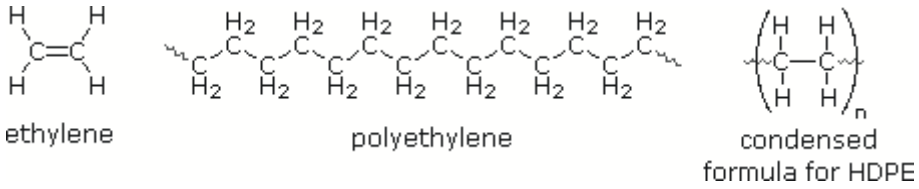

Figure 1.1: *ethylene, polyethylene and condensed formula of polyethylene. n is the number of the repeating units in a polyethylene molecule*

1.1.1 Homochain polymers and heterochain polymers

In the case of polyethylene the backbones of the molecular chains are built up by carbon (**C**) atoms. However, this isn't always the case. In some polymers the backbones are constructed by atoms of another element, or even by atoms of several elements. Take PDMS(Polydimethylsiloxane) for example, the molecular chains of PDMS are constructed by silicon **Si** and oxygen **O** atoms.

If the backbone is formed by atoms of one single element, the polymer is called a *Homochain polymer*. If the backbone is formed by atoms of two or more elements,

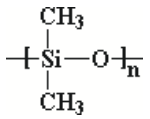

Figure 1.2: *polydimethylsiloxane*

the polymer is called *heterochain polymer*[4]. In the present work only homochain polymers will be studied and the atoms used to build the backbone are all carbon **C** atoms.

1.1.2 Homopolymers and co-polymers

Homopolymers are polymers built up of one type of monomers, and *Co-polymers* are those by two or more types of monomers.

Homopolymers are often sorted by *tacticities*. Take polypropylene for example, as illustrated by Fig. 1.3, the sequence of the appearance of the two side groups, **H** and $\mathbf{CH_3}$, may be quite different in different polypropylene polymers. Also the two side groups may appear at one side of the molecular chain or the other. These detailed structures are determined by the coupling of the monomers. If monomers couples in such a way that the side groups are always on the same position relative to the backbone, this polymer is said to be *isotactic*. If monomers couples in an irregular way, this polymer is said to be *atactic*. *Syndiotactic* describes coupling of monomers which is non-unique but varies in a regular way. The term *tacticity* is not used in polymers where the two side groups are the same.

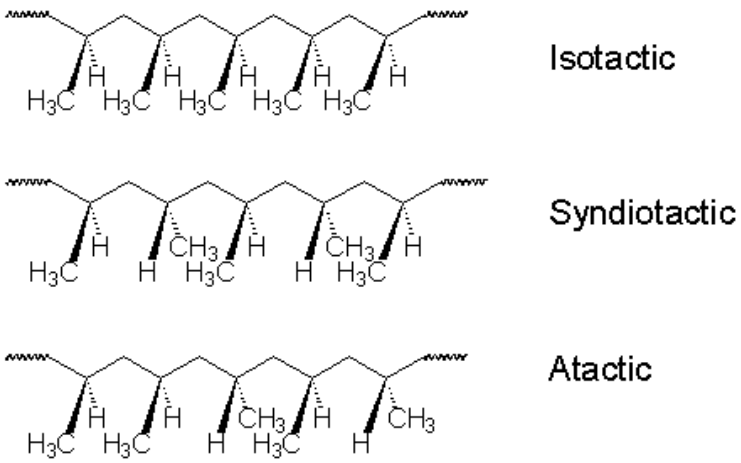

Figure 1.3: *Molecular structures of polypropylene of different tacticities*

1.1.3 Thermoplastics and thermosetting plastics

Polymers are divided into two categories, *thermoplastics* and *thermosetting plastics*. Thermoplastics, such as polyethylene, nylon and polystyrene are mixture of molecules and can be heated up to liquid state and be remoulded. Thermosetting plastics such as vulcanized rubber and epoxy resin have highly cross-linked molecular structures, that is, all molecules are chemically bonded together to form a percolating network. If thermosetting plastics are heated up they will decompose before becoming liquids.

In this work, the factor of cross-linking will not be taken into consideration, and only thermoplastics will be studied.

1.1.4 Sizes and radius of polymer molecules

Some concepts to be discussed in the present work are related to the size and weight of polymer molecules.

Contour length

For a linear polymer chain, the maximum end-to-end distance is named *contour length*. The contour length of the polymer chain is equal to the sum of the lengths of all monomer segments. Fig. 1.4 shows the contour length of a polyethylene molecule.

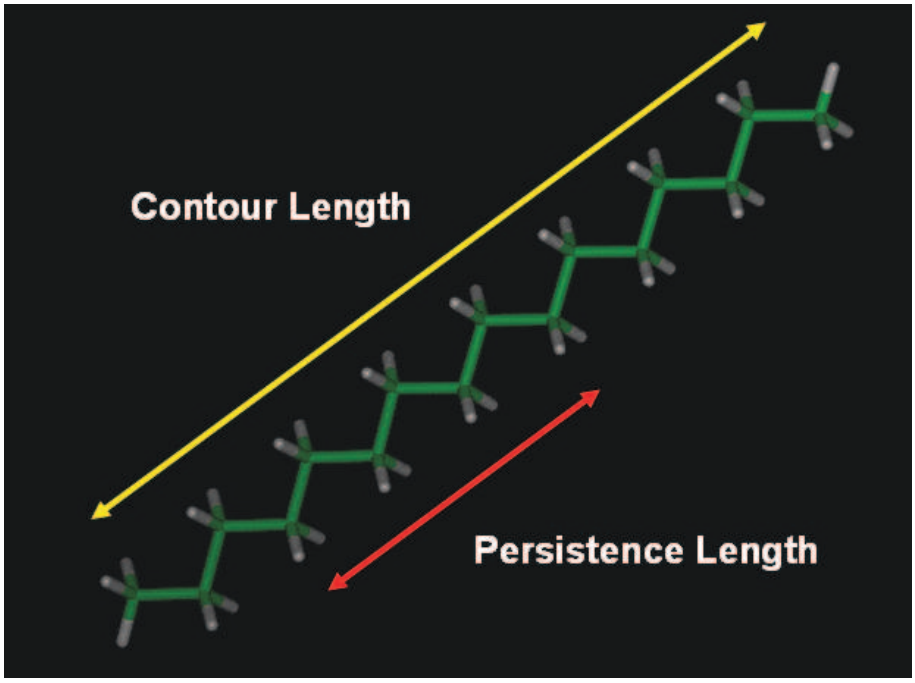

Figure 1.4: *Illustration of the contour length and the persistence length of a polyethylene molecule. The contour length is the maximum end-to-end distance and the persistence length of polyethylene molecules is* $\sim 0.65nm$ *[5], which depends on temperature.*

Persistence length

The *persistence length* indicates the stiffness of polymer molecular chains, and large persistence length values indicate rigid molecular chains. For example, the persistence length of a double-helical DNA molecule is about 50 nm, which is quite large and makes the double-helical chain very stiff. But the persistence length of polyethylene molecules is only 0.65nm [5], and those molecules are very flexible. The persistence of a polymer molecule depends on temperature.

End-to-End distance

The distance between the two loose ends of a polymer molecular chain is called end-to-end distance (R_{EE}). In dilute solutions or in polymer mass, the molecular chain can be described by the model of 'random walk'. Using this model R_{EE} can be evaluated by $\sqrt{n}l$, where n represents the number of covalent bonds along the backbone of the chain and l represents the length of each covalent bond. So R_{EE} is a function of molecular weight, and increases with increasing molecular weight.

Stokes radius

The *Stokes radius*, or the *hydrodynamics radius* of a polymer is defined in the following way. Suppose we have a solution of hard spheres diffusing at the same rate as that of a polymer molecule, the Stokes radius of the polymer molecule will be defined to be the radius of the hard sphere.

Gyration radius

Gyration radius is defined by:

$$R_g^2 = \frac{1}{N}\sum_{k=1}^{N}(\mathbf{r}_k - \mathbf{r}_{mean})^2 \tag{1.1.1}$$

where N is the number of the repeating units of a molecule, $\mathbf{r}$ is the position of the repeating units, and $\mathbf{r}_{mean} = \sum_{k=1}^{N} \mathbf{r}_k$.

R_g is also defined by:

$$R_g^2 = \frac{1}{2N^2}\sum_{i,j}(\mathbf{r}_i - \mathbf{r}_j)^2 \tag{1.1.2}$$

The above two definitions are equivalent. Fig. 1.5 schematically shows a linear polymer molecule chain and its gyration radius.

1.1.5 Weight of polymer molecules

If all molecular chains of a polymer sample have one uniform molecular weight, the sample is said to be *monodisperse*. Strict monodispersity can be found in some biopolymers where molecular chains are copies of a template. In most cases not all molecular chains are the same length. Polymers usually contain a mixture of

Figure 1.5: *A linear polymer molecule chain that is randomly distributed in space. The black arrow shows the gyration radius of it.*

chains of different lengths. The distribution of polymer chain lengths is quantified in terms of the polydispersity. Polydispersity is quantified using the polydispersity coefficient, which will be defined in the following paragraphs.

The *number average* of molecular weight, $\overline{M_n}$, is defined to be

$$\overline{M_n} = \int p(M) M \mathrm{d}M \tag{1.1.3}$$

where M is molecular weight and $p(M)$ is the number density distribution function.

In this work, and in many other literatures, the *weight average* of molecular weight, $\overline{M_w}$, is used instead of the number average. $\overline{M_w}$ is defined by:

$$\overline{M_w} = \frac{\int p(M) M M \mathrm{d}M}{\int p(M) M \mathrm{d}M} \tag{1.1.4}$$

M_w is always larger than M_n. This can be proved by

$$0 < \langle \Delta M^2 \rangle = \int p(M)[M - M_n]^2 dM = \int p(M) M^2 dM - M_n^2 = (M_w - M_n) M_n \tag{1.1.5}$$

The width of the molecular weight distribution can be specified by the polydispersity coefficient U

$$U = \frac{\langle \Delta M^2 \rangle}{M_n^2} = \frac{\overline{M_w}}{\overline{M_n}} - 1 \tag{1.1.6}$$

U becomes zero when and only when the sample is perfectly monodisperse.

1.2 Glass transition

1.2.1 Introduction to glass transition

The term 'Glass' in the scientific sense refers to amorphous solids, such as common window glasses and many polymers. The term 'amorphous' means that atoms of these solids are not arranged in any sort of regular order. In contrast to crystalline solids such as metals and salts which have long range periodic order of atoms in their structure.

Amorphous solids are usually formed in the following ways. Firstly the complex molecular structures of some materials make periodical ordering of molecules difficult. Take polymers for example, their large molecular size makes crystallization difficult. Secondly, additives may interfere with the crystallization process and help to produce amorphous solids. For example, addition of soda to silicon dioxide results in window glass [6]. Finally, when some crystalline materials are cooled down from liquid state, if the cooling rate is faster than the rate at which atoms can reorganize, these materials could become amorphous solids.

At low temperatures amorphous polymers are in a 'glassy' state, or a 'vitreous' state. When being heated up, amorphous polymers soften and finally become liquids. When being cooled back down from liquid state, they transit back to glassy state, and this transition is called the 'glass transition'. For semi-crystalline polymers, only the glassy portion will undergo glass transition, the crystalline portion will undergo crystallization, which usually occurs at a higher temperature than the glass transition of the glass portion.

At the molecular level the glass transition is explained by kinetically 'frozen' molecular motion. That is, when glassy materials are cooled down from liquid state to glass state, the mobility of molecules drops down by a large factor ($\sim 10^{13}$) as a result of densification (to be described in detail in a following section), and the viscosity at macroscopic level increases tremendously. Glassy materials lose fluidity and are considered as solids. A definition of glass transition temperature T_g (dynamic definition)

is the temperature at which the viscosity of the liquid exceeds 10^{13} pascal-seconds (Pa.S).

At liquid state, glassy materials establish equilibrium quickly, while when these materials are cooled down to glass state, approaching to equilibrium of these materials becomes longer and longer due to the slow molecular motion. For example, it may take 10^{-10}mins to establish equilibrium at 30K above T_g and 10^{10}mins ($\sim 10^5$ years) to establish equilibrium at 30K below T_g [7].

A main difference between glass transition and crystallization is that there is no abrupt change of physical parameters in glass transition (such as volume). This is illustrated in Fig. 1.6. Another main difference between the glass transition and a true thermodynamic phase transition is the dependence of glass transition on heating/cooling rate. As illustrated in Fig. 1.7, curve (1) shows volume variation as a function of temperature measured at a higher cooling rate, and curve (2) shows the result measured at a lower cooling rate. The lower the cooling rate is the lower glass transition temperature (T_g) will be obtained. The cooling rate dependence of the measured T_g can be explained by that, a slower cooling rate allow molecules to have more time to establish equilibrium, and dropping off from equilibrium will therefore occur at a lower temperature.

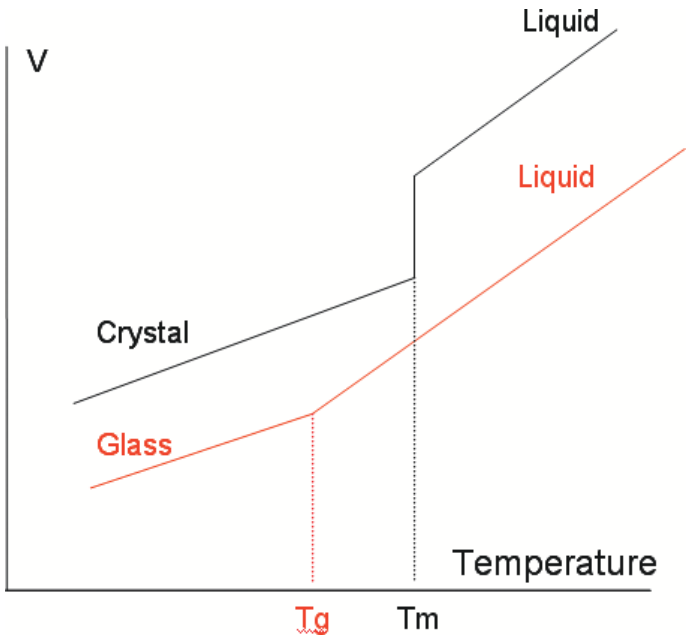

Figure 1.6: *Comparison of glass transition and crystallization. In crystallization the variation of the volumes of crystalline materials as a function of temperature will be like the black solid line. The temperature T_m where the volume jumps is defined to be freezing temperature. In glass transition the variation of the volumes of glassy materials as a function of temperature will be like the red solid line. The temperature T_g where the expansion rate changes is defined to be glass transition temperature.*

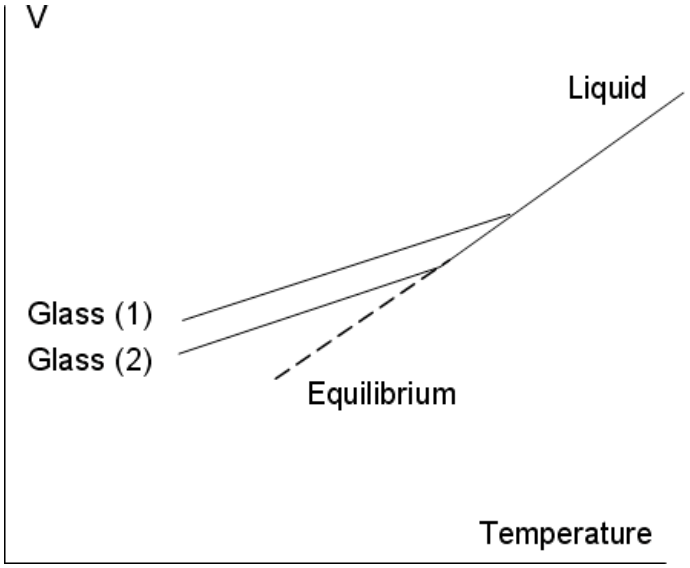

Figure 1.7: *Heating/cooling rate effect on glass transition. Curve (1) shows volume variation as a function of temperature measured at a higher cooling rate, and curve (2) shows volume variation as a function of temperature measured at a lower cooling rate.*

1.2.2 Techniques used to study glass transition

The variation of many physical parameters, such as enthalpy, heat capacity, shear modulus, dielectric permittivity and dielectric loss are measured to study glass transition. In the present work, ellipsometry was used to monitor the volume variation as a function of temperature during the glass transition of thin polymer films. Fig.1.8 shows an example of experimental data obtained in our experiment. The sample is a 486nm thick PVAc film supported on an aluminum substrate. The sample was heated up to liquid state and then cooled down at 9K/min. During the cooling process ellipsometry was used to monitor changes in the thickness of the films (which is proportional to the sample volume). The data shows that the volume expansion coefficient is constant in the glass and liquid states, and it gradually changes around the glass transition temperature. Fig: 1.8 also shows how to determine the *glass*

transition temperature (denoted by T_g), from a volume vs temperature plot. T_g here is defined as the temperature where the two linear fits to the glass and liquid regions intersect.

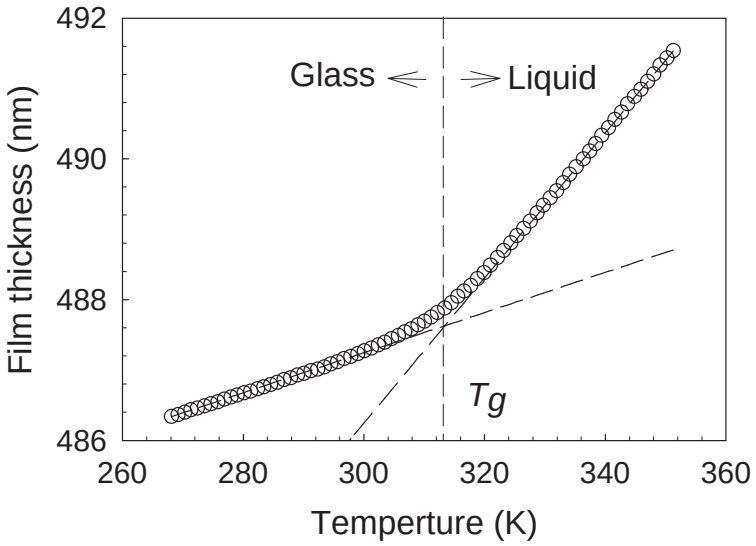

Figure 1.8: *An example of experiment data of volume variation as a function of temperature during glass transition. The sample is a 486nm thick PVAc film supported on an aluminum substrate. The sample was heated up to liquid state and then cooled down at 9K/min. During the cooling process ellipsometry was used to monitor the thickness of the films. The changing of the film thickness is proportional to the changing of the sample volume. The dashed lines show the best linear fits to the liquid and glass regions. The vertical dashed line indicates the temperature where the two fits intersect, and this temperature is defined to be* T_g.

1.2.3 Detailed description of the glass transition

A detailed description of glass transition often divides it into five regions. This five-region model is often illustrated using a diagram similar to Fig. 1.9, which shows the

variation of Young's modulus as a function of temperature.

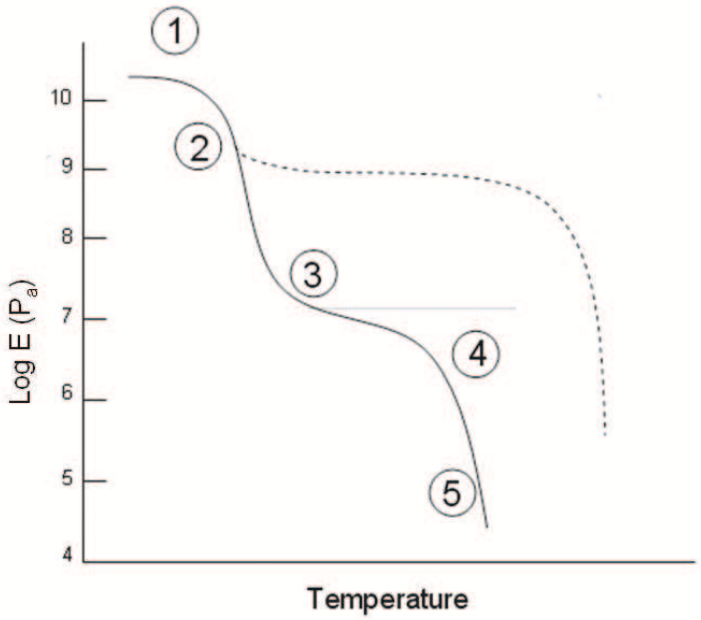

Figure 1.9: *Variation of Young's modulus of polymers as a function of temperature. The solid line, the dashed line and the dotted line in turn represent the Variation of Young's modulus of linear, semi-crystalline and cross-linked polymers [8].*

The first region indicates the glass state. It was found that for a wide range of polymers the Young's modulus remains constant throughout this temperature range. The value of Young's modulus is approximately 3×10^{10}dynes/cm^2, or 3×10^9 Pa. Local vibrations and short-range rotational motions prevail in molecular motions in this state. Some studies [9, 10, 11] [12] reported that coordinated molecular motions involves typically less than 4 main chain atoms.

The second region is the glass transition region. The Young's modulus varies by

a factor of 1000 in this narrow temperature range. In this region long-range, coordinated molecular motions become significant. The number of main chain atoms involved in these motions was reported to be $\sim 10 - \sim 15$. [9, 10, 11, 12]

The next region is called rubbery plateau region, where the modulus becomes almost constant. A typical value of the modulus is $2 \times 10^7 \text{dynes/cm}^2$, or 2×10^6 Pa. At this region the mechanical dynamics is different for different polymers. For linear amorphous polymers, the plateau slowly drops off as temperature increases. In this plateau region, linear amorphous polymers exhibit rubber elasticity. For cross-linked polymers, the modulus follows the dotted line, and for semi-crystalline polymers the modulus follows the dashed line. These two kinds of polymers are not in our research interest.

In region 4 polymers exhibit both elasticity and flow properties. In short-time-scale experiments polymers are predominantly elastic materials, because the molecular chains have not enough time to rearrange themselves. In long-time scale experiments polymers behave more like viscous materials, because the molecular chains have sufficient time to move around. There is no such region for cross-linked polymers.

On region 5 polymers flow like liquid. At this temperature range the molecules motion is strong enough to easily overcome potential barriers.

1.2.4 Constitutional influence on glass transition

Molecular weight was found to be an important factor that affects the T_g, and that's why in this work we use polymers with narrow M_w distributions. Polymers with higher M_w usually have higher T_g values. An example is the observation by Fox and Flory [13, 14] of the linear relationship between T_g and the reciprocal of molecular weight $1/M_n$, which is described by:

$$T_g = T_{g,\infty} - \frac{K}{(\alpha_R - \alpha_G)M_n} \tag{1.2.1}$$

where K is a constant specific to each kind of polymers. α_R and α_G in turn represent the expansion coefficient ($\mathrm{d}V/\mathrm{d}T$) of the polymer at liquid and glass state. $T_{g,\infty}$ represents the T_g of this polymer with $M_w = \infty$. Fox et al. suggested that larger density of end groups of molecular chains will elevate the specific volume of polymer samples, and larger specific volume will allow molecules to move more easily and therefore reduce the T_g. Since low-molecular-weight polymer samples have larger end group densities, their specific volumes are bigger and their T_g values are lower.

Fig. 1.10 shows the experimental result [15] measured on polystyrene. In this case the linear relation can be described by:

$$T_g = 106^{\circ}C - \frac{2.1 \times 10^5}{M_n} \tag{1.2.2}$$

It is noteworthy that those parameters in Eqn. 1.2.4 rely on the experimental time

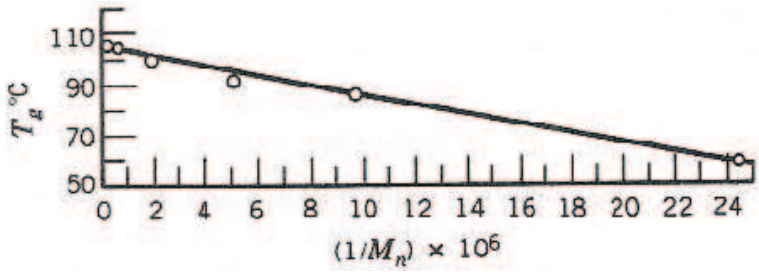

Figure 1.10: *Molecular weight dependence of T_g measured polystyrene. Taken from reference [15] and reproduced with permission from Rubber Chem. Technol.*

scale.

The stiffness of main chains is one of the key factors determining T_g. For example, the backbones of polydimethylsiloxane molecules are composed of repeating Si-O units, which is highly flexible and results in a very low T_g, which is -120°C. The backbones of poly(phenylene oxide) molecules are composed of repeating phenyl-O units, which is very stiff and results in a very high T_g value, which is 200°C.

In some polymers, tacticity affects T_g significantly. For example atactic and syndiotactic pMMA (poly methacrylate) always display the same T_g, which is around 103°C, but T_g of isotactic pMMA can be as low as 42°C. The general relationship between tacticity and T_g isn't totally clear yet, but it's widely accepted that tacticity affects the rotational freedom of the side groups, and therefore affects the stiffness of the main chains.

Side groups have a strong and complex effect on T_g. It is usually thought that bulky side groups, such as benzene substituent, block the movement of main chain and therefore elevate T_g. For example, as illustrated in Fig: 1.11, the T_g of polyethylene

is $\sim -80°$C; T_g of atactic polypropylene is $\sim -10°$C; and T_g of atactic polystyrene is $\sim 100°$C. However, studies made on polyacrylic acid [16], polymethacrylic acid [17] and some other polymers [18] revealed that these linear polymers usually have higher T_g than their counterparts with aliphatic side groups. It is suggested that these pendant groups act as 'internal diluents' and make the movement of backbones easier. More complex side group effects are found in studies on polymers with aliphatic side groups [19, 20].

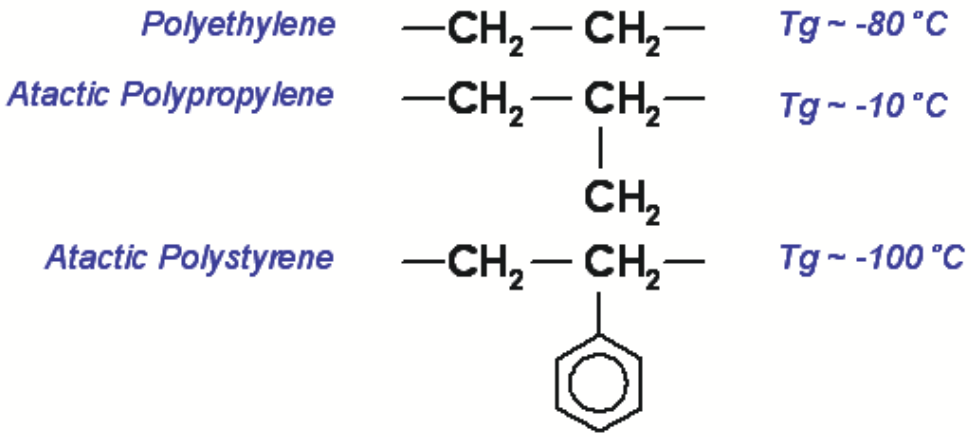

Figure 1.11: *Illustration of molecular structure and T_g of polyethylene, atactic polypropylene and atactic polystyrene. It is suggested that side groups block the inter-chain movement and elevate T_g. Bigger side groups have stronger effect.*

Given a knowledge of the composition of copolymers, we can calculate their T_g using an empirical function. For a polymer built up with units A and B the function is given by:

$$\frac{1}{T_G} = \frac{w_A p_{AA}}{(T_G)_{AA}} = \frac{w_A p_{AB} + w_B p_{BA}}{(T_G)_{AB}} + \frac{w_B p_{BB}}{(T_G)_{BB}} \tag{1.2.3}$$

where w_A and w_B are the mass function of the units A and B, and p is the probabilities of occurrence of AA, AB, and BB along the molecular chains. In this function the effect of AB and BA on T_g are assumed to be the same [21].

Polymer properties can be significantly affected by additives. For example, plasticiser molecules (such as small molecules and solvents) embed themselves inside the polymer matrix and increase the spacing between molecular main chains. This results in an enhancement of the mobility of those chains and a reduction of the T_g [22]

Factors that affect T_g values are summarized in Table 1.1

Factors that increase T_g	Factors that decrease T_g
Rigid main chains	Flexible main chains
Intermolecular forces	In-chain groups promoting flexibility
	flexibility (double-bonds and ether linkage)
Bulky and stiff side groups	Flexible side groups
Intrachain steric hindrance	symmetrical substitution

Table 1.1: Factors affecting T_g

1.2.5 Glass transition theories

Free volume theory

Eyring (US, Nobel, Laureate 1950's) was the first person to deal with the concept of '*free volume*',[23], which is defined to be vacancies among the polymer molecule matrix. It is assumed that the chain segments movement is passing through these vacancies, and without the presence of these vacancies, chain segmental motion can not happen. It is also assumed that larger free volume makes the movement easier. The volume of a polymer sample, represented by V, should be the sum of the free volume V_f and the volume occupied by the molecules V_m, i.e. $V = V_f + V_m$. In glass state, the segmental molecule motion is 'frozen' and the chain configuration is therefore expected to be the same at any temperatures below T_g, so the free volume is expected to be constant in glass state. The expansivity of V in glass state originates from the expansivity of V_m only, which suggests the expansion coefficient of V_m is equal to that of V in glassy state.

In liquid state, the expansivity of V_m are expected to be the same value as that in glass state, but the segmental molecule motion won't be 'frozen' any more, and will change the molecular chain configuration. This means that the free volume will not be constant. Since in liquid state both V and V_m are proportional to temperature, it can be concluded that the V_f in this state is proportional to temperature too. The expansivity of V_f and the expansivity of V_m both contribute to the sample expansivity in liquid state, which makes the expansivity of the sample in liquid state larger than in glass state.

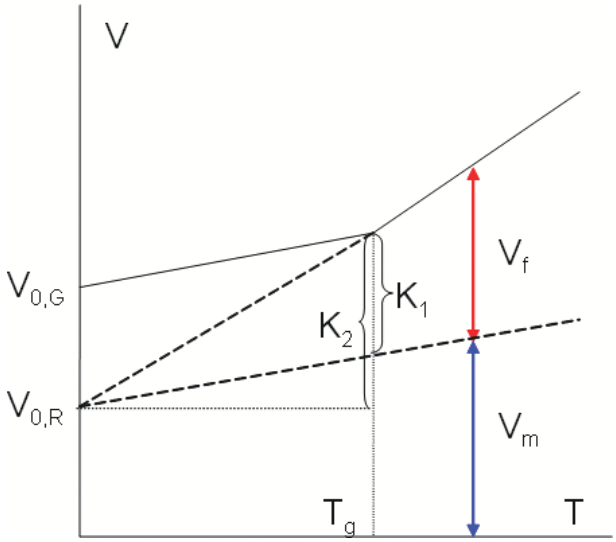

Figure 1.12: *The free Volume model to describe glass transition. The solid line represents the sample volume V as a function of temperature. The upper dashed line represents the equilibrated state at temperatures below T_g, and the lower dashed line represents the variation of the volume occupied by the molecules throughout the whole temperature range. The horizonal dotted line helps to illustrate the meaning of the parameters K_1 and K_2, which are defined in Eqn. 1.2.6 and Eqn. 1.2.6. The vertical dotted line indicates the position of T_g. $V_{0,\mathrm{G}}$ and $V_{0,\mathrm{R}}$ in turn represent the value of V and V_m when $T = 0K$. V_f and V_m in turn represent the free volume and the volume occupied by the molecules. This plot shows that at temperatures below T_g, V_f is constant and the expansivity of V originates from the expansivity of V_m. At temperatures above T_g, both the expansivity of V_f and that of V_m contribute to the expansivity of V, and that makes the expansivity of V in liquid state larger.*

The above relationships are usually illustrated in plots like Fig. 1.12. Since V_f has the same expansion coefficient in both glassy and liquid state, which is equal to the expansion coefficient of the sample in glass state, it can be expressed with $V_{0,\mathrm{R}}+\alpha_G T$, where T is temperature, $V_{0,\mathrm{R}}$ is the value of V_m when $T = 0\mathrm{K}$ and α_G is the expansion coefficient of the polymer sample in the glass state.

At temperatures below T_g, the sample volume V can be expressed by:

$$V = V_{f,\text{ constant}} + V_m = (V_{f,\text{ constant}} + V_{0,\mathrm{R}})(1 + \alpha_G T) \tag{1.2.4}$$

At temperatures above T_g, V can be expressed by:

$$V = V_{0,\mathrm{R}}(1 + \alpha_R T) \tag{1.2.5}$$

where α_R and α_G in turn represent the expansion coefficients of V in liquid and glass state, i.e. $\alpha_R = 1/V(\mathrm{d}V/\mathrm{d}T)$ when $T > T_g$ and $\alpha_G = 1/V(\mathrm{d}V/\mathrm{d}T)$ when $T < T_g$

Two parameters K_1 and K_2 are often used in free volume theory. The definition of them are:

$$K_1 = (\alpha_R - \alpha_G)T_g \tag{1.2.6}$$

$$K_2 = \alpha_R T_g \tag{1.2.7}$$

The meaning of K_1 and K_2 is illustrated in Fig. 1.12. It was found that K_1 and K_2 do not change very much from polymer to polymer, as shown in Table 1.2 (data from [8]), where some polymers and their specific values of T_g, K_1 and K_2 are listed. This makes K_1 and K_2 useful to determine the T_g of a new polymer, or to find the T_g of a polymer whose volume vs temperature plot doesn't clearly show the glass transition break.

According to the free-volume theory, the variation in the viscosity of a glass forming liquid with varying volume can be described by the Doolittle equation [24, 25]:

$$\eta = \eta_0 \exp(B\frac{V}{V_f}) \tag{1.2.8}$$

with η_0 and B being empirical constants. Combined with the Eqn. 1.2.4 and Eqn. 1.2.5, Eqn. 1.2.8 becomes:

$$\eta = \eta_0 \exp(\frac{B}{T-T_0}) \qquad \text{or} \qquad \tau = \tau_0 \exp(\frac{B}{T-T_0}) \tag{1.2.9}$$

Eqn. 1.2.9 leads to the widely used Vogel-Fulcher-Tammann (VFT) law. (VFT) law describes the relationship between viscosity and temperature in glassy forming materials at temperatures above T_g. τ approaches experiment times scale τ_{exp} when the sample is cooled down from the liquid state, and when τ becomes comparable to τ_{exp} the translational motion of the molecules can't establish equilibrium, which indicates the beginning of the glass transition. The more slowly we do the experiment, the

larger the τ_{exp} is, and the lower T_g will be obtained.

An equivalent empirical equation that was introduced by Williams, Landel and Ferry, called WLF equation, is more widely used. The WLF equation is like:

$$\log A_T = \frac{C_1(T - T_0)}{C_2 + (T - T_0)} \tag{1.2.10}$$

where $\log A_T = \log \eta / \log \eta_0$ or $\log A_T = \log \tau / \log \tau_0$. C_1 and C_2 are both universal constants for all polymers ($C_1 = -17.44\text{K}^{-1}$ and $C_2 = 51.6\text{K}$.). In the range of T_g to $T_g + 100°\text{C}$, the fits of WLF equation to the experimental results are good.

WLF equation can be derived from free volume theory too. If P is defined to be the probability of the segmental molecule relaxation per unit time, and ΔE_{act} the free energy of activation of the relaxation process, these two variables will be related by an arrhenius-type relationship:

$$P = \exp(-\Delta E_{act}/kT) \tag{1.2.11}$$

For a smaller probability P, longer time is required for the onset of the relaxation, or for a bigger P, the time required for the onset of the relaxation is smaller. In the WLF theory it is assumed that Pt (or in logarithm scale $\ln(Pt)$, defined as the possibility of the segmental molecule motion of the relaxation process) must be a constant value for the onset of the relaxation. That is

$$\ln(Pt) = -\Delta E_{act}/kT + \ln t = \text{Constant} \tag{1.2.12}$$

Take the derivative of $\ln t$ with respective to T results in the relationship

$$\Delta \ln t = -\frac{\Delta E_{act}}{kT^2}\Delta T \tag{1.2.13}$$

According to the free volume theory, the relaxation probability P is decided by the specific free volume, which leads to

$$\frac{\Delta E_{act}}{kT} = \frac{B}{f} \tag{1.2.14}$$

where $f = V_f/V$, and B is the constant in Doolittle equation. Combined with Eqn. 1.2.14, Eqn. 1.2.13 becomes:

$$\Delta \ln t = B\Delta\frac{1}{f} \tag{1.2.15}$$

The specific free volume is a linear function of temperature at temperatures above T_g, So the specific free volume f can be replaced by temperature T with Eqn. 1.2.4 and Eqn. 1.2.5, which leads to

$$\Delta \ln t - \Delta \ln t_0 = -\frac{(B/f_0)(T - T_0)}{f_0/(\alpha_R - \alpha_G) + (T - T_0)} \tag{1.2.16}$$

where f_0 is the fractional free volume at T_g, and T_0 is the reference temperature.

Compare Eqn. 1.2.16 to Eqn. 1.2.10, we find $B/f_0 = C_1 = -17.44\text{K}^{-1}$ and $f_0/(\alpha_R - \alpha_G) = C_2 = 51.6\text{K}$.

An important prediction made by WLF equation is that change of temperature by 3°C near the T_g will result in change of τ (or η) by a decade, or, if the experimental time scale changes by a decade, the measured T_g will change by 3°C.

Cooperative relaxation theory

Adam and Gibbs built up another theoretical approach to describe glass forming materials [26]. They proposed that in glass forming materials, each successful relaxation of a molecule/segment is accompanied with cooperative rearrangement of a group of neighboring units. The units involved in the cooperative rearrangement is called 'Cooperative Rearranging Region (CRR)', and the number of the units, represented by z, is called the size of CRR. Adam and Gibbs further argued that z has a lower limit z^*, and only when $z > z^*$ could a successful relaxation happen. Adam and Gibbs further assume the energy barrier for each relaxation is proportional to the CRR size. That is, $E = z\Delta\mu$, where $\Delta\mu$ is the activation energy barrier for cooperative rearrangement if only one single unit is involved. They also assume that the distribution function of the CRR size z follows the Boltzmann form. Thus the probability of a cooperative relaxation can be described by:

$$W(T) = A\exp(-\frac{z^*\Delta\mu}{kT}) \tag{1.2.17}$$

where $W(T)$ represents the possibility of the cooperative relaxation as a function of temperature, and A is a constant. The average possibility of the cooperative relaxation can be described by:

$$\overline{W(T)} = \sum_{z=z^*}^{\infty} A \exp(-\frac{z^* \Delta\mu}{kT}) \tag{1.2.18}$$

which leads to

$$\overline{W(T)} = \frac{A}{1 - \exp(-\Delta\mu/kT)} \exp(-\frac{z^* \Delta\mu}{kT}) \tag{1.2.19}$$

Because $A/(1 - \exp(-\Delta\mu/kT)) \approx A$, we may use $\overline{A}$ to replace this pre-exponential factor, and transform Eqn. 1.2.20 to

$$\overline{W(T)} = \overline{A} \exp(-\frac{z^* \Delta\mu}{kT}) \tag{1.2.20}$$

Therefore an important conclusion is made that most CRR sizes are very close to the smallest CRR size z^*.

Many experimental efforts have been put into the measuring the CRR size, and this size is generally estimated to be a few nanometers [27, 28].

1.3 Physical aging

1.3.1 Experiment observations of physical aging

It was not recognized until seventy years ago [29] that glassy materials are not in equilibrium. After being cooled down from above T_g to a temperature below T_g, the density of a glass becomes higher and the free volume decreases. The composite units don't have enough mobility to establish equilibrium on experimental time scales. However, due to thermal fluctuation, some units still have enough mobility to relax, and glassy materials will slowly evolve to equilibrium. This process is called 'physical aging'.

A most remarkable observation of physical aging is the slow decrease of free volume, which is reflected by the slow decrease of the sample volume (as illustrated by Fig.1.13). The volume variation is accompanied by changing of many other properties such as entropy, enthalpy, heat capacity, compliance, modulus, dielectric permittivity, loss factor etc. Some theoretical approaches were devised to address this phenomenon. [30, 31, 32, 33].

At lower aging temperatures the higher density of the glass forming materials have higher density and less free volume than in the liquid state, this makes the aging rate very slow and strongly temperature dependent. The aging rate is relatively fast at a temperature close to T_g, but in most cases at $\sim -15°$C below T_g, the aging rate is so slow that equilibrium won't be established within an accessible time scale. In practice, properties of the equilibrated state below T_g can only be predicted by extrapolation, instead of being directly measured. Eqn. 1.3.1 is an estimation of the time needed

Polymers	T_g(K)	K_1	K_2
polystyrene	369	0.113	0.164
polyethylene	143	0.105	0.192
Poly(dimethylsiloxane)	150	0.140	0.180
polyurethane	213	0.129	0.171
PVC	256	0.115	0.146
PMMA	378	0.113	0.182

Table 1.2: *T_g, K_1 and K_2 for different polymers* [8, 21]

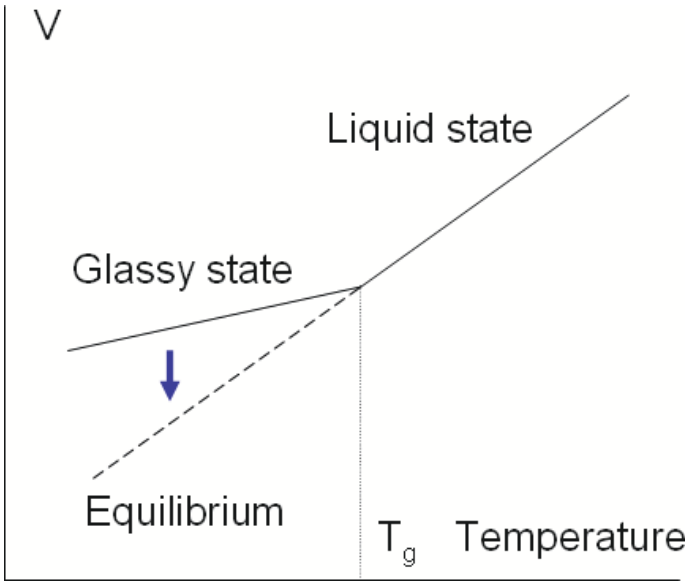

Figure 1.13: *Glassy materials are not in equilibrium in glass state. They undergo slow physical process towards the equilibrium. The solid line indicates the volume variation as a function of temperature in glass transition. The dashed line indicates the equilibrium and the dotted line indicates T_g. During the process volume and some other physical parameters slowly evolve to equilibrated values.*

to establish equilibrium, which is proposed by Struik based on the WLF equation [30].

$$t_\infty \approx 100/3 \times 10^{T_g - T} = 100\mathrm{e}^{0.77(T_g - T)} \tag{1.3.1}$$

In this equation t is in seconds and T_g and T are in °C. Physical aging are usually very slow. According to Eqn. 1.3.1, at 17K below T_g it takes $\sim 10^{10}$ years (~ 3 times of the age of the universe) to establish equilibrium in a glassy material.

It is surprising that not much effort was put in the research area of constitutional effects on physical aging. Several experiments [34, 35, 36, 37, 38] have been done to study the effect of the molecular weight on physical aging, and they showed that the aging rates are faster for polymers with smaller molecular weights, and this was attributed to the higher molecular mobility in polymers with smaller molecular weights. Some studies [34, 38] revealed that at temperatures above a critical molecular weight, aging rate will settle down at the lowest limiting value. The critical molecular weight was found to vary for different polymers and for different aging temperatures. For example, Marshall and Petrie [34] found that with atactic polystyrene at aging temperatures just below T_g, the critical molecular weight is $\sim 5 \times 10^4$g/mol.

One of the most important findings is that physical aging exists in all glassy materials, and in these materials physical aging proceeds in a similar way, no matter how different the polymers are. This suggests that for all glassy materials the mechanisms underlying physical aging are essentially the same.

1.3.2 Theory of physical aging

An early model introduced by Alfrey [39] takes polymers as a lattice of molecules and vacant holes, and these holes simulate the free volume. This model suggests that the aging process is equivalent to the diffusion of the holes to the polymer surface. During the process, the number of vacant holes decreases, which is equivalent to the decreasing of free volume in physical aging. Diffusion of the holes is described by equation:

$$\partial f/\partial t = \nabla \cdot (D \nabla f) \tag{1.3.2}$$

where $f = V_f/V$ and D is a diffusion constant. D would follow the well know Doolittle equation:

$$D = D_0 \exp\left[-Z(\frac{1}{f} - \frac{1}{f_0})\right] \tag{1.3.3}$$

D_0 and f_0 in turn denote the value of D and f at a reference state, which for convenience is usually taken as the state at glass transition temperature. This model has been used to describe small scale (submicron) polymer samples [40].

A more famous and more useful model is Struik's theory, which assumes that free volume relaxation rate is determined by segmental mobility, and that segmental mobility is determined by the specific free volume. In this model a closed-loop scheme,

as is sketched in Fig. 1.14, is thought to be the underlying mechanism.

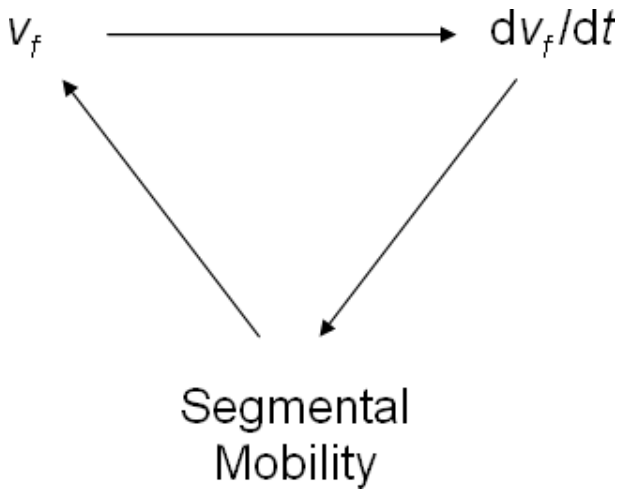

Figure 1.14: *Self-reduction in Physical aging. v_f represents the specific free volume and t represents the aging time.*

In Fig. 1.14 v_f is the specific free volume, and t is the aging time. In a physical aging process, the specific free volume decreases, which suppresses the segmental mobility, and the suppressed segmental mobility in turn slows down the decreasing rate of the specific free volume. This logical loop suggests that physical aging is a self-retarding process, and the equation to describe the aging process will be non-linear. It also suggests that in an isothermal aging process free volume won't decrease infinitely and the segmental mobility will not be zero. This loop can be described by Eqn.1.3.4,

$$\frac{\mathrm{d}v_f}{\mathrm{d}t} = \frac{v_f - v_{f\infty}}{\tau(T, v_f)} \tag{1.3.4}$$

where t is the relaxation time, $v_{f,\infty}$ is the equilibrated value of the specific free volume at temperature T. $\tau(T, v_f)$ represents the characteristic relaxation time of the

polymer sample at temperature T and free volume v_f. Struik proposed that:

$$\tau = \tau_0 \exp(\frac{\Delta G}{KT} - \gamma(v_f - v_{f\infty})) \tag{1.3.5}$$

where ΔG is the activation energy of the relaxation process, τ_0 is a pre-exponential factor, and γ is a constant. Many studies agree with the theoretical prediction based on Struik's theory.

Despite the non-linearity of physical aging, it's useful in practice to fit isothermal physical aging process with an empirical function. The most frequently used empirical function is Kohlrausch-Williams-Watts (KWW) function:

$$V(t) = V_{t=\infty} + V_{(f,t=0)} \exp(-t/\tau)^{\beta} \tag{1.3.6}$$

where β is a non-exponential factor which is between 0 and 1. When $\beta = 1$ KWW function will describe an exponential relaxation, otherwise the sample has a broad distribution of relaxation time.

Bibliography

[1] Gauri Shankar Misra. *Introductory Polymer Chemistry.* New Age International, 1993.

[2] Rob Perrée. *Bakelite.* Cadre, 1997.

[3] Rolf Mülhaupt. Hermann staudinger and the origin of macromolecular chemistry. *Angew. Chem. Int. Ed.*, **43**:1054, 2004.

[4] IUPAC. A classification of linear single-strand polymers. *Pure Appl. Chem.*, **61**:243, 1989.

[5] H.Yamakawa. *Annu. Rev. Phys. Chem.*, **35**:23, 1984.

[6] Institution of Engineers (India). *Journal of the Institution of Engineers (India).* The Institution, 1950.

[7] Editors: G. E. Zaikov, Yu. B. Monakove, and A. Jiménez. *Homolytic and Heterolytic Reactions: Problems and Solutions.* Nova Publishers, 2004.

[8] L. H. Sperling. *Introduction to Physical Polymer Science(Fourth edition).* Wiley Interscience, 2006.

[9] D. Katz and I. G. Zervi. *J. Polym. Sci.*, **46C**:139, 1974.

[10] D. Katz and G. Salee. *J. Polym. Sci.*, **A-2(6)**:801, 1968.

[11] K. Ueberreiter and G. Kanig. *J. Chem. Phys.*, **18**:399, 1950.

[12] G. M. Martin and L. Mandelkern. *J. Res. Natl. Bur. Stand., 2nd ed.*, **62**:141, 1959.

[13] T. G. Fox and P. J. Flory. *J. Appl. Phys.*, **21**:581, 1950.

[14] E. Jenckel and K. Ueberreiter. *Z. Phys. Chem.*, **A182**:361, 1938.

[15] A. Eisenberg and M. Shen. *Rubber Chem. Technol.*, **43**:256, 1970.

[16] J. A. Shetter. *Polymer Letter*, **1**:209, 1963.

[17] S. S. Rogers and L. Mandelkern. *J. Phys. Chem.*, **61**:985, 1957.

[18] W. G. Barb. *J. Polym. Sci.*, **37**:515, 1957.

[19] H. van Hoorn. *Rheologica Acta*, **10**:208, 1971.

[20] I. Negulescu and O. Vogl. *J. Polym. Sci.: Polymer Letters Edition*, **13**:17, 2003.

[21] F. W. Billmeyer. *Textbook of Polymer Science*. Wiley Interscience, 1984.

[22] V. R. Gowariker, N. V. Viswanathan, and Jayadev Sreedhar. *Polymer science*. New Age Publishers, 1994.

[23] H. N. W. Lekkerkerker, W. C. K. Poon, P. N. Pusey, A. Stroobants, and P.B. Warren. *Europhys. Lett.*, **20**:559, 1992.

[24] AK. Doolittle. *J. Appl. Phys.*, **22**:1741, 1951.

[25] AK. Doolittle. *J. Appl. Phys.*, **23**:236, 1952.

[26] G. Adam and J.H. Gibbs. *Journal of Chemical Physics*, **43**:139, 1965.

[27] D. Cangialosi, A. Alegría, and J. Colmenero. *Phys. Rev. E*, **76**:2007, 011514.

[28] N. Delpouve, A. Saiter, J. F. Manob, and E. Dargent. *Polymer*, **49**:2008, 3130.

[29] F. Z. Simon. *anorg. allgem. Chem.*, **203**:219, 1931.

[30] L. C. E. Struik. *Physical Ageing in Amorphous Polymers and Other Materials*. Elsevier, New York, 1978.

[31] C. T. Moynihan, A. J. Easteal, M. A. DeBolt, and J. Tucker. *J. Am. Ceram. Soc.*, **59**:12, 1976.

[32] G. Williams and D. C. Watts. *Trans. Faraday Soc*, **66**:80, 1970.

[33] A. J. Kovacs, J. J. Aklonis, J. M. Hutchinson, and A. R. Ramos. *Journal of Polymer Science: Polym. Phys. Ed.*, **17**:1097, 1979.

[34] A. S. Marshall and S. E. B. Petrie. *J. Appl. Phys.*, **46**:4223, 1975.

[35] K. Takada and H. Matsuya et al. *J. Appl. Polym. Sci.*, **30**:1605, 1985.

[36] M. W. Muggli and T. C. Ward et al. *J. Appl. Polym. Sci.*, **30**:1605, 1985.

[37] R. Wimberger-Friedl and de Bruin. *J. Macromolecules*, **29**:492, 1996.

[38] L. M. Nicholson, K. S. Whitley, and T. S. Gates. *Mechanics of Time-Dependent Material*, **5**:199, 2001.

[39] T. Alfrey, G. Goldfinger, and H. Mark. *J. Appl. Phys.*, **14**:700, 1943.

[40] Y. Huang and D. R. Paul. *Polymer*, **45**:8377, 2004.

Chapter 2

Background and Motivation

Great effort has been put into the study of ultrathin (<100nm) polymer films due to the increasing technology importance, such as sensors, dielectric layers, lubricants and bio-compatible materials. The ultrathin polymer films supported on substrates [1-19] and those non-supported films [1, 2] were studied by a variety of technological methods, which includes dielectric spectroscopy [3, 4, 5, 6], X-ray reflectivity [7, 8], fluorescence spectroscopy [9, 10, 11, 12], positron lifetime spectroscopy [13], Brillouin scattering [14, 15, 1, 2], optical waveguide spectroscopy [16], optoelectronic integrated sensor [17], differential scanning calorimetry (DSC) [18] and ellipsometry [19, 20, 21, 22].

These studies have revealed that many physical processes of polymer films in this thickness range differ from those in bulk samples. These include properties such as the glass transition temperature [8, 19, 21, 22, 6], dielectric relaxation [3, 6, 23, 24, 25, 26, 27, 28], physical aging rate [9, 19, 29, 30, 31], adhesion [32], friction [33], semiconducting properties and others. Understanding why thin film properties differ from the bulk properties will help to understand the molecular dynamics in confined glass forming systems, and will lay a sound basis for the research of new materials and the development of nano-structures and devices. However, despite the fact that more and more efforts are being put into this research area, a lot of unanswered questions

still remain. The experiments described in this thesis are dedicated to the study of polymer films in this thickness range and use two complementary technological techniques (namely ellipsometry and dielectric spectroscopy).

2.1 Thickness dependence of glass transition in thin polymer films

A pioneering experiment in this area was the study of thin polystyrene (PS) films by Keddie et al. [34]. It was found that in films thinner than 40nm the T_g was significantly reduced below the bulk value, as is shown in Fig. 2.1 (reproduced from [34] with permission from Europhys. Lett.)

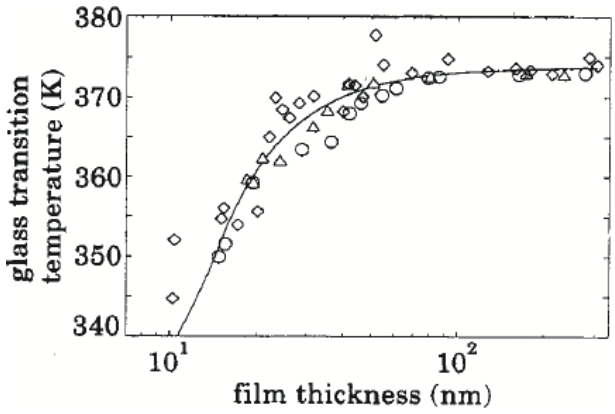

Figure 2.1: *Thickness dependence of T_g in PS films supported by silicon wafers. The solid line is the best fit to the experiment data. The data from the two thinnest films wasn't used in fitting because of the large error bars. PS of three molecular weights were used in this study, and the thickness dependence of T_g is quite the same for all molecular weights studied. $\triangle$ $M_w = 120K$, $\circ$ $M_w = 500.8K$, $\Diamond$ $M_w = 2900K$. Taken from reference [34] and reproduced with permission from Europhys. Lett.*

The solid fitting line can be described by an empirical function [34]:

$$T_g(d) = T_g(\infty)\left[1 - \left(\frac{A}{d}\right)^{\delta}\right] \tag{2.1.1}$$

where $T_g(\infty)$ is the bulk glass transition temperature, which is 373.8±0.7K in this study. d is the film thickness. A is a characteristic thickness which in this study equals to 3.2±0.6nm. δ is a shape parameter which in this study is 1.8±0.2.

One possible explanation to this experiment was the argument [7] that in polymer films thinner than the natural size of polymer molecules in bulk samples, the size, conformation and dynamics of polymer molecules will be different from those of the molecules in bulk samples, and that difference could hopefully account for this new observation. However, in that study, chain confinement effects are not responsible for the T_g reduction in ultra-thin supported polymer films. This is because the thickness dependence of the T_g was found to be the same within error for the three molecular weights studied. Keddie et al. proposed that, since the surface-to-volume ratios of those film samples are $\sim$ 6 orders of magnitude larger than that of the bulk samples, the cooperative molecular motion in ultrathin PS films was significantly affected by the free surface and the interface between the polymer films and the silicon substrates. They postulated a sandwich model to describe the ultrathin polystyrene films supported on the silicon wafers. As illustrated in Fig. 2.2, the sample is composed of three layers: the top, the middle and the bottom layers. The top layer has enhanced molecule mobility. The reason is the molecules on the surface have less neighbor molecules surrounding them, which makes the segmental motion of them easier. This layer is suggested to be liquid-like when the polymer is in glassy state. The bottom layer has less molecule mobility because of the solid silicon wall. Since simulation results [35] showed that only about two layers of segments were confined by the film-substrate interface, they argued that the effect of the PS film-substrate interface is not significant in this study. This is confirmed by the fact that $T_g(h)$ in

PS is independent of substrate used for simple supported films. The free surfaces of these samples are expected to be the dominant reason for the decreased T_g reduction in these ultrathin films.

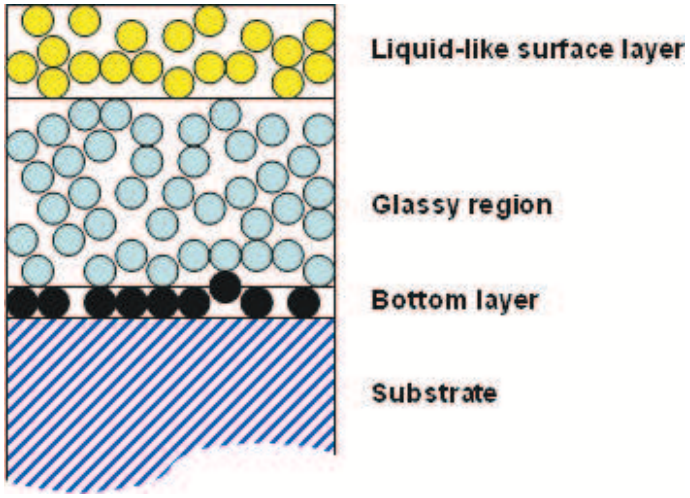

Figure 2.2: *Sandwich model of an ultrathin polystyrene film supported by a silicon wafer.*

Keddie et al. proposed the thickness of the free surface layer ξ increases with increasing temperature, and will become infinite at temperatures above T_g. This dependence can be described by: [34]:

$$\xi = A\left[1 - \left(\frac{T}{T_g(\infty)}\right)^{-\nu'}\right] \tag{2.1.2}$$

where $\nu' = 1/\delta$, and δ is the exponential factor in Eqn. 2.1.1. A is the thickness of the liquid like layer when the temperature is 0K.

The model postulated by Keddie et al. explained another important observation in their experiment: while the expansion coefficients of the polymer films in liquid

state were all the same, the glassy expansion coefficients of those films were found the be thickness dependent, as shown in Fig. 2.3 (taken from [34]).

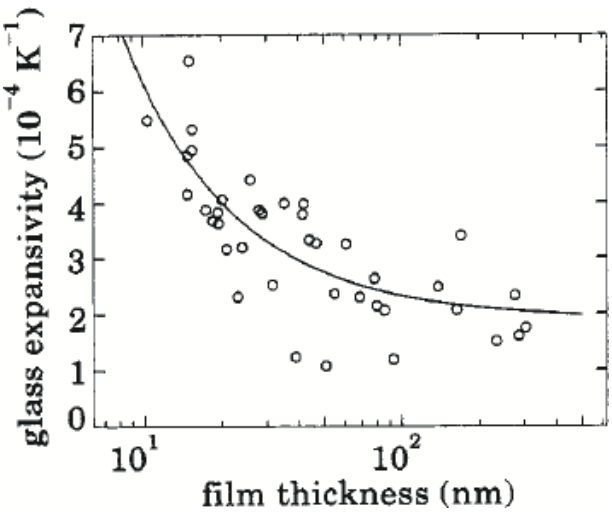

Figure 2.3: *Thickness dependence of expansion coefficient of PS films in glass state. Taken from reference 2.1 and reproduced with permission from Europhys. Lett.*

Keddie et al. suggested that the expansion coefficient of the liquid surface layer is the same as that of the polymer liquid, which are usually larger than the expansion coefficient of the glassy region. In the glass state the expansivity of both the liquid like surface layer and the glassy region contribute to the expansivity of the polymer samples, but in bulk polymer samples, the contribution from the former can be reasonably ignored because the liquid like surface layer is very thin (<4nm). Therefore the expansion coefficient of a bulk glassy polymer sample is equal to that of the glassy region. In ultrathin films, where the surface to volume ratio becomes $\sim$6 orders of magnitude larger, the contribution from the liquid like surface layer can not be ignored. The expansivity of these films will become closer to that of the liquid like layer, and that's the reason why in ultrathin polymer films the glassy expansion coefficients are larger than those of the corresponding bulk polymer sample.

The expansivity α of a film can be determined by: [34]

$$\alpha = \frac{\overline{\xi}}{d}\,\alpha_{\text{melt}} + \frac{d-\overline{\xi}}{d}\,\alpha_{\text{bulk,glass}} \tag{2.1.3}$$

where $\overline{\xi}$ is the average thickness of the liquid like layer over the temperature range to be measured, and d is the total film thickness. α_{melt} and $\alpha_{\text{bulk,glass}}$ in turn represent the expansion coefficients of the polymer sample at melt state, and the expansion coefficients of a bulk polymer sample at glassy state.

Sharp et al. [22] performed experiments which provided direct evidence for the existence of a liquid-like surface layer in ultra-thin glassy polymer films. In their experiment Au nano-spheres, with radius R, were scattered on PS film surface, and then an AFM tip was used to scan across the film surface to measure the height of the spheres as a function of time. This was done by holding the samples at constant temperature and was repeated for a range of temperatures above and below the bulk T_g of the polymer. Quantitative analysis showed that if the PS films are in liquid state, the nano-spheres will immerse into the film surface slowly and will settle down at an equilibrium height determined by the geometry of the spheres and the equilibrium contact angle of PS on gold. This was proved in their experiments. When nano-spheres with $R = 5$nm were used, $\sim$8nm of those spheres was immersed into the liquid PS films, and when nano-spheres with $R = 10$nm were used, $\sim$16nm of those spheres was immersed. Quantitative analysis also pointed out that if the surface of the PS films were glassy, no embedding would be expected. Sharp et al. pursued the embedding experiments on PS films at temperatures below T_g, with Au nano-spheres of those sizes. In those experiments they observed the embedding of nano-spheres by $\sim$4nm (independent of nanosphere radius), which strongly suggests the existence of liquid like surface layers at temperatures below T_g. At temperatures as low as $\sim$7 K below T_g, the embedding depth of nano-spheres of both sizes was $\sim$4 nm, At

higher temperatures (which is still below T_g), the embedding depth depends on the temperature, which suggests that the thickness of the surface layer is temperature dependent. These quantitative observations confirmed Keddie et al.'s theory about the liquid like surface layer on polymer films.

Indirect proof of the existence of liquid like surface layer comes from an experiment done on 'free-standing' PS films, which have no supporting substrate and are expected to have twice the surface-to-volume ratios of simple supported films, as illustrated in Fig. 2.4. T_g measurement on these films revealed that the T_g reduction in a thin supported film (the film thickness is h) is the same as the T_g reduction in a free-standing film whose film thickness is $2h$. These studies also revealed that for a free-standing film with thickness h, the T_g of it is roughly the same as that of a supported film with thickness $h/2$. These results provide additional evidence to support the theory postulated by Keddie et al.

However, some studies [36, 14, 2] on free-standing films also revealed some contradictory results that suggests the mechanism underlying this phenomenon could be much more complex. In Keddie et al.'s study of supported films, it was found that the molecular weight has no effect on thickness dependence of T_g, and they concluded that the molecule confinement in thin polymer films are not the origin of T_g reduction. This was confirmed by Ellison et al. who studied supported PS films and found that in a broad M_w range of 5K - 3000K g/mol M_W has no effect on thickness dependence of T_g. However, further studies on free-standing PS films [36, 14, 2] revealed that although there is no molecular weight dependence of T_g reduction when $M_n < 514$K, the thickness dependence of the T_g is affected by molecular weight in polymers with larger molecular weights. This is illustrated in Fig. 2.5. From the plot we can see in polymer films where $M_n > 514$K, the molecular weights have strong effect on the thickness dependence of T_g. Further quantitative analysis shows that h_0/R_{EE} is quite

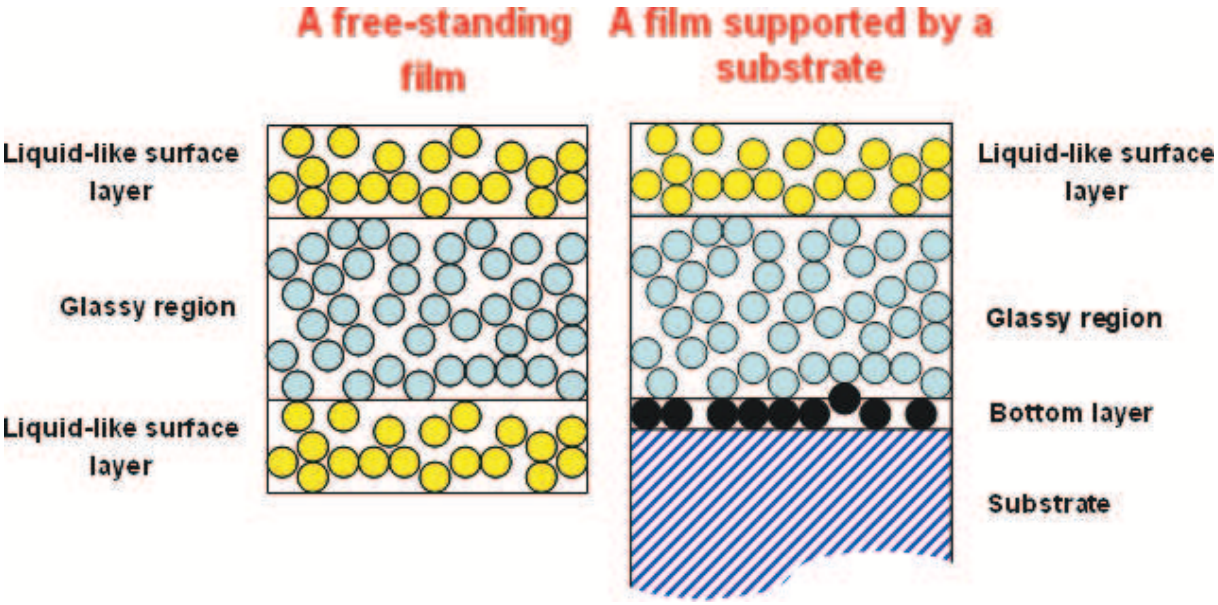

Figure 2.4: *Comparison of a free-standing polymer film and a polymer film supported by a substrate. No supporting substrate exists in a free-standing film, and therefore a free-standing film is expected to have liquid-like free surfaces on both sides.*

constant for all molecular weights, where h_0 is the threshold film thickness at which T_g reductions start to occur, and R_{EE} is the end-to-end distance which increases with increasing molecular weight, as was discussed in chapter 1. The constant h_0/R_{EE} for all molecular weights strongly suggests that for the samples with bigger molecular weights, the chain confinement becomes the dominant origin of the thickness dependence of T_g in free standing films.

Another method of verifying the existence of the free surface with enhanced mobility was also developed. This was done in an attempt to cover the free surface with a rigid layer to remove effect of the mobile surface. An example is the experiments that were performed on PS films [2] coated with $\mathbf{SiO_2}$ layers. The thickness dependence of T_g was found to be essentially the same as those for un-coated PS films. Another study performed on PS films with thermally evaporated Al capping layers [3] obtained similar results. These results seem to contradict Keddie et al.'s free surface theory.

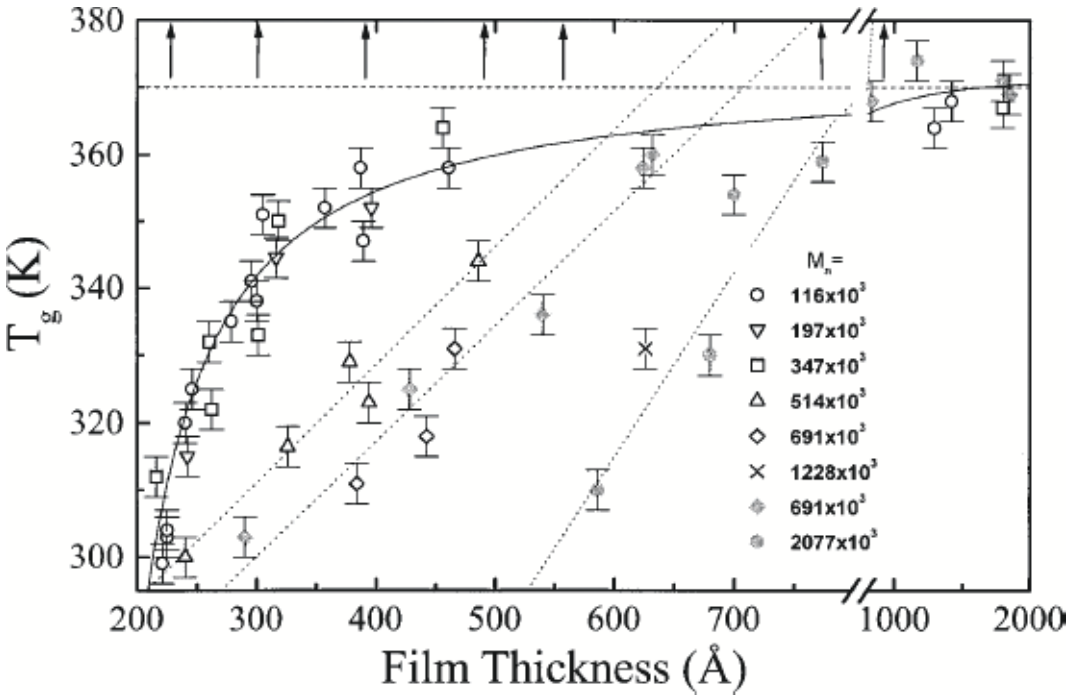

Figure 2.5: *Thickness dependence of T_g for free-standing PS films of different molecular weights. The plot is taken from reference [36] and reproduced with permission from Phys. Rev. E. The arrows indicate the R_{EE} values of PS molecules in bulk samples for each molecular weight. The solid line is the fit to the data sets measured on free-standing PS films with smaller ($M_n < 514K$) molecular weights. The horizonal dotted line indicates bulk T_g value, and the rest of the dotted lines are fits to data sets measured on samples with larger molecular weights. Eqn. 2.1.1 was used as the fitting function in those fits.*

However, Sharp et al. [22] designed an experiment to address this contradiction. They revealed that removal of the effect of free surface by evaporating layers depends highly on the coating procedure. In their experiments PS films were capped with both evaporated Al layers and evaporated Au layers. It was found that thickness dependence of T_g exists in Al capped PS films, as is consistent with some previous studies, but it doesn't exist in Au capped PS films. This result suggests that to remove the free surface effect with metal capping layer is possible, but the Al evaporated capping layer may not actually contact well with the polymer films. Sharp et al. further prepared a series of PS film samples (named '$2(h/2)$' samples) with Al capping layers, using a special procedure to be described in a later chapter. In those '$2(h/2)$' samples the Al capping layers were expected to be in good contact with film surfaces. The thickness dependence of the T_g was found to be suppressed in these samples. It was also found that in Au evaporatively capped films and in $2(h/2)$ samples the thickness depedence of expansivity in glassy state also disappeared. Furthermore, they demonstrated that removal of the Al capping layers in the $2(h/2)$ samples using a simple chemical treatment resulted in the restoration of the free surface effect, and the recovery of the thickness dependent T_g. All these observations suggest that the microstructure of the interface between polymer films and the capping layers is an important factor in determining whether the free surface effects are removed during the capping procedures.

There are further experiments that don't agree with the theory postulated by Keddie et al. Kawana et al. reported some results [20] that suggested the thickness of the liquid like surface layer was independent of temperature. Fig. 2.6 is taken from reference [20], where the thickness of the liquid like surface layer is calculated from ellipsometry data using Equ. 2.1.3. It is found that, below glass transition region, there is no strong evidence that the thickness of the liquid like surface layer is temperature dependent within the limits of experimental uncertainty. These authors also

found that at temperatures below T_g the thickness of this layer is $\sim$ 10nm for all films studied regardless of their total thicknesses. This was attributed to a much weaker temperature dependence of the thickness of this layer at temperatures below T_g.

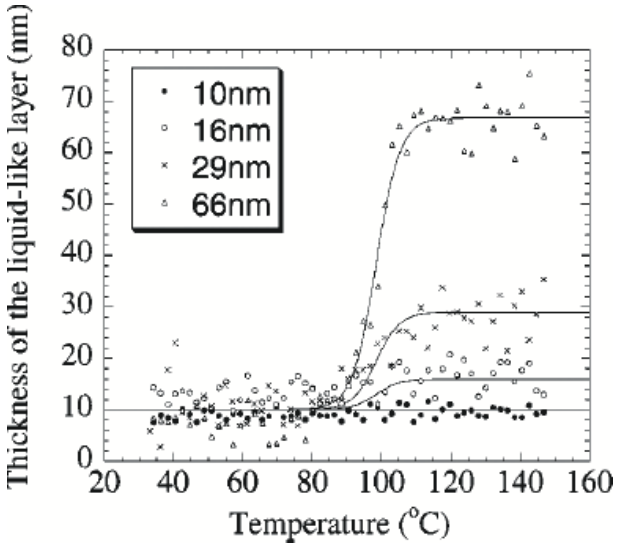

Figure 2.6: *Temperature dependence of the thickness of the liquid like surface layer in PS films supported on silicon substrates. The thickness of the liquid like surface layer is calculated with Equ. 2.1.3, and it is found that below glass transition region this value is neither temperature dependent nor thickness dependent. The plot is taken from reference [20] and reproduced with permission from Phys. Rev. E.*

Detailed experiments and analysis have been performed in an attempt to study the width of the glass transition region in thin PS films. Kawana et al. [20] reported that the upper temperature limits of glass transition region (T_+) don't significantly depend on film thickness, while the lower temperature limits of glass transition region (T_-) are depressed in thinner ($<\sim$40nm) PS films. This results in widening of the glass transition region with decreasing film thickness. Kawana et al [20]. proposed an explanation using a three-layer model that was originally proposed by DeMaggio et al.[13]. In that model a supported polymer film consists of three layers, the liquid like surface layer, the layer near to the substrate with reduced mobility, and the middle

layer. During a cooling process the layer near to the substrate drops out of equilibrium first, which indicates the onset of the glass transition. This is followed by the vitrification of the glassy region. The liquid-like surface layer drops out of equilibrium last, which indicates the T_+ of the glass transition. For all films measured in the experiments, the bottom layers dropped out of equilibrium at the same temperature, which explained why the onset temperature of the glass transition are all the same for all film thicknesses. In the thinner films the relative contributing of the surface and middle layer change with film thickness, making T_- of the glass transition be smaller than those in the bulk samples. Kawana et al. [19] further reported some consistent results. In these experiments PS films supported on Si wafers were heated above T_g to establish equilibrium, and then cooled down to a temperature below T_g and kept at that temperature for as long as 7 days. This ensured that all samples had the same thermal history. The samples were then heated up at a constant rate and the thickness was monitored by ellipsometry. The upper limit temperatures of the glass transition were found to be quite the same for all film thicknesses, and the lower limit temperatures were found to decrease with decreasing film thickness. This confirmed their previous observations. In this study (to be described in detail in Chapter 4) we used ellipsometry to study the thickness dependence of the T_g in ultra-thin poly (tert-butyl methacrylate) (PtBMA) films [37]. We also found that T_+s and T_-s as functions of film thickness is similar to Kawana et al.'s observations, which suggests that thickness dependence of T_+ and T_- may not rely on the chemical constituents of polymers.

Influence of molecular microstructure

Micro-structure of polymer films and their thermal history were found to significantly affect the glass transition in thin polymer films. Fig. 2.7 is taken from [8],

where the thickness dependence of glass transition in spin-coated PtBMA films, and PtBMA Langmiur-Blodgett (LB) films with and without annealing were measured. Spincoated PtBMA films and annealed LB PtBMA films exhibit essentially the same bulk T_g values ($\sim$ 110°C), and display a similar thickness dependence of T_g with large T_g reductions ($\sim$ 60K) in thin films ($<\sim$ 40nm). In contrast, the LB PtBMA films that were prepared without being annealed showed no thickness dependence of glass transition, and their bulk T_g values ($\sim$ 80°C) are much smaller. This could be attributed to the presence of the solvent in the un-annealed LB films. In the present work (to be described in detail in Chapter 4) we studied the thickness dependence of glass transition with annealed PtBMA films. Our results showed the bulk T_g values of PtBMA films are the same as those presented in these other studies ($\sim$ 110°C), but the T_g reduction observed is much smaller. However, the T_g reductions reported in our work are consistent with reports of the thickness dependence of the T_g in other polymers). All these results showed the effect of thermal history and molecular microstructure on the thickness dependence of glass transition in thin polymer films.

The role of substrate effect

In some cases the interaction between polymer films and their supporting substrates had a significant influence on the thickness dependence of T_g in thin polymer films. For example, Fryer et al. [38] measured the thickness dependence of T_g in atactic PMMA (a-PMMA) films supported by hexadimetyldisilazane (HMDS) treated silicon wafers and SiO_x substrates. They obtained quite different results from samples on different substrates. For the a-PMMA films spincast on HMDS treated silicon wafers (which are thought to be hydrophobic), a reduction of T_g ($\sim 20°C$) was observed on a thin (35nm thick) a-PMMA film, and samples spin-cast onto SiO_x substrates displayed an elevated T_g by $\sim$ 8°C was observed on a sample with the same film thickness.

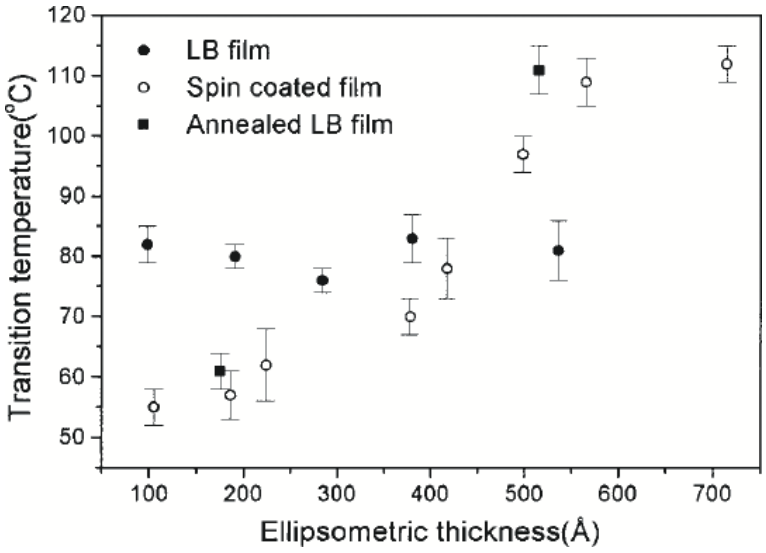

Figure 2.7: *thickness dependence of T_g in spincoated PtBMA films on silicon substrates ∘ and PtBMA films with ■ and without • being annealed. The plot is taken from reference [8] and reproduced with permission from Langmuir*

Different measurement methodologies have been reported to affect the measured dynamic properties in ultra-thin polymer films. Fig. 2.8 (from [39]) shows thickness dependence of T_g in thin syndiotactic (s-PMMA) films and isotactic (i-PMMA) films, which were measured using both ellipsometry and dielectric spectroscopy. It has been well known since the work of Karastz [40] that bulk i-PMMA and s-PMMA samples have quite different T_g values. These results measured from thinner films of PMMA stereoisomers makes the problem more complex. The most striking observation is that the $T_g(h)$ is different when the samples were measured using ellipsometry and dielectric spectroscopy. For s-PMMA samples, the dielectric measurements results gave a smaller T_g reduction in thin film samples than the ellipsometry measurement results. For i-PMMA samples, the results measured by different measurement techniques have much larger difference. While the T_g decreases with decreasing film thickness in the dielectric measurements, in the ellipsometry measurements the T_g increased with decreasing film thickness. An explanation for these observations is

related to the different samples used in these two kind of measurements. The films used in dielectric measurements were sandwiched between two alumium electrodes, but those used in ellipsometry measurements were simply supported on substrates.

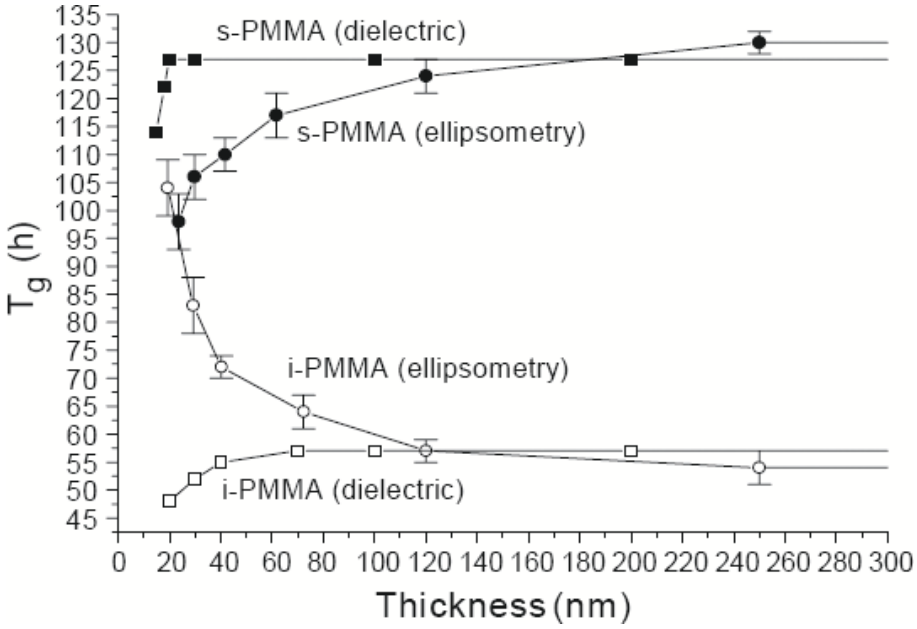

Figure 2.8: *thickness dependence of T_g in s-PMMA films and s-PMMA films measured by both ellipsometry (● ○) and dielectric spectroscopy (□ ■). The plot is taken from reference [39] and reproduced with permission from Eur. Phys. J. E*

Influence of experiment time scale/measurement frequency

The experiment time scale/measurement frequency is also a potentially important factor in determining the thickness dependence of T_g in polymer films. Fig. 2.9 is taken from reference [39], where the T_g of i- and s- PMMA films on silicon substrates were measured using DSC. The T_g of a bulk i-PMMA film decreases with decreasing heating rate, and the T_g of a 35nm i-PMMA film remains constant with decreasing

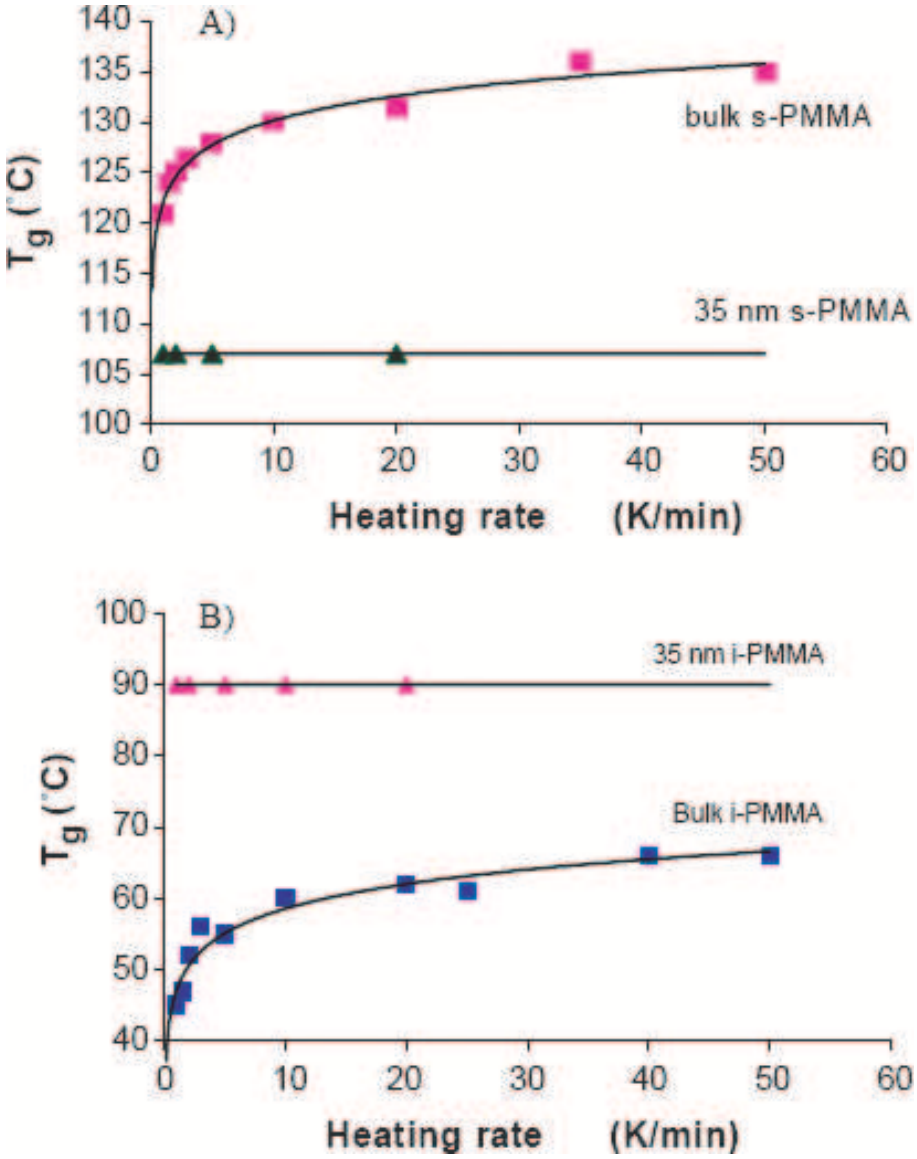

Figure 2.9: *T_g as a function of heating rate for bulk s-PMMA films (pink ■), 35nm s-PMMA films (▲), bulk i-PMMA films (blue ■) and 35nm i-PMMA films (pink ▲). The plot is taken from reference [39] and reproduced with permission from Eur. Phys. J. E*

heating rate. The T_g of a bulk s-PMMA film also decreases with decreasing heating rate, and the T_g of a 35nm i-PMMA film also remains constant with decreasing heating rate. In reference [21] PS films were measured with ellipsometry and displayed a quite different behavior. For all films the T_g is was found to be larger at higher cooling rates. The thickness dependence of the T_g obtained at higher cooling rate tends to diminish. Fig. 2.10 is taken from [21], which shows the log (cooling rate) vs $1/T_g$. This plot suggests that at a certain cooling rate the T_gs obtained from all films become the same (T_*). In the cooling rate range $1 - 130\text{Kmin}^{-1}$ the data obtained from the thicker films was fitted accurately with VFT function, while the thinner films were found to obey an Arrhenius law. Fakhraai et al. explained this using theory of finite size effect [21]. They suggested that in thinner films, The size of cooperative relaxation region (CRR) Z^* increases with decreasing temperatures. When a polymer film sample is cooled down from the liquid state, Z^* may become larger than the film thickness h. This can be illustrated in Fig. 2.11. When $Z^* > h$ the authors argued that the cooperative segmental motion become a simple activated process (Arrhenius relaxation) and the activation energy is a function of the film thickness. This theory is confirmed by the data shown in the inset in Fig. 2.10, where activation energy of thin films is plotted against film thickness.

2.2 Thickness dependence of physical aging in thin polymer films

Developing an understanding of the molecular level processes that underly the glass transition and physical aging are central challenges in condensed-matter physics [41]. Many studies have concentrated on the study of glass transition in thin polymer films,

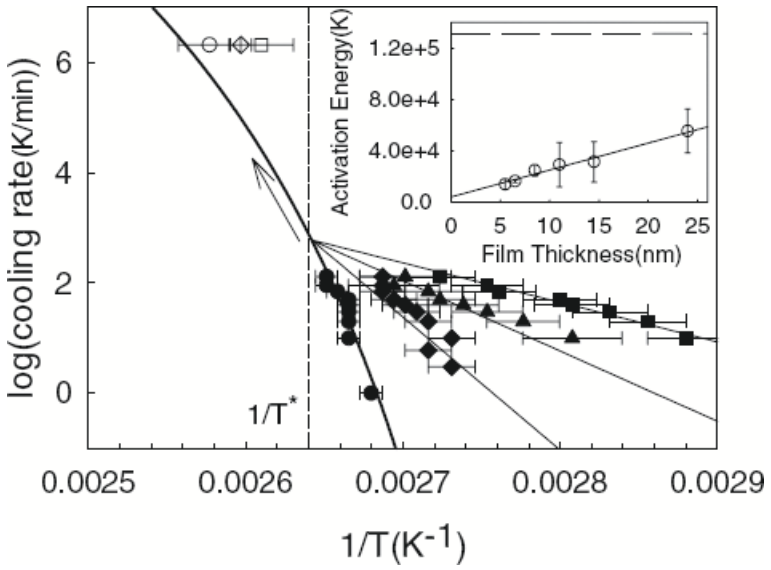

Figure 2.10: *Cooling rate vs* $1/T_g$ *for 90* •*, 24* ♦*, 11* ▲ *and 6* ■ *nm PS films. This plot suggests that at a certain cooling rate the* T_g*s obtained from all films become the same* (T_*)*. The inset shows the activation energy as a function of film thickness. The dashed line in the inset of the figure indicates the activation energy of bulk PS samples. The plot is taken from reference [21] and reproduced with permission from Phys. Rev. Lett.*

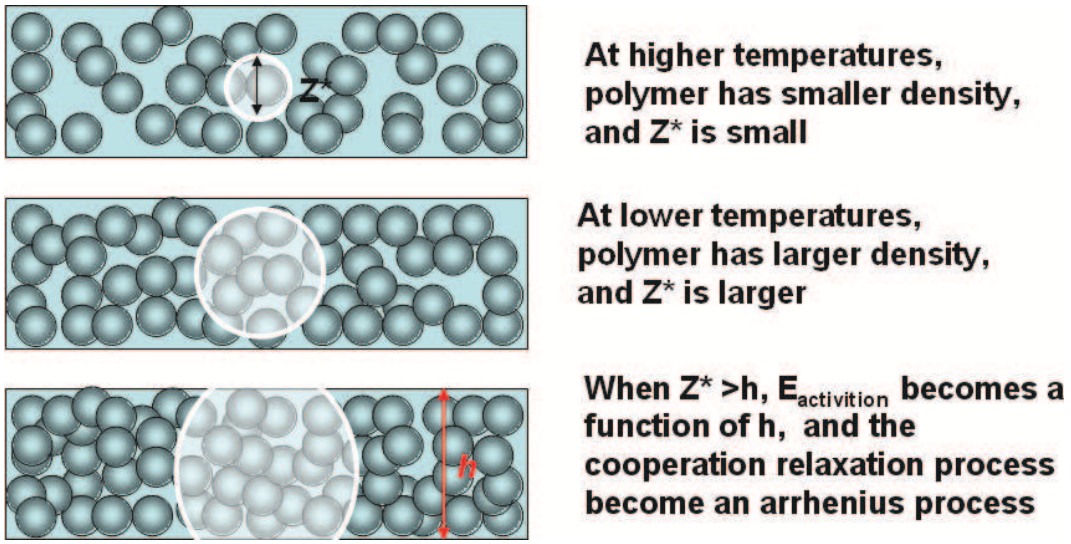

Figure 2.11: *The size of cooperative relaxation region (CRR) Z^* increases with decreasing temperatures. When a polymer film sample is cooled down from the liquid state, Z^* may become larger than the film thickness h. When $Z^* > h$ the cooperative segmental motion become a simple activated process (Arrhenius relaxation) and the activation energy $E_{\text{activation}}$ is a function of the film thickness.*

but only a few studies were aimed to study physical aging processes in thin polymer films. Recent studies [42, 43, 44, 45] of aging in thin PS films showed that, for a bulk PS sample physical aging was observed at temperatures below T_g, but disappeared at temperatures above T_g as expected. In thinner PS films (<40nm thick), where reductions in the measured T_g were reported, physical aging was not observed when these samples were held above their measured T_g but below the bulk T_g of the polymer. Only when the aging temperature was smaller than their measured T_g could physical aging be observed.

Fig. 2.12 is reproduced from ref. [46] and shows physical aging obtained from 500nm thick ◊ and 200nm thick □ PMMA films. The quantity r_f shown in this figure is proportional to the physical aging rate, defined by $r = (1/V)(\mathrm{d}V/\mathrm{d}\log(t))$, where V is the sample volume and t is the aging time. In the first plot the aging rate is plotted

against the measured temperature. In the second plot the aging rate is plotted against quench depth $T_{\mathrm{g,bulk}} - T_{\mathrm{aging}}$. The most remarkable observation is that the aging rate vs temperature measured from the thicker films is quite different from that measured from the thinner films. For a 500nm thick sample, the aging rate increases with decreasing aging temperature, and settles down at a low aging temperature. This can be explained by the competing mechanisms underlying the physical aging. The physical aging rate is determined by two factors, the distance to equilibrium, which serves as the driving force of the physical aging, and the polymer density, which is a function of temperature. At a lower aging temperature, the distance to equilibrium becomes larger which can accelerate the physical aging rate, but the lower temperatures result in a larger polymer density and smaller specific free volume. The smaller specific free volume determines that the physical aging process is slow. The increasing aging rate with decreasing aging temperature observed in this experiment suggests that the enlarged distance to equilibrium serves as a dominant factor in determining the aging rate in this case. A thinner PMMA films exhibits maximum aging rate at 20°C below T_g. This can be explained by that the competition between the driving force and the molecular dynamics, as is illustrated in Fig. 2.13.

Polymer molecules near the free surface, the substrate and the central region of the film may relax in different ways after being quenched from melt state to glass state. Priestley et al. [47] studied molecular relaxation at different distances from the free surface. To measure the molecular relaxation at a given distance, a thin layer of the film was doped with fluorescent molecules. Microscopy was used to measure the relaxation rates of the doped layers by monitoring the quenching rates during energy transfer. The relaxation rate is plotted against the depths of the doped probe layers (Fig. 2.14). Relaxation rates of the layers near the two interfaces (polymer-air and polymer-substrate) were found to be slower than those in the central layers. Priestley

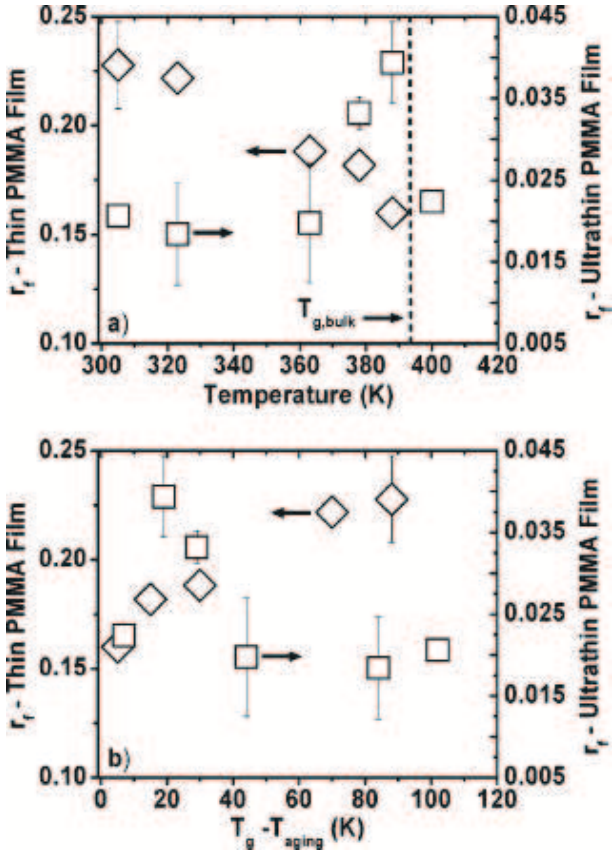

Figure 2.12: *The first plot shows physical aging rate as a function of aging temperature, and the second one shows physical aging rate as a function of quench depth.* ◊ *represents data measured from 500nm PMMA film and* □ *represents data measured from 20nm PMMA films.* r_f *is proportional to physical aging rate* $r = (1/V)(\mathrm{d}V/\mathrm{d}\log(t))$. *The plot is taken from reference [46] and reproduced with permission from Macromolecules*

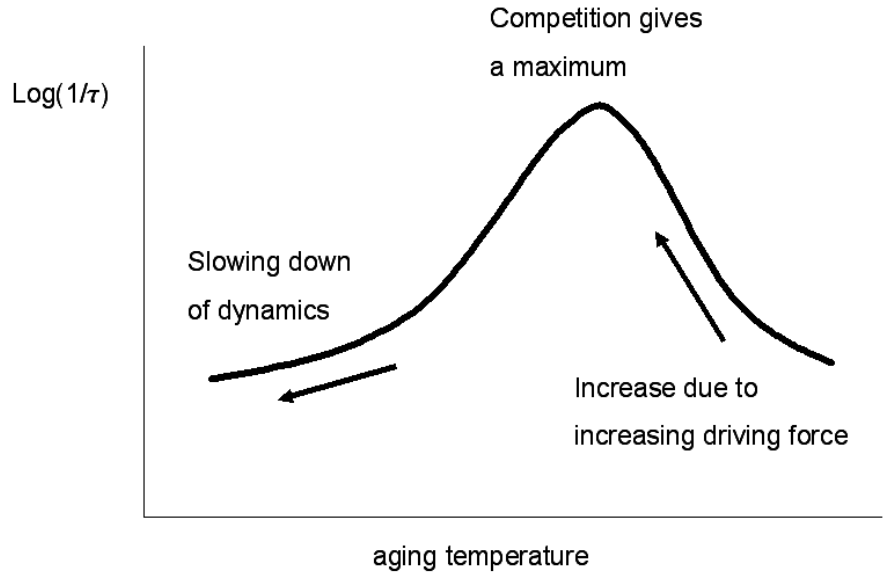

Figure 2.13: *The competition of the driving force and the molecular dynamics gives a maximum in physical aging rate* τ^{-1}

et al. [47] proposed that the origins of aging rate reduction for the layers near the free surface and the layers near the interface are not the same. For the layers near the free surface, because these layers have smaller T_g values, the driving force is smaller in these layers. For the layers near the substrates, the origin of the reduced relaxation rate is the suppressed segmental mobility as a result of the H-bonds between the film and the substrate. Another remarkable observation is that the effect of the free surface and the substrate interface penetrates a long way (>100nm and <250nm) into the central region of the film compared with the estimates of the thickness of the liquid-like surface layer.

Several studies [29, 30] found that even in a very wide thickness range (several nms to less than one hundred microns) physical aging is dependent on the film thickness. Fig. 2.15 (taken from [30]) shows the thickness and temperature dependence of aging rate (defined as $r = \partial \log \rho / \partial \log t$) in Polysulfone (PSF) films. Physical aging rate was found to be higher in thinner films or at higher temperatures. At higher

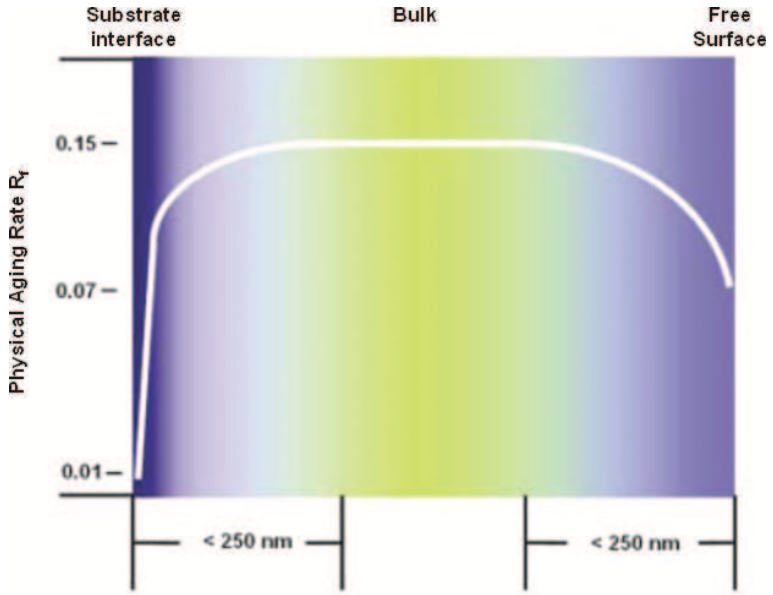

Figure 2.14: *Distribution of the structural relaxation rate. The data is obtained from PMMA film measured at* $305K$*. The color gradient represents the gradient of the relaxation rate, which is lower near the free surface and the substrate. The molecules near the free surface exhibit a factor of 2 reduction in relaxation rate and the molecules near the substrate exhibit a factor of 15. The effects of the free surface and the substrate both penetrate a long way (>100nm and <250nm) into the central region of the film compared to the estimates of the thickness of the liquid-like surface layer. The plot is taken from reference [47] and reproduced with permission from Science*

temperatures (close to, but below the $T_{\mathrm{g,bulk}}$), thickness dependence of physical aging becomes weaker. In thinner films, the temperature dependence of physical aging also becomes less significant. Huang et al. [30] suggest that the accelerated physical aging in thinner films was due to easier diffusion of free volume from the central regions of the film to the surface. It is remarkable that in their experiment the thickness dependence of physical aging was observed in a wide thickness range (up to 1 μm), which is quite different from the results obtained from the studies of the thickness dependence of the glass transition and the nano particle embedding. That makes it unlikely to explain it with the theory of liquid like free surface. In reference [29] this dependence is found extend further to 50μm. These observations are from films much thicker than the films in our interests.

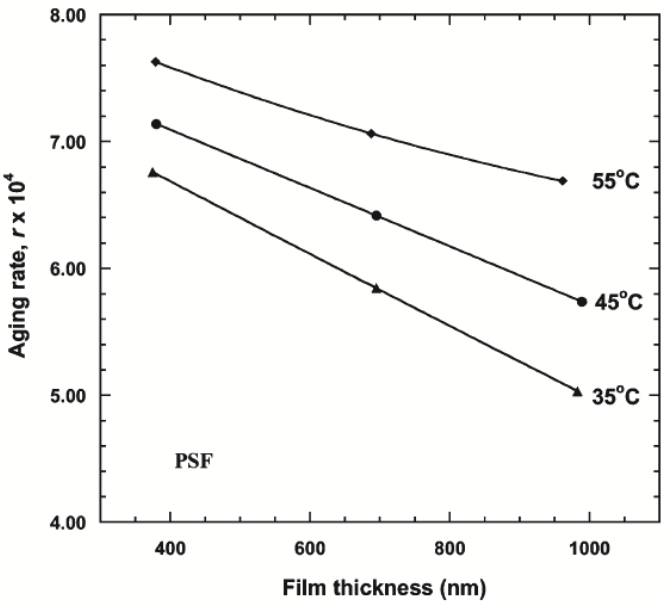

Figure 2.15: *Physical aging rate as a function of polymer film thickness. The data are shown for PSF sample measured at different temperatures. The plot is taken from reference [30] and reproduced with permission from Macromolecules.*

2.3 Motivation for experiments

Although the glass transition and relaxation process in bulk polymer material has been extensively studied, the nature of relaxation processes in ultra-thin films hasn't been clarified. A number of important questions regarding are still not answered, which are summarized below:

1. What influence do the free surfaces and confinement effects have on molecular relaxation processes in glass forming liquids? What is the relationship between polymer segmental relaxation dynamics and those of entire polymer chains in thin films?

2. Are there any intrinsic differences in the mobility of polymer molecules near free surfaces relative to the bulk polymer? If so, how do these differences affect the T_g of the thin polymer films?

3. Why, and how exactly does T_g reduction in thin polymer films depend on cooling rate/measurement frequencies? In dielectric spectroscopy studies, is the α relaxation/glass transition dependent on film thickness over a large frequency range? Can a concensus be reached about how cooling rates and measurement frequencies influence the measured properties of thin polymer films?

In the present study the relaxation process will be studied on several types of polymer film samples. Some types of samples are expected to have a free surface on top and some others are expected to have no free surface. Complementary measurement techniques (ellipsometry and dielectric spectroscopy) were used in these studies. We also used several kinds of polymers (polystyrene, poly tert-butyl methacrylate and polyvinyl acetate) in these studies, to show that the results are generic and are not

specific properties of a single polymer chemistry. The comparison of the results measured from different polymers, different sample structures and the results measured by complementary techniques will hopefully provide some information that will help to address the problems discussed above.

Bibliography

[1] J. A. Forrest and J. Mattsson. *Phys. Rev. E*, **61**:R53, 2000.

[2] J. A. Forrest, K. Dalnoki-Veress, J. R. Stevens, and J. R. Dutcher. *Phys. Rev. Lett.*, **77**:2002, 1996.

[3] K. Fukao, S. Uno, Y. Miyamoto, A. Hoshino, and H. Miyaji. *Phys. Rev. E*, **64**:051807, 2001.

[4] K. Fukao and Y. Miyamoto. *Europhys. Lett.*, **46**:649, 1999.

[5] K. Fukao and Y. Miyamoto. *Phys. Rev. E.*, **61**:1743, 2000.

[6] J. S. Sharp and J. A. Forrest. *Phys. Rev. E*, **67**:031805, 2003.

[7] G. Reiter. *Macromolecules*, **27**:3046, 1994.

[8] Y. See, J. Cha, T. Chang, and M. Ree. *Langmuir*, **16**:2351, 2000.

[9] C. J. Ellison and S. D. Kim et al. *Eur. Phys. J. E*, **8**:155, 2002.

[10] C. J. Ellison and J. M. Torkelson. *J. Polym. Sci. Part B: Polym. Phys.*, **40**:2745, 2002.

[11] C. J. Ellison and J. M. Torkelson. *Nat. Matter.*, **2**:695, 2003.

[12] C. J. Ellison, R. L. Ruszkowski, and et al. *Phys. Rev. Lett*, **92**:095702–1, 2004.

[13] G. B. Demaggio, W. E. Frieze, D. Gidley, M. Zhu, H. A. Hristov, and A. F. Yee. *Phys. Rev. Lett*, **78**:1524, 1997.

[14] J. A. Forrest, K. Dalnoki-Veress, and J. R. Dutcher. *Phys. Rev. E*, **56**:5705, 1997.

[15] J. A. Forrest, K. Dalnoki-Veress, and J. R. Dutcher. *Phys. Rev. E*, **58**:6209, 1998.

[16] O. Prucker, S. Christian, H. Bock, J. Ruhe, C. Frank, and W. Knoll. *Macromol. Chem. Phys.*, **199**:1435, 1998.

[17] A. Cusano, G. V. Persiano, M. Russo, and M. Giordano. *IEEE Sensors Journal*, **4**:837, 2004.

[18] M. Yu., Efremov, E. A. Olson, M. Zhang, Z. Zhang, and L. H. Allen. *Phys. Rev. Letters*, **91**:085703–1, 2003.

[19] S. Kawana and R. A. L. Jones. *Euro. Phys. J. E*, **223**:10, 2003.

[20] S. Kawana and R. A. L. Jones. *Phys. Rev. E*, **63**:021501, 2001.

[21] Z. Fakhraai and J. A. Forrest. *Phys. Rev. Lett.*, **95**:025701, 2005.

[22] J. S. Sharp, J. H. Teichroeb, and J. A. Forrest. *Eur. Phys. J. E*, **8**:473, 2004.

[23] K. Fukao. *Euro. Phys. J. E.*, **12**:119, 2003.

[24] J. Hauwede L. Hartmann, W. Gorbatschow and F. Kremer. *Eur. Phys. J. E.*, **8**:145, 2002.

[25] A. Serghei and F. Kremer. *Review of Scientific Instruments*, **77**:116108, 2006.

[26] A. Serghei, H. Huth, M. Schellenberger, C. Schick, and F. Kremer. *Physical Review E*, **71**:061801, 2005.

[27] A. Serghei and F. Kremer. *Phys. Rev. Letters*, **91**:165702, 2003.

[28] A. Serghei, Y. Mikhailova, H. Huth, C. Schick, K. J. Eichhorn, B. Voit, and F. Kremer. *Eur. Phys. J. E*, **17**:199, 2005.

[29] C. Zhou, T. S. Chung, R. Wang, and S. H. Goh. *J. Appl. Polym. Sci.*, **92**:1758, 2004.

[30] Y. Huang and D. R. Paul. *Macromolecules*, **39**:1554, 2006.

[31] Y. Huang and D. R. Paul. *Macromolecules*, **38**:10148, 2005.

[32] J. A. Forrest. *Eur. Phys J. E*, **8**:261, 2002.

[33] V. I. Trigub, A. V. Plotnov, and A. N. Kiselev. **27**:35, 2001.

[34] J. L. Keddie, R. A. L. Jones, and R. A. Cory. *Europhys. Lett.*, **27**:59, 1994.

[35] I. Bitsanis and G. Hadziioannou. *J. Chem Phys*, **92**:3827, 1990.

[36] J. Mattsson, J. A. Forrest, and L. Börjesson. *Phys. Rev. E*, **62**:5187, 2000.

[37] H. Yang and J. S. Sharp. *Macromolecules*, **41**:4811, 2008.

[38] D. S. Fryer, R. D. Peters, E. J. Kim, J. E. Tomaszewski, J. J. de Pablo, P. F. Nealey, C. C. White, and W. L. Wu. *Macromolecules*, **34**:5627, 2001.

[39] Y. Grohens, L. Hamon, RG. eiter, A. Soldera, and Y. Holl. *Eur. Phys. J. E*, **8**:217, 2002.

[40] F. E. Karastz and W. J. Macknight. *Macromolecules*, **6**:537, 1968.

[41] J. I. Brauman. *Science*, **267**:1887, 1995.

[42] P. G. Debenedetti and F. H. Stillinger. *Nature*, **410**:259, 2001.

[43] C. A. Angell. *Science*, **267**:1924, 1995.

[44] V. N. Novikov and A. P. Sokolov. *Nature*, **431**:961, 2004.

[45] P. G. de Gennes. *Eur. Phys. J. E*, **2**:201, 2000.

[46] R. D. Priestley, L. J. Broadbelt, and J. M. Tokelson. *Macromolecules*, **38**:654, 2005.

[47] R. D. Priestley et al. *Science*, **309**:456, 2005.

Chapter 3

Experimental Techniques

3.1 Spin-coating

In the present work polymer films are prepared by spin-coating, which is an easy, quick, and reproducible approach to prepare uniform thin polymer films with well-controlled thickness. Spin-coating is a well established technique and is a widely used film-forming method. It has been applied in microlithographic process to produce photoresists in microelectronics industry. Some papers have been dedicated to the study of this phenomenon [1, 2].

The home-built spin-coater used in our experiments is sketched in Fig. 3.1:

As illustrated in Fig. 3.1, the hollow hole at the axis is kept in vacuum by a rotary pump, and the different pressure between the vacuum and the environment holds the sample substrate tightly on the rubber pad. To prepare a polymer film, firstly a small amount of polymer solution is dropped on the sample substrate; secondly the axis is rotated by a motor, and in this experiment the rotation speed is several thousand revolutions per minute; finally most of the solution is thrown off and the solvent residue drys out in the air and the content left on the substrate forms a uniform film. Volatile organic solvents are usually used to accelerate evaporation during spin-coating. The

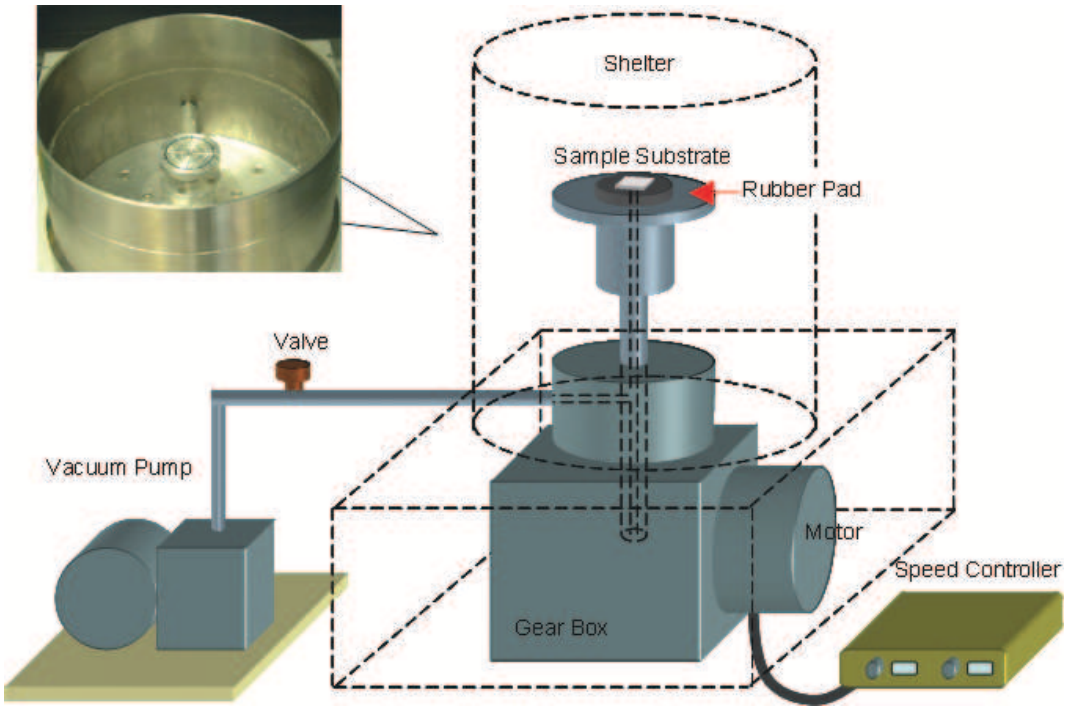

Figure 3.1: *The structure of our spin-coater*

system is put in a fume cupboard so that the evaporated solvents, often poisonous, can be vented quickly and won't harm the operator.

Film thickness can be controlled both by varying the concentration of the solution and by varying the spin speed. In the present work, film thickness is controlled by varying the concentration of solutions. Film thickness isn't always a simple function of the solution concentration, and the relationship often needs to be determined by experiment.

Films formed by spin-coating often contain internal stresses, and before being used they are usually heated up to melt state, held at the melt state for several hours and then cooled down to room temperature to remove the stress as well as any excess solvent. This process is called annealing. In the present work samples are annealed

in vacuum or dried nitrogen gas to exclude the possibility of influence from oxygen and humidity, and to remove possible stress formed in spin-coating.

3.2 Thermal evaporation of metal layers

In the present work all metal layers were prepared with vacuum evaporation. Vacuum evaporation is a method used to prepare thin and uniform metal layers. Fig. 3.2 shows the structure of the evaporator used in this work. In an evaporation the chamber covered by the bell jar is pumped into vacuum firstly. In this system a rotary pump and a diffusion pump is combined to create a low vacuum environment (in the present experiments the pressure is $< 1 \times 10^{-5}$) so that neither the boat nor the metal inside are oxidized during evaporation. The low vacuum environment also prevents contamination of the samples. The metal in the boat is then heated up to its boiling point, and the metal vapor will form a film on the cold sample surface. A mask is put beneath the samples so that only the area to be coated is exposed to the metal vapor while the remaining area remains clean. A quartz sensor is put close to the samples to monitor the film thickness during evaporation, and once the metal layer is found to grow to the required thickness, the shelter is closed immediately to prevent further metal film growth.

3.3 Ellipsometry

3.3.1 Introduction to ellipsometry

Ellipsometry measures optical properties of thin films and bulk materials. In the case of thin films this technique is particularly useful for determining the film thickness.

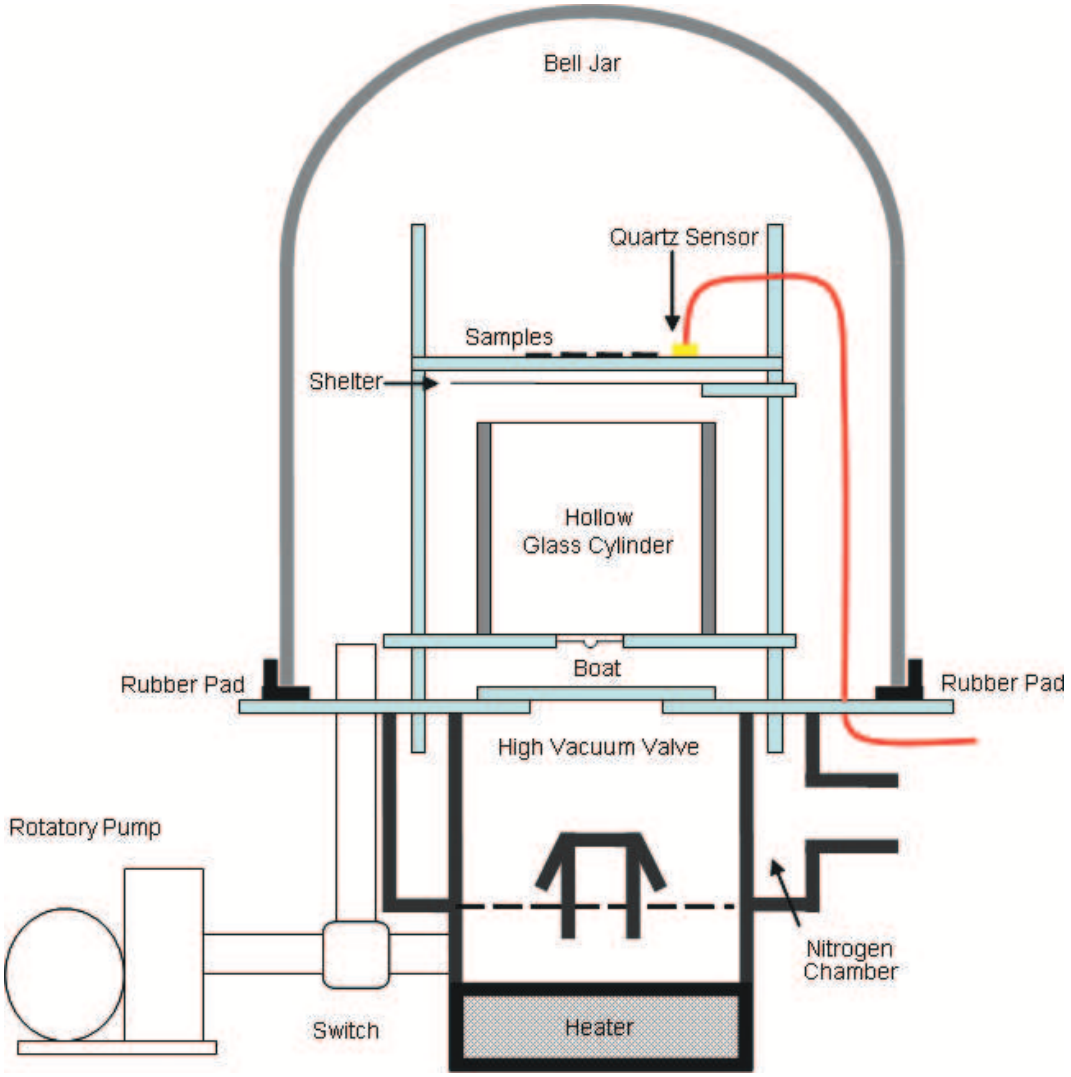

Figure 3.2: *The structure of the evaporator used in this work. a combined use of the rotatory pump and diffusion pump is able to make a low air pressure* (1×10^{-5} *torr) in the bell jar. Metal is put in the boat and then heated up to boiling point. The metal vapor deposits on the sample surfaces and form uniform metal layers. The thickness of the layers is monitored by a quartz sensor which is placed close to the samples.*

It can also be used to measure birefringence of materials.

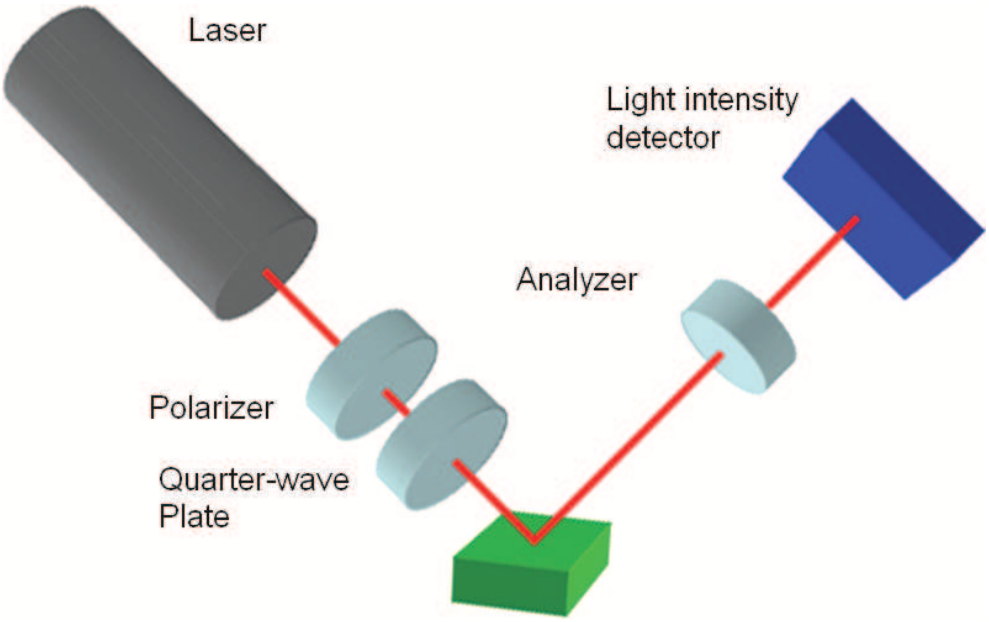

Figure 3.3: *The basic structure of an ellipsometry*

As illustrated by Fig. 3.3, a monochromatic light beam, usually generated from a laser, passes through a polarizer and a quarter-wave plate in turn. The laser is initially randomly or circularly polarized, and it becomes linearly polarized after passing through the polarizer. After passing through the quarter-wave plate, it becomes elliptically polarized, and this is where the name 'ellipsometry' is from. The elliptically polarized laser then illuminates a region on the sample surface at a certain angle of incidence and is reflected. At last it passes through a second polarizer, called the analyzer, and then is received by a light intensity detector (such as a photodiode). In a measurement, the fast axis of the quarter-wave plate is held at a fixed direction relative to the plane of incidence, and the two polarizers are rotated until a light intensity minimum (or null) is detected. The two angles, formed between the polarization of the polarizer/analyzer and the plane of incidence, are recorded and can be used to calculate the optical properties of the sample. If the sample is a substrate, one can

find its refractive index. If there is a film on the substrate, the film thickness, or the refractive index of the film, or the refractive index of the substrate can be determined in a single measurement (given the values of all other parameters). Ellipsometry is often used in the case of multiple film layers, where the film thicknesses and the refractive indexes of the layers can be determined at the same time. If samples are birefringent (no birefringent sample will be used in this work), analysis of the data is much more complex.

Fig.3.4 sketches the structure of the Ellipsometry system used in the present work. A low power Helium-Neon laser serves as the source of monochromic and highly collimated light. The two polarizers are both high quality Glan-Thompson prisms, and each prisms is mounted on a rotation stage (Newport Corporation) so that the polarization angle can be adjusted accurately (resolution $\sim 0.0001^{\circ}$). The rotation stages are controlled by software through a motion driver. The fast axis of the quarter-wave plate in this work forms an angle of 45° with the incident plane. The sample is mounted on a sample stage which can adjust the sample precisely both in the direction and in the position. Before a measurement, the direction of the surface of the sample is finely adjusted until the reflected laser shines on the centre of the photo-detector. Through adjusting the position of the sample we can also select a sample area of interests for the measurement. The signals of the light intensity and the sample temperature (measured by a thermo-couple placed close to the sample) are converted to analogue electrical signals to be measured by a computer.

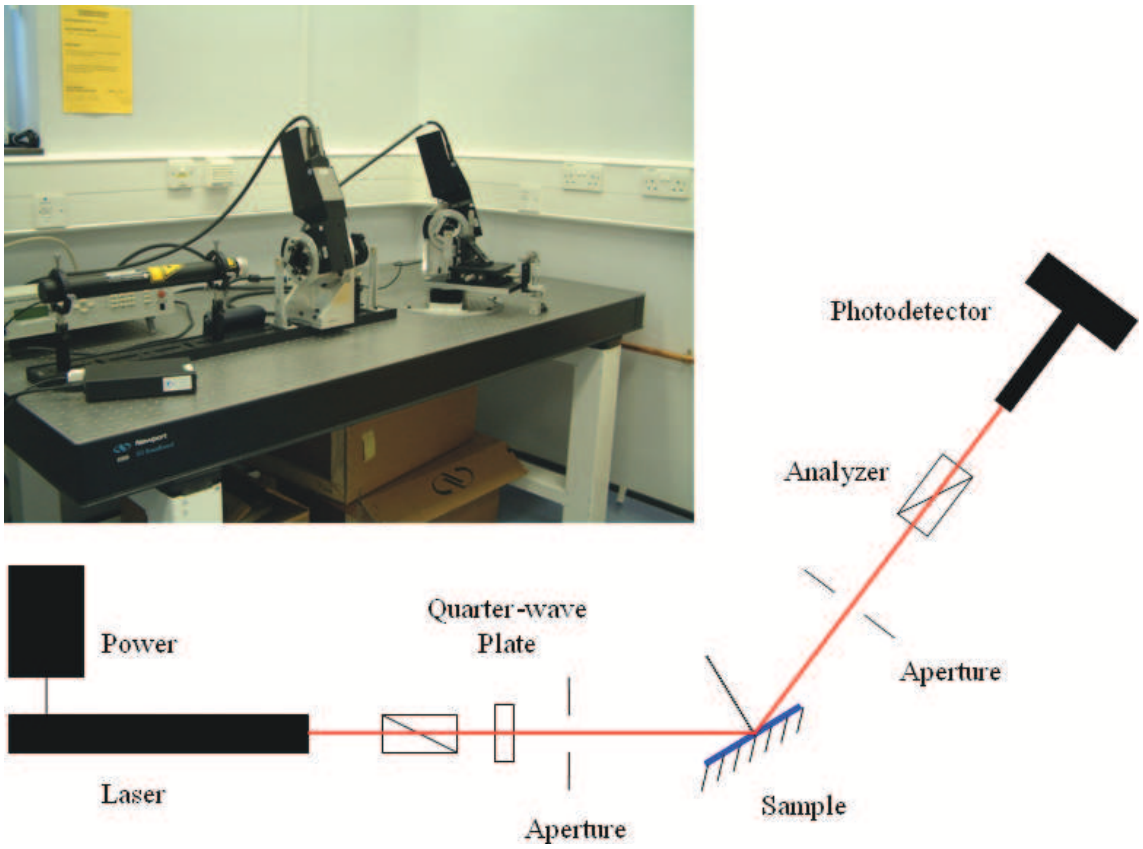

Figure 3.4: *Ellipsometry system in the lab*

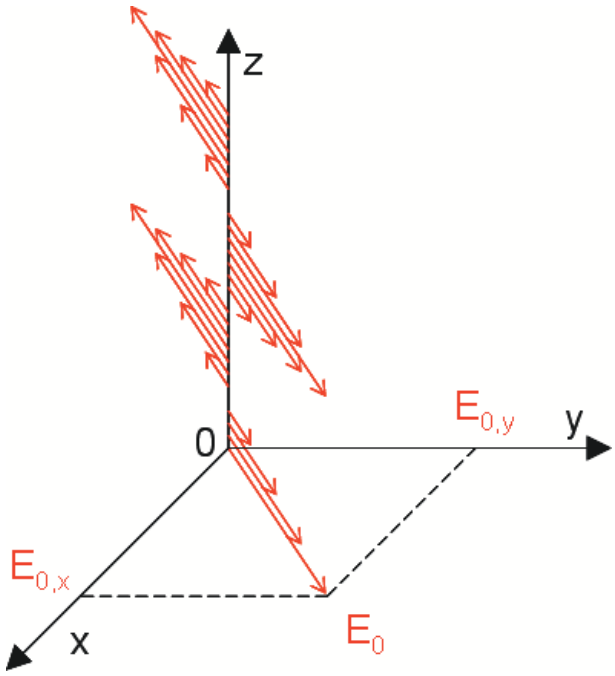

Figure 3.5: *A monochromatic light travels in +z direction. E_0 represents the oscillating electric field that lies in the x-y plane. The two components of E_0 in the x direction and the y direction are in turn represented by $E_{0,x}$ $E_{0,y}$.*

3.3.2 Theory of ellipsometry

The Jones' calculus

Consider a beam of monochromatic light traveling in the +z direction (see Fig. 3.5), if E_0 is a complex number representing the oscillating electric field that lies in the x-y plane, E_0 has two perpendicular electric vector components, one in the x direction and another in the y direction. The two polarizations (x and y) of the light at $z = 0$ can be described by a vector:

$$\begin{pmatrix} E_{0,x} \\ E_{0,y} \end{pmatrix}$$

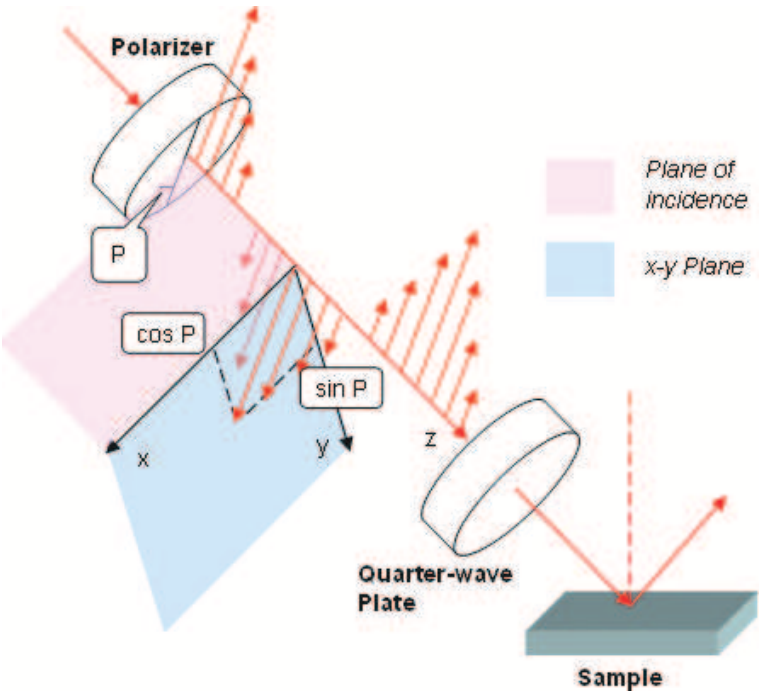

Figure 3.6: *A monochromatic light travels in +z direction. x axis is perpendicular to z and is set in the incident plane. E_0 represents the oscillating electric field that lies in the x-y plane. The two components of E_0 in the x direction and the y direction are in turn represented by $E_{0,x}$ $E_{0,y}$.*

The upper element represents the x component of the electric field and the lower one represents the y component.

The polarization state of a light is determined by the relative amplitudes of the two components of that vector, and the relative phase difference of the two components. If the two components are both multiplied with a certain complex number, neither the relative amplitudes of the two components, nor their relative phase difference will be changed. This means the vector will represent the same polarization state after its two components being multiplied with the same complex number. This can be used to remove time dependence $e^{i\omega t}$ which affects both x and y component in the same way.

For example, to describe the polarization state of the laser that has passed through the polarizer, we set the x axis to be in the plane of incidence and the z axis to be in light traveling direction, as illustrated in Fig. 3.6. Then the polarization state of light passing through a polarizer with its fast axis oriented at an angle P relative to the plane of incidence has its polarization modified by a factor of

$$\begin{pmatrix} \cos P \\ \sin P \end{pmatrix}$$

where P is the angle of the transmission axis of the polarizer referring to the incident plane. A vector like this which only describes the change in polarization state is called a *Jones' vector*.

After passing through an optical component, the light will change to another polarization state, and will be described by another Jones vector. Each optical component can be described by a 2×2 matrix, called a Jones matrix, and the effect of this optical component on the light passing through it can be described by multiplication of the matrix with a Jones vector (which describe the polarization state of the light before

being affected by this optical component). To save length, the Jones' matrix of most optical components will be given without derivation.

For example, after the linearly polarized light passes through the quarter-wave plate, the fast axis of which form an angle Q with the plane of incidence, the Jones vector becomes:

$$\begin{pmatrix} E_{p,i} \\ E_{s,i} \end{pmatrix} = \begin{pmatrix} \cos Q & -\sin Q \\ \sin Q & \cos Q \end{pmatrix} \begin{pmatrix} 1 & 0 \\ 0 & -i \end{pmatrix} \begin{pmatrix} \cos Q & \sin Q \\ -\sin Q & \cos Q \end{pmatrix} \begin{pmatrix} \cos P \\ \sin P \end{pmatrix} \quad (3.3.1)$$

where $E_{p,i}$ and $E_{s,i}$ in turn represent the p and s components of the incident light. The Jones' vector of incident light and light reflected from the sample can be related by:

$$\begin{pmatrix} E_{p,r} \\ E_{s,r} \end{pmatrix} = \begin{pmatrix} R_p & 0 \\ 0 & R_s \end{pmatrix} \begin{pmatrix} E_{p,i} \\ E_{s,i} \end{pmatrix} \quad (3.3.2)$$

where $E_{p,r}$ and $E_{s,r}$ in turn represent the x and y components of the reflected light, and R_p and R_s in turn represent the reflectivity ratio of the x component and the y component.

Rotation of the polarizer (that is, to change P) will change of the polarization state of the reflected laser. When the polarizer forms a certain angle with the plane of incidence, the reflected laser will be linearly polarized, and can be extinguished by the analyzer. Under this condition

$$i(\rho E_{p,i} E_{s,i}^{*}) = 0 \quad (3.3.3)$$

where $E_{p,r}$ and $E_{s,r}$ in turn represent the p and s components of the reflected light.

In Eqn. 3.3.3 ρ is a complex number and $\rho = R_p/R_s$. ρ is often expressed by:

$$\rho = \tan\Psi\exp(i\Delta) = \tan\Psi\cos\Delta + i\tan\Psi\sin\Delta \tag{3.3.4}$$

If Eqn. 3.3.1, Eqn. 3.3.3 and Eqn. 3.3.4 are combined together we can relate P and A to ρ. It is found that for a given ρ there are four solutions for P and four solutions for A in the range of $0° \sim 360°$. Two solutions of P are

$$P = \frac{1}{2}\tan^{-1}(-\sin 2Q\tan\Delta) + Q \tag{3.3.5}$$

$$P = \frac{1}{2}\tan^{-1}(-\sin 2Q\tan\Delta) + Q + \pi/2 \tag{3.3.6}$$

The other two others differing from these by π, which are actually the same as the above two solutions. Eqn. 3.3.5 and Eqn. 3.3.6 suggest that P is determined only by Δ.

Quite often in practice $Q = +45°$ or $Q = -45°$. Because with these two parameters, the amplitudes of the two perpendicular electric vectors of the incident light are equal. If $Q = +45°$, from equation 3.3.5 and 3.3.6 the two solutions for P will be

$$P_2 = -\Delta/2 - \pi/4 \quad \text{and} \quad P_4 = -\Delta/2 + \pi/4 \tag{3.3.7}$$

and the corresponding values of A are

$$A_2 = \Psi \quad \text{and} \quad A_4 = -\Psi \tag{3.3.8}$$

If $Q = -45°$,

$$P_1 = \Delta/2 - \pi/4 \quad \text{and} \quad P_3 = \Delta/2 + \pi/4 \tag{3.3.9}$$

and the corresponding values of A are

$$A_1 = \Psi \quad \text{and} \quad A_3 = -\Psi \tag{3.3.10}$$

These results show that for a fixed Q, there are two sets of P and A solutions that can extinguish the light. Sometimes for accuracy purpose, both the two sets of the solutions are measured and are used to calculate the P_{ave} and A_{ave} in the following equation.

$$P_{ave} = \frac{P_1 + (P_3 - 90^\circ)}{2} \quad \text{and} \quad A_{ave} = \frac{A_1 - A_3}{2} \tag{3.3.11}$$

P_{ave} and A_{ave} are expected to be more accurate, and this kind of averaging is referred to as zone averaging. The above equation assumes that $Q = -45^\circ$

Maxwells' equations

The other half of the problem is relating the Δ and Ψ to the optical properties of the sample. Mathematical approaches, especially matrix methods have been developed to address this issue. To save length only the non-matrix mathematical method will be discussed below.

According to Maxwell's equation

$$\nabla \times \overrightarrow{E} = -\frac{1}{c}\frac{\partial \overrightarrow{B}}{\partial t} \tag{3.3.12}$$

where $\overrightarrow{E}$ is electric field and $\overrightarrow{B}$ is magnetic induction. for traveling light wave described by the equation

$$\overrightarrow{E} = \overrightarrow{E_0}\exp(i\omega t - i\,\overrightarrow{k}\,\overrightarrow{r}) \tag{3.3.13}$$

where $\overrightarrow{k}$ is the wave vector of light. we can develop the relationship

$$\overrightarrow{k} \times \overrightarrow{E} = \frac{\omega}{c}\overrightarrow{B} \tag{3.3.14}$$

$\overrightarrow{k}$ can also be written as

$$\overrightarrow{k} = \frac{n\omega}{c}\overrightarrow{\mu} \tag{3.3.15}$$

where n is the refractive of index of the material where this light is traveling. $\overrightarrow{\mu}$ is the permeability of the material and is parallel to $\overrightarrow{k}$. Since at the frequency range of visible light $|\overrightarrow{\mu}| = 1$, we have $\overrightarrow{B} = \mu\overrightarrow{H} = \overrightarrow{H}$ where $\overrightarrow{H}$ is the magnetic field. Equ.3.3.15 therefore can be written in the form:

$$\overrightarrow{H} = n\overrightarrow{\mu} \times \overrightarrow{E} \tag{3.3.16}$$

The Fresnel reflection coefficients of a bare substrate

We will calculate the Fresnel reflection coefficient of semi-infinite bare substrate first. When light crosses an interface between two materials, the E and H components

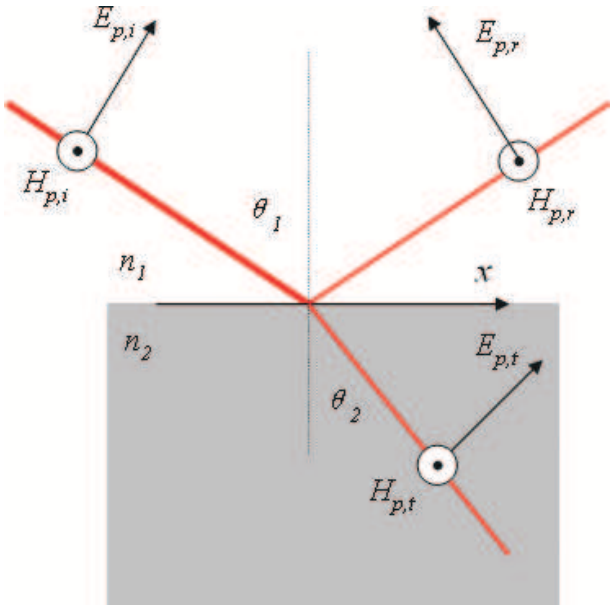

(a)

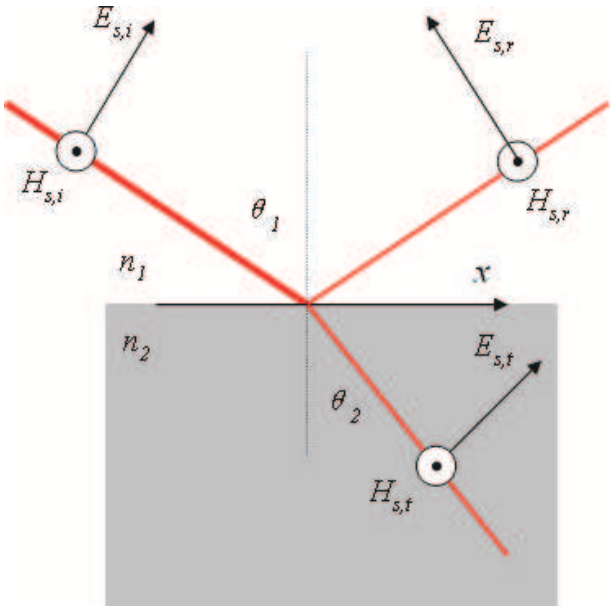

(b)

Figure 3.7: *Reflection and refraction of p-polarized light and s-polarized light on a bare semi-infinite substrate.* n_1 *and* n_2 *in turn represent the refractive index of the upper media and that of the semi-infinite bare substrate.* θ_1 *and* θ_2 *in turn represent the incident angle and the refractive angle.* $E_{p,i}$ *and* $H_{p,i}$ *in turn represent the electric field and magnetic field of the incident p-polarized light;* $E_{p,r}$ *and* $H_{p,r}$ *in turn represent the electric field and magnetic field of the reflected p-polarized light;* $E_{p,t}$ *and* $H_{p,t}$ *in turn represent the electric field and magnetic field of the refracted p-polarized light;* $E_{s,i}$ *and* $H_{s,i}$ *in turn represent the electric field and magnetic field of the incident s-polarized light;* $E_{s,r}$ *and* $H_{s,r}$ *in turn represent the electric field and magnetic field of the reflected s-polarized light;* $E_{s,t}$ *and* $H_{s,t}$ *in turn represent the electric field and magnetic field of the refracted s-polarized light;*

parallel to the interface have to be conserved on either side, as illustrated by Fig.3.7. considering only the p component, we have

$$E_{p,i}\cos\theta_1 - E_{p,r}\cos\theta_1 = E_{p,t}\cos\theta_2 \tag{3.3.17}$$

$$H_{p,i} + H_{p,r} = H_{p,t} \tag{3.3.18}$$

Since the magnititude of H is given by nE by Eqn. 3.3.16, Equ.3.3.18 becomes

$$n_1 E_{p,i} + n_1 E_{p,r} = n_2 E_{p,t} \tag{3.3.19}$$

Equation 3.3.17 and 3.3.19 can be combined together to obtain the reflection coefficients r_p and transmission coefficients t_p of the p-polarized light.

$$r_p = \frac{n_2\cos\theta_1 - n_1\cos\theta_2}{n_2\cos\theta_1 + n_1\cos\theta_2} = \frac{E_{p,r}}{E_{p,i}} \tag{3.3.20}$$

$$t_p = \frac{2n_1\cos\theta_1}{n_2\cos\theta_1 + n_1\cos\theta_2} = \frac{E_{p,t}}{E_{p,i}} \tag{3.3.21}$$

According to Snell's law, $n_1\sin\theta_1 = n_2\sin\theta_2$, so θ_2 can be eliminated and

$$r_p = \frac{n_2\cos\theta_1 - n_1\sqrt{1 - n_1^2\sin^2\theta_1/n_2^2}}{n_2\cos\theta_1 + n_1\sqrt{1 - n_1^2\sin^2\theta_1/n_2^2}} \tag{3.3.22}$$

$$t_p = \frac{2n_1\cos\theta_1}{n_2\cos\theta_1 + n_1\sqrt{1 - n_1^2\sin^2\theta_1/n_2^2}} \tag{3.3.23}$$

Similarly for the s component we have

$$r_s = \frac{n_1\cos\theta_1 - \sqrt{n_2^2 - n_1^2\sin^2\theta_1}}{n_1\cos\theta_1 + \sqrt{n_2^2 - n_1^2\sin^2\theta_1}} \tag{3.3.24}$$

$$t_s = \frac{2n_1\cos\theta_1}{n_1\cos\theta_1 - \sqrt{n_2^2 - n_1^2\sin^2\theta_1}} \tag{3.3.25}$$

Since $\rho = r_p/r_s$, it is found that given n_1 and the angle of incidence, n_2 can be calculated by

$$n_2 = n_1 \tan\theta_1 \sqrt{1 - \frac{4\rho\sin^2\theta_1}{(1+\rho)^2}} \tag{3.3.26}$$

In a single measurement the refractive index of a semi-infinite substrate can be calculated from ρ (i.e. Ψ and Δ), which in turn is calculated from the measured P and A values.

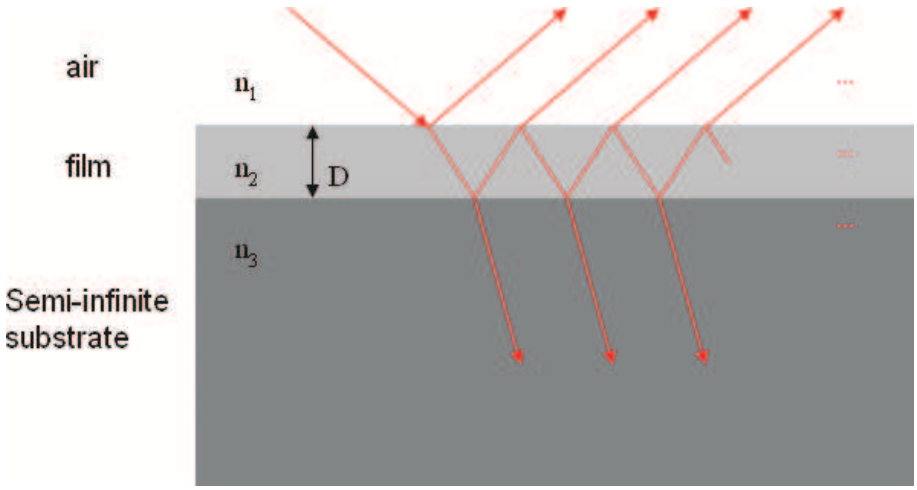

Figure 3.8: *The light path formed by multiple reflection when a beam of light shines on a film supported by a semi-infinite substrate. n_1, n_2, n_3 in turn denote the refractive index of the environment, the film and the substrate. D represent the film thickness*

The Fresnel reflection coefficients of a thin film

Next we will calculate the reflectivity of a thin film supported on a semi-infinite substrate. When a beam of light shines on the sample, It is reflected at each interface and 'bounces' around inside the film, as illustrated in Fig. 3.8. At each interface some of the light is reflected and some is transmitted. The absorption processes will not be discussed because the absorption of all the samples used in the present work can be ignored. The total reflected amplitude of light of a given polarization can be described by

$$E = E_0(r_{12} + t_{12}e^{-i\delta}r_{23}e^{-i\delta}t_{21} + t_{12}e^{-i\delta}r_{23}e^{-i\delta}r_{21}e^{-i\delta}r_{23}e^{-i\delta}t_{21} + \cdots) \qquad (3.3.27)$$

Following are the definitions of the symbols used in this equation. When a portion of light shines from the fist media on the surface of the second media, r_{12} is defined to be the ratio of the amplitudes of the reflected and incident light. r_{21}, r_{23} are defined in the similar way. t_{12}, t_{23}, t_{21} represent the amplitude ratios of the transmitted light at each corresponding interface. $e^{-i\delta}$ is the phase shift that's introduced when light passes through media 2. δ can be calculated by $\delta = k\cos\theta 2D = 2\pi n_2 \cos\theta 2D/\lambda$, where D is the film thickness and λ is the wavelength.

so for a given polarization the total reflection coefficient is:

$$R_{\text{total}} = r_{12} + t_{12}t_{21}r_{23}e^{-2i\delta}[1 + r_{21}r_{23}e^{-2i\delta} + (r_{21}r_{23}e^{-2\delta})^2 + \cdots] \qquad (3.3.28)$$

The following equation can help to simplify Eqn. 3.3.28

$$(1-x)^{-1} = 1 + x + x^2 + x^3 + \cdots \qquad (|x| < 1) \qquad (3.3.29)$$

To do that, just let $x = r_{12}r_{23}e^{-2i\delta}$, and Equ. 3.3.28 becomes:

$$R_{\text{total}} = \frac{r_{12} + r_{23}\text{exp}^{(-2i\delta)}}{1 + r_{12}r_{23}\text{exp}^{(-2i\delta)}} \tag{3.3.30}$$

The total transmission coefficient can be derived in a similar way to give

$$T_{\text{total}} = \frac{t_{12}t_{23}\text{exp}^{(-2i\delta)}}{1 + r_{12}r_{23}\text{exp}^{(-2i\delta)}} \tag{3.3.31}$$

Through Eqn. 3.3.30 ρ can be expressed by the refractive indexes, film thickness and the angle of incidence. The detailed expression is:

$$\rho = \frac{R_p}{R_s} = \frac{(r_{12,p} + r_{23,p}\exp^{-2i\delta})(1 + r_{12,s}r_{23,s}\exp^{-2\delta})}{(r_{12,s} + r_{23,s}\exp^{-2i\delta})(1 + r_{12,p}r_{23,p}\exp^{-2\delta})} \tag{3.3.32}$$

In a single measurement, ρ is determined from P and A, and then is used to calculate the refractive indexes or film thickness. This is done by minimizing $|\Delta P|^2 = (P_{\text{exp}} - P_{\text{theory}})^2$ with respect to n and D.

3.4 Dielectric spectroscopy

Dielectric spectroscopy is used to study the dielectric properties of materials as a function of measurement frequency and temperature. The measured dielectric spectra can be used to provide quantified insights to the molecular level dynamics of polymeric materials. Since measurement frequency can range from 10^{-7} Hz all the way up to 10^{17} Hz, a broad variety of dynamics in this wide frequency range can be studied by this method.

The basic structure of a dielectric spectrometer is illustrated in Fig. 3.9. The dielectric media to be measured is put between the two electrodes which forms a capacitor. An oscillating voltage is applied to the media by the system and the feedback current, or the voltage between the two electrodes, is monitored. The dielectric permittivity ε' and the dielectric loss ε'' can be calculated from the oscillating voltage applied to the sample, the feedback current and the geometric configuration of the capacitor (the calculation will be described in the theoretical subsection). Some measurements keep the sample at a constant temperature and scan through a frequency range, and the ε' or ε'' vs frequency is used as the measurement results. Some measurements keep the frequency at a constant value and heat up/cool down the sample during the measurement, and the ε' or ε'' vs temperature is used as the measurement results.

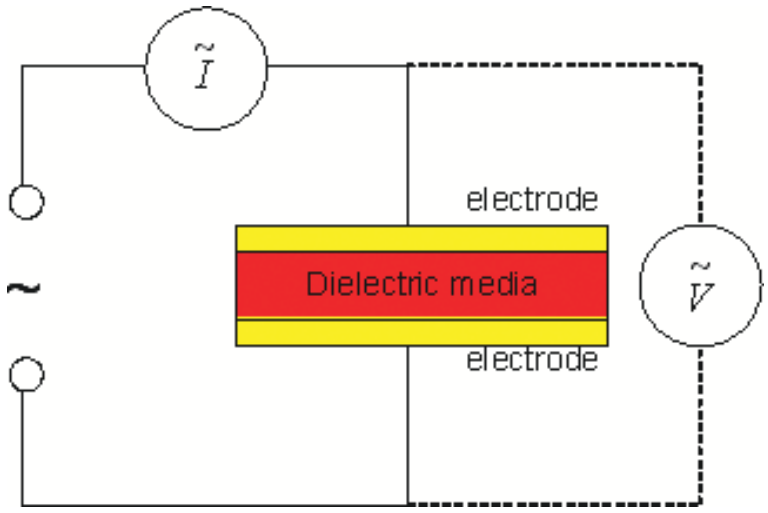

Figure 3.9: *The basic structure of a dielectric spectroscopy*

In the present work the dielectric properties of polymers are measured using a TA 2970 DEA, which can take measurements within a temperature range of -150°C to 500°C and through a frequency range of 0.1 - 100kHz. Fig. 3.10 schematically illustrates this system. The samples are located on top of a heater and are in good

thermal contact with it, so that the temperature of the sample surface can follow the temperature of the heater. A frame in the bell jar can move up and down under the driving of a motor. Four gold pins are fixed on top of the frame. Two of them are for the connection with the electrodes of the capacitor and two others are for the connection with RTD circuit, which is used to measure the temperature of the sample. Before a measurement, the sample to be measured is mounted on the heater, and then the frame moves down until the gold pins connect with the circuits. At this stage the circuit as been connected and the system is ready for a measurement.

If purging is required, as is the case where water can be a problem (such as in the present work), nitrogen gas or dried air should be connected as illustrated in Fig. 3.10. Purging rate has to be adjusted so that the purging media gently blows the sample surface.

In some cases cooling media such as water or liquid nitrogen are required to be circulated through the system, for example, some experiments require dielectric properties to be monitored when temperature is cooled down at a certain constant rate. In these measurements cooling media are connected as illustrated in Fig. 3.10. TA 2970 DEA system has special functions to deal with liquid nitrogen circulation. In the present work a lot of measurements had to be done, in which samples were required to be heated up and cooled back frequently, so water was used to accelerate heating-cooling cycles.

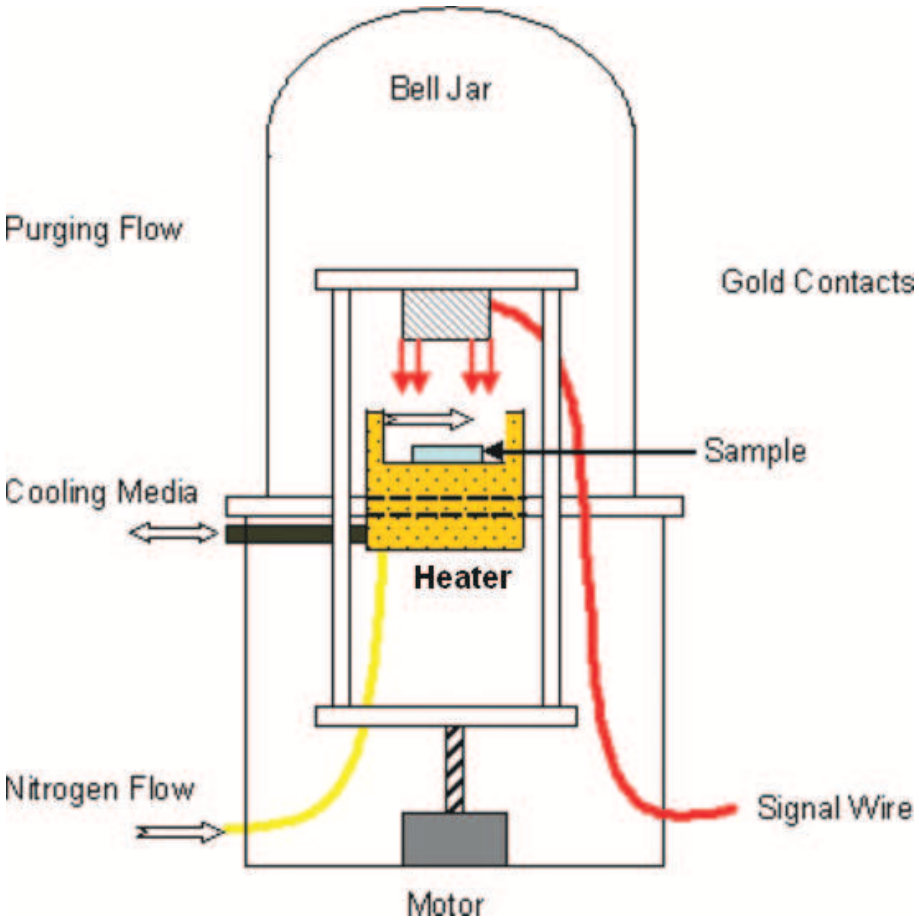

Figure 3.10: *The structure of TA 2970 DEA*

Figure 3.11: *TA 2970 DEA*

3.4.1 Models of media with one single relaxation time

The interactions between the atoms/molecules and the exerted external electric field are usually very complex, and it is quite difficult to build an extensive model for dielectric dynamics. In the following paragraphs several dielectric relaxation models are discussed and the 'bistable model', possibly the simplest and most useful one, is described in detail.

The bistable model, first treated by Fröhlich[3], assumes that a particle of charge e can be in two positions, and the distance between these two positions b. At these two positions the charge is at the minimum of the potential energy, as illustrated by Fig.3.12. When the sample is not in electrical field, the number of charges in the two wells are equal. When the two locations is in a local electric field E, A potential

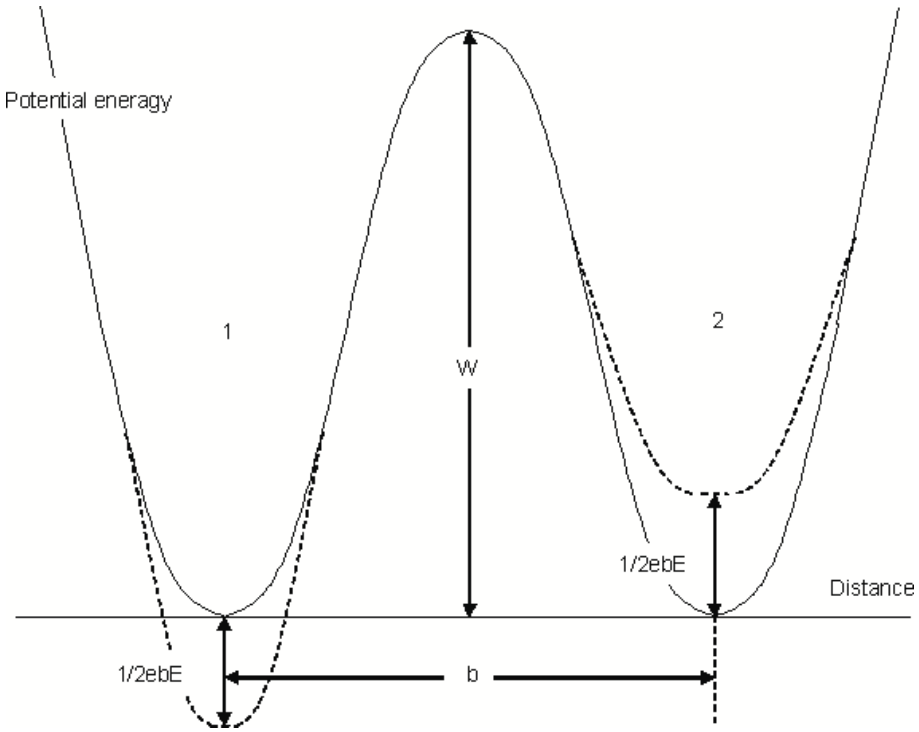

Figure 3.12: *The bistable model*

difference arises by $ebE\cos\theta$, where θ denotes the angle between direction of external electric field and the direction determined by the two potential energy wells. To make the calculation easier, we can just assume θ to be 0, which won't affect the conclusion. This movement is equivalent to a turn by 180° of a dipole of moment $\mu = \frac{1}{2}eb$.

The model assumes that the energy of charges obey statistical thermodynamics distribution, and the charges with energy higher than the potential energy barrier will jump from one well to the other. The number of charges jumping from the first well to the second one per unit time, represented by w_{12}, will be

$$w_{12} = Ae^{-\frac{W-\mu E}{kT}} \tag{3.4.1}$$

Where T is the absolute temperature, k is the Boltzmann constant, and A a factor which may or may not depend on temperature. W is usually described as activation energy.
In practice, $\mu E/kT \ll 1$, hence equ.3.4.1 can be simplified to

$$w_{12} = Ae^{-\frac{W}{kT}}\left(1 - \frac{\mu E}{kT}\right) \tag{3.4.2}$$

The rate of charges jumping back is

$$w_{21} = Ae^{-\frac{W}{kT}}\left(1 + \frac{\mu E}{kT}\right) \tag{3.4.3}$$

In equilibrium, the rate of charges jumping forward and the rate of those jumping back are equal, i.e.

$$N_1 w_{12} = N_2 w_{21} \tag{3.4.4}$$

where N_1 and N_2 in turn denote the number of the charges in the first and the second potential wells respectively.

The dipole P formed by these charges is

$$P = (N_1 - N_2)\mu \tag{3.4.5}$$

using Eqn.3.4.2, Eqn.3.4.3 and Eqn.3.4.4 we get

$$N_1 - N_2 = N\frac{\mu E}{kT} \tag{3.4.6}$$

where $N = N_1 + N_2$ remains constant. Equ.3.4.5 therefore becomes

$$P = N\frac{\mu^2 E}{kT} \tag{3.4.7}$$

This equation gives an explanation why the polarization of media is directly proportional to the electric field.

In non-equilibrated state, The charge flow between the two wells is

$$\frac{\mathrm{d}N_1}{\mathrm{d}t} = -N_1 w_{12} + N_2 w_{21} \tag{3.4.8}$$

and

$$\frac{\mathrm{d}N_2}{\mathrm{d}t} = N_1 w_{12} - N_2 w_{21} \tag{3.4.9}$$

Comparing the two above equations results in

$$2\frac{\mathrm{d}N_1}{\mathrm{d}t} = \frac{\mathrm{d}(N_1 - N_2)}{\mathrm{d}t} \tag{3.4.10}$$

combining Equ.3.4.2, 3.4.3, 3.4.5, 3.4.8 and 3.4.10 one get

$$\frac{1}{2w} \cdot \frac{\mathrm{d}P}{\mathrm{d}t} + P = \frac{N\mu^2 E}{kT} \tag{3.4.11}$$

where $w = Ae^{-WkT}$. The above equation can be written in this form:

$$\tau\frac{\mathrm{d}P}{\mathrm{d}t} + P = \alpha E \tag{3.4.12}$$

where $\tau = 1/2w$ and $\alpha = N\mu^2/kT$. This relationship suggests that relaxation rate $\mathrm{d}P/\mathrm{d}t$ is proportional to the distance to the equilibrium state $\alpha E - P$. This is an important base for the dielectric theory. As is shown in the later discussion, some other models also lead to this relationship. In this model, τ is the characteristic time scale for charges to jumping between the potential wells. If the sample is polymeric material, it can be understand as the time scale for molecular segments to reorganize themselves after an applied perturbation.

Another model that results in the same relationship is Debye's classic model, which treats dipolar molecules in non-polar liquids. This model assumes that the dipolar molecules concentration is very small and that the electrostatic interaction between dipoles can be ignored. The dipolar molecules experience Brownian motion in the solvent, and the rotation of dipole orientation is hindered by friction force. When samples are not in external electric field, the distribution of the orientation of the dipoles is random and the total dipole equals to zero.

When an external electric field is applied to the medium, more dipoles will point to the direction of the external electric field. Calculation of this model found that the relaxation rate obey Equ. 3.4.12, and the parameter τ is determined by

$$\tau = \frac{\zeta}{2kT} \tag{3.4.13}$$

where ζ is a constant which characterize the friction hindering the rotation of the dipoles.

The above models, however, didn't consider the interaction between dipoles. In many cases the interaction cannot be ignored. A variety of approaches have been brought up with to address different types of the interactions between the dipoles. Discussion of these approaches will be somewhat lengthy and will not be included.

3.4.2 Debye equations

The polarization of a medium as the response to an external electric field is usually composed of two components. One follows the changing of the external electric field intimately and the other one lags behind. As illustrated in Fig.3.13, when a step external electric field is applied to a medium, the polarization of the media jumps immediately to another level, and then the polarization slowly evolves to a saturated level. The quick polarization is thought to be related to relaxation processes with very short relaxation times, such as the polarization of the atoms. The slow polarization is related to relaxation processes with long relaxation times, such as the cooperative relaxation of polymer molecules. Hereby the quick component is represented by P_∞, the slow component is represented by P_D and the saturated value of polarization by P_s. P_∞ and P_s are both proportional to the change of the electric field, so we can

define two parameters ε_∞ and ε_s to be:

$$\varepsilon_\infty = \frac{4\pi P_\infty}{E} - 1 \qquad \varepsilon_s = \frac{4\pi P_s}{E} - 1 \tag{3.4.14}$$

The relaxation process of P_D can be described using the model discussed in the previous section, that is:

$$\tau \frac{\mathrm{d}P_D}{\mathrm{d}t} + P_d(t) = (\varepsilon_s - \varepsilon_\infty)\frac{E(t)}{4\pi} \tag{3.4.15}$$

Oscillating electrical field is much more useful in dielectric spectroscopy. For a periodic field that is applied on the medium,

$$E(t) = E_0 e^{i\omega t} \tag{3.4.16}$$

The general solution of equation 3.4.15 is

$$P_D^*(t) = Ke^{-\frac{t}{\tau}} + \frac{1}{4\pi}\frac{\varepsilon_s - \varepsilon_\infty}{1+\omega\tau}E_0 e^{i\omega t} \approx \frac{1}{4\pi}\frac{\varepsilon_s - \varepsilon_\infty}{1+\omega\tau}E_0 e^{i\omega t} \tag{3.4.17}$$

where K characterizes the initial polarization. The first term decays with time and that's why it's neglected. In the case of oscillating electric field, a complex dielectric constant is defined to be:

$$\varepsilon^*(\omega) = 4\pi\frac{P_D^*(\omega,t) + P_\infty}{E^*(\omega,t)} + 1 \tag{3.4.18}$$

Combining Eqn. 3.4.14, Eqn. 3.4.16, and Eqn. 3.4.17 and Eqn. 3.4.14, we can

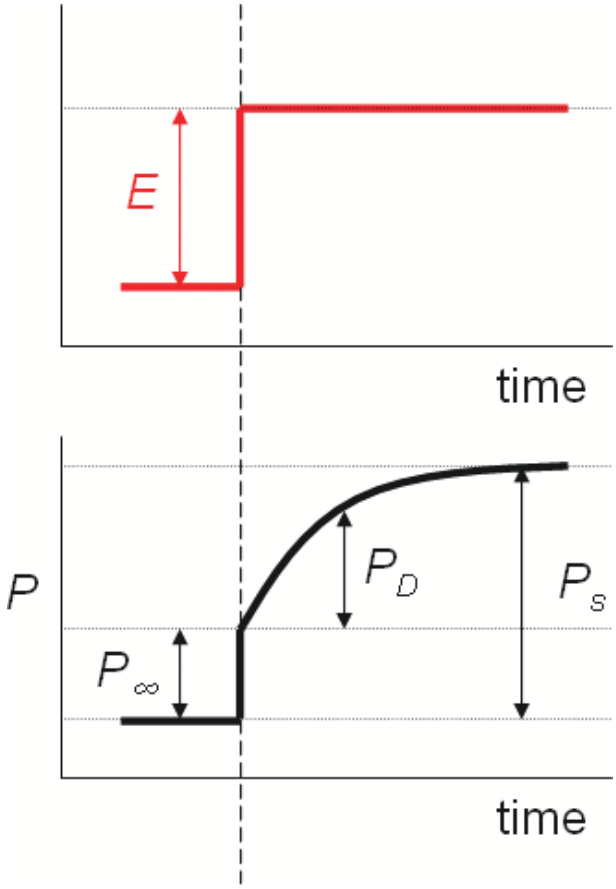

Figure 3.13: *A step electric field is exerted on a medium, and the polarization of the medium is composed of two components:* P_∞ *and* P_D*.* P_∞ *follows the electric field intimately and* P_D *slowly evolves to a saturated level, which is represented by* P_s*.*

represent $\varepsilon^*(\omega)$ by

$$\varepsilon^*(\omega) = \frac{\epsilon_s - \epsilon_\infty}{1 + i\omega\tau} + \epsilon_\infty \tag{3.4.19}$$

The real part (represented by ε') and imaginary part (represented by ε'') of ε^* are

$$\varepsilon'(\omega) = \varepsilon_\infty + \frac{\varepsilon_s - \varepsilon_\infty}{1 + \omega^2\tau^2} \tag{3.4.20}$$

$$\varepsilon''(\omega) = (\varepsilon_s - \varepsilon_\infty)\frac{\omega\tau}{1 + \omega^2\tau^2} \tag{3.4.21}$$

ε' and ε'' vs frequency or temperature is used as the results of dielectric spectroscopy measurements. ε' and ε'' are plotted out in Fig. 3.14 against $\log(\omega\tau)$, where the parameters $\varepsilon_s = 8$ and $\varepsilon_\infty = 2$. $\tan\delta$, defined by

$$\tan\delta = \frac{\varepsilon''}{\varepsilon'} = \frac{(\varepsilon_s - \varepsilon_\infty)\omega\tau}{\varepsilon_s + \varepsilon_\infty\omega^2\tau^2} \tag{3.4.22}$$

is also plotted out in that figure. The relaxation frequency is at the peak point in the ε'' vs frequency plot, or at the maximum slope in the ε' vs frequency plot.

The solution of P as a function of time provides a proof to an important assumption that with electric field disturbance dielectric response complies with linearity and causality. Linearity means that the response at a certain time point is the sum of all responses to stimuli, and the causality means that only previous stimuli will affect current response. While it's easy to accept that the response of a dielectric medium follows the causality. The linearity of dielectric system wasn't realized until Boltzmann [4] proposed it in 1874 and J. Hopkinson [5] verified it in 1876. Later experiments showed that under small electric fields dielectric systems hold linearity

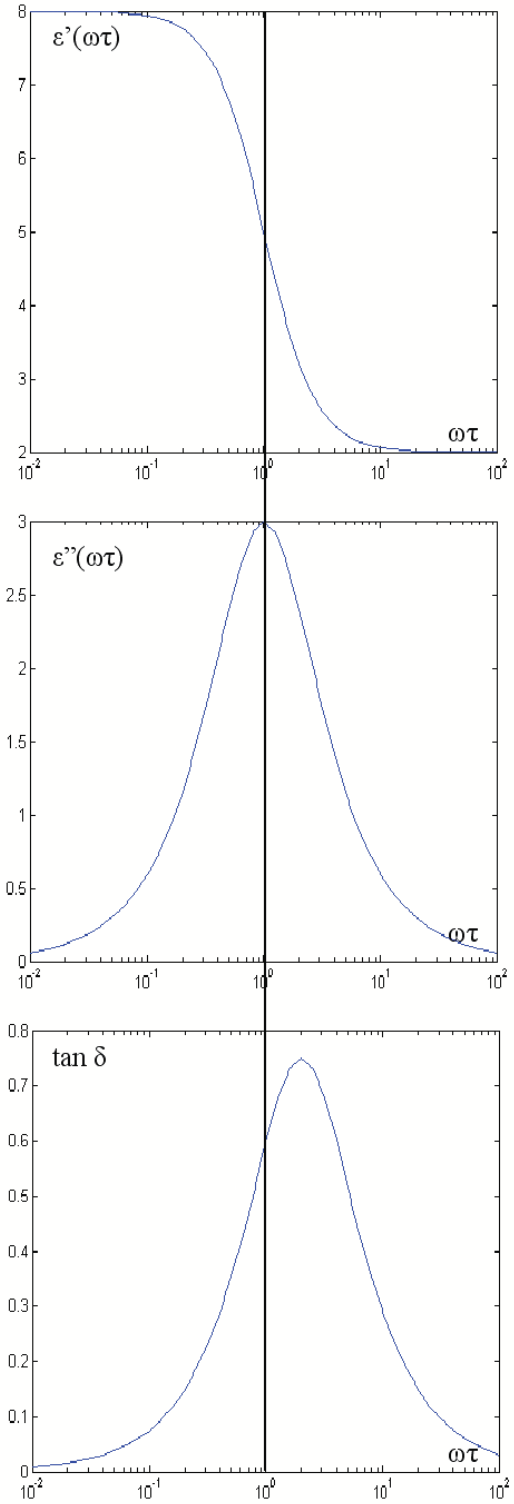

Figure 3.14: ε', ε'' *and* $\tan\delta$ *as a function of* $\log(\omega\tau)$. *The peak point of* $\tan\delta$ *isn't at the same place as that of the* ε''

pretty well. In this context, the response $P(t)$ can be calculated by:

$$P(t) = \int_{-\infty}^{t} E(\mu)\dot{\Psi}(t-\mu)\mathrm{d}\mu \tag{3.4.23}$$

where $\dot{\Psi}$ is a decay function called current decay function.

3.4.3 Models of media with multiple relaxation time

The Debye equation fits well to many dielectric spectra, especially to those measured from dilute solutions of large polar molecules in non-polar solvents. It also gives us basic understanding of the origin and properties of dielectric spectra. In practice there could be several relaxation processes exist in a sample. An example is in polymer samples where several relaxation processes often exist. The most pronounced one is the segmental cooperative relaxation which follows the VFT law, and this relaxation process is called α relaxation. The weaker relaxation processes are usually related to some chemistry processes which follows the arrhenius law, and these weaker relaxation processes are called β, γ... relaxations. The dielectric spectrum of a polymer like this can be theoretically treated as the overlap of several Debye relaxation spectrums. There are also some cases where the dielectric spectrum cannot be described by Debye equation (or overlap of several Debye equations). For example, the peaks of ε'' as a function of $\log\omega$ are often observed to be wider than expected, or to have asymmetric shapes, or even to behave further away from Debye relaxation. There exist three popular treatments to this issue. One of them is to describe the relaxation with an empirical function, which is usually an altered Debye relaxation function. In polymer physics one of the most important empirical function is the Havriliak-Negami (H-N) function [6, 7]. It describes the widening and asymmetry of the relaxation peaks of ε'' vs $\log\omega$ by two extra exponential parameters. Below is the

Havriliak-Negami function:

$$\varepsilon^* = \varepsilon_\infty + \frac{\Delta\omega}{(1 + (i\omega\tau)^\alpha)^\beta} \tag{3.4.24}$$

The second one is to describe the relaxation in second order differential equations, rather than keep using the first order ones. A second order differential equation is like:

$$\omega_0^2 \frac{\mathrm{d}^2(Ay)}{\mathrm{d}t^2} + \tau \frac{\mathrm{d}(Ay)}{\mathrm{d}t} + Ay = Ax \tag{3.4.25}$$

This treatment is usually used at very high frequencies, and won't be used in this work.

The last one is to assume that these peaks are produced by overlapping of more than one Debye peaks, and each peak reflects the relaxation of one kind of charge in the material. The number of overlapping Debye relaxations can range from two to continuous distributions. If K kinds of charges are supposed to exist, and each kind is supposed to have n polarisable elements, $\dot{\Psi}(t)$ can be expressed by:

$$\dot{\Psi}(t) = \sum_K \frac{n_k \alpha_K}{\tau_K} e^{-\frac{t}{\tau_K}} \tag{3.4.26}$$

where the α is the polarizability. In this case $P(t)$ can be obtained by calculating the response of each charge, and then summing up those responses. The treatment of $\varepsilon^*(\omega)$ is similar.

For a dielectric with a continuous set of charges. A distribution function $y(\tau)$ is often used, which is defined by:

$$y(\tau) = \frac{\mathrm{d}\varepsilon_s(\tau)}{\mathrm{d}\tau} = 4\pi\alpha(\tau)f(\tau) \tag{3.4.27}$$

where $f(\tau)$ is the density function of charges. The distribution function was first introduced in 1893 by Wiechert [8]. With this function dielectric constant can be calculated by:

$$\varepsilon_s - \varepsilon_\infty = \int_0^\infty y(\tau)\mathrm{d}\tau \tag{3.4.28}$$

$$\varepsilon'(\omega) - \varepsilon_\infty = \int_0^\infty \frac{y(\tau)\mathrm{d}\tau}{1+\omega^2\tau^2} \tag{3.4.29}$$

$$\varepsilon''(\omega) = \int_0^\infty \frac{y(\tau)\omega\tau}{1+\omega^2\tau^2}\mathrm{d}\tau \tag{3.4.30}$$

In practice in stead of calculating ε^*, ε_s, ε' and ε'' from $y(\tau)$, $y(\tau)$ is calculated from ε^* etc. which, can be obtained in experiments.

3.5 Atomic force microscope

The Atomic Force Microscope (AFM) is an important tool for imaging and manipulating nanoscale objects. It was invented in 1985 by Binnig, Quate and Gerber [9].

Fig. 3.16 gives the typical structure of an AFM. A sharp tip is fixed on a flexible and reflective cantilever, and the cantilever is fixed on a piezo tube. To obtain an AFM image, The piezo tube and the cantilever move toward the sample surface under the driving of a step motor until the tip is in contact with the sample surface.

The interaction energy between the AFM tip and the sample surface in most cases are a competition between Pauli repulsion, approximated by a $1/r^{12}$ variation and the attractive van der Waals (VDW) interactions, which vary as $1/r^6$. Hence the tip-sample potential is given by

$$E(r) = 4\varepsilon \left[\left(\frac{\sigma}{r}\right)^{12} - \left(\frac{\sigma}{r}\right)^{6} \right] \tag{3.5.1}$$

where ϵ is the depth of the potential well, r is the tip-sample distance and the minimum in the potential occurs at $2^{1/6}\sigma$. Fig 3.15 illustrates the tip-sample force as a function of the tip-sample distance. Since VDW's force is proportional to $-\nabla E(r)$, it drops off quickly with distance ($\sim 1/r^7$) and only the very end of the AFM tip interacts with the surface. This makes the AFM highly sensitive.

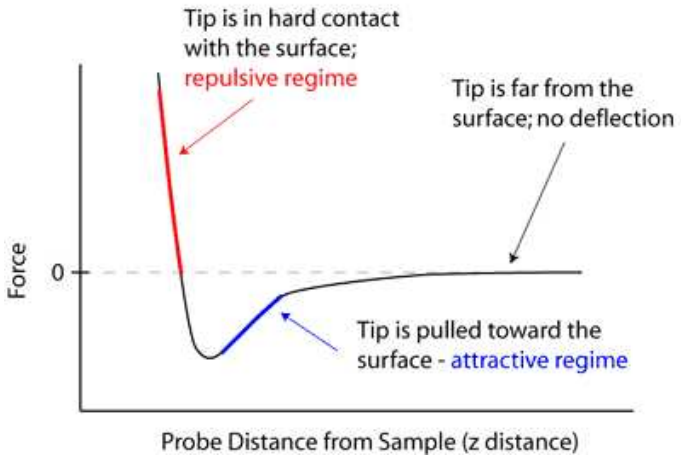

Figure 3.15: *The tip-sample force as a function of the tip-sample separation*

After the AFM tip is in contact with the sample surface the piezo tube drives the cantilever and the AFM tip to scan across the sample surface. The piezo tube can provide precise positioning. A laser beam is used to illuminate onto the top surface

of the tip and is reflected back to a photodiode. The photodiode is divided into two or four sectors, and the out put voltage of those sectors are coupled to differential amplifiers. The angular movement of the deflected light results in the sectors of the split photodiode collect more light intensity that others. This difference is used to determine the position of the laser beam, and hence the height of the tip. Voltage can be fed back to the z piezo motor to keep the tip at a constant distance with respect to the surface.

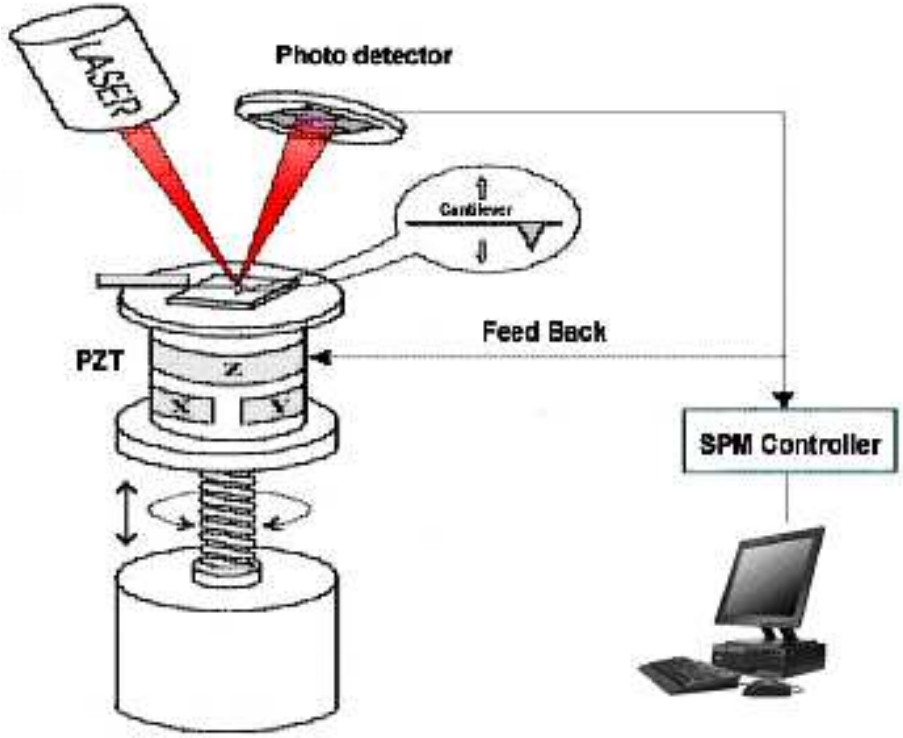

Figure 3.16: *Diagram of typical AFM arrangement*

Most modern commercial AFM tips and cantilevers are made of silicon or silicon nitride. Fig.3.17(a) shows SEM images of an pyramid-like tip. Fig.3.17(b) is the cantilever, with the common shape V, at the end of which stands the sharp tip.

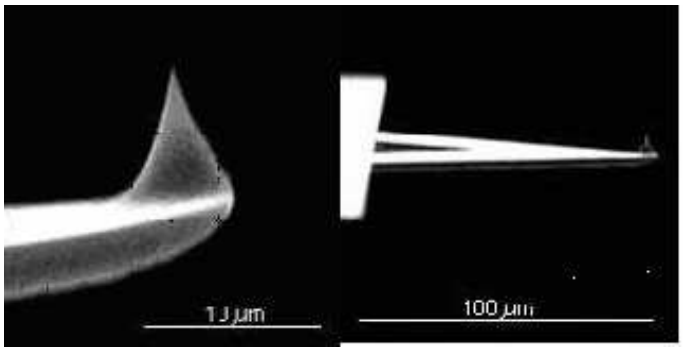

Figure 3.17: *SEM image of an AFM cantilever*

AFM usually works in the following imaging modes.

1. **Contact Mode** In this Mode the sample and tip are always in contact. The feedback voltage from the photodiode keeps a constant cantilever deflection. In this mode the repulsive wall of the interaction between the tip and the sample is imaged. The main disadvantage of the contact mode is that it's not suitable for sticky or fragile samples. Because in this mode the tip is always in contact with the sample, if the sample is sticky the surface corrugation does not only cause vertical deflections but also a tiny twisting of the cantilever [10], which is often unwanted because this lateral forces affect the images usually in a complex way [11]; if the sample is fragile, the contact mode may simply damage the sample.

2. **Tapping Mode (Also known as AC mode)**. In this mode when the tip is driven to oscillate by the piezo tube. The frequency is usually just below the resonant frequency of the cantilever. As the tip comes into contact with the surface, the surface damps the oscillation of the cantilever, and the resonant frequency of the cantilever shifts downward. The amplitude reduction is fed back to computer, and the computer adjusts the PZT according to the feedback to keep a constant tip-sample distance. The tapping mode is comparatively less

destructive to samples the tip is only in contact with the surface for a small percentage of each oscillation. This mode is more suitable for the imaging of sticky and fragile samples.

3. **Phase Mode** Phase Mode The tip oscillates in the same way as that in the Tapping mode. An image is built up according to the phase difference between the driving oscillation and the cantilever oscillation.

Bibliography

[1] D. E. Bornside, C. W. Macosko, and L. E. Scriven. *J. Imag. Techn.*, **13**:122, 1987.

[2] A. Weill and E. Dechenaux. *Polym. Eng. Sci.*, **28**:945, 1988.

[3] H. Fröhlich. *Theory of Dielectrics*. Oxford University Press, London, 1939.

[4] L. Boltzmann. *Akad. Wissenschaft, Wien.* 1874.

[5] J. Hopkinson. *Original Papers*. Cambridge University Press, Cambridge, 1901.

[6] S. Havriliak and S. J. Negami. *Polym. Sci. C*, **14**:99, 1966.

[7] S. Havriliak and S. J. Negami. *Polymer*, **8**:161, 1967.

[8] E. Wiechert. *Wied. Ann. Phys.*, **50**:335, 1893.

[9] Binnig et al. *Phys. Rev. Lett.*, **56**:9, 1981.

[10] C. M. Mate, G. M. McClelland, R. Erlandsson, and S. Chiang. *Phys. Rev. Lett.*, **59**:1942, 1987.

[11] A. J. den Boef. *Rev. Sci. Instrum.*, **62**:88, 1991.

Chapter 4

Interfacial effects and the glass transition in ultrathin films of poly (tert-butyl methacrylate)

4.1 Introduction

Ultrathin polymer films provide an excellent model system for studying the effects of surfaces, interfaces and molecular confinement on the nanoscale properties of polymeric materials [1]. Of particular interest are the role played by interfacial effects in determining the glass transition in thin polymer films. [2, 3, 4, 5, 6]. The T_g reductions that are routinely observed in these samples have been attributed to the existence of a liquid like surface layer in thin polymer films or to finite size effects, and many studies have been performed to test these theories. As discussed in chapter 2, despite many consistent results, there also exist many other contradictory observations. These have resulted in a significant amount of controversy and our understanding of the nature of the dynamic properties of polymers near surfaces and the interfaces, and their relationship to the physical properties in ultrathin polymer films remains incomplete.

Interpreting the wealth of results and resolving the controversy that already exists

regarding the dynamic properties of thin polymer films has proven to be a challenging task. When comparing techniques that are designed to probe similar properties of these samples a number of experimental considerations need to be taken into account. For example, great care has to be taken to differentiate between experiments that are designed to probe local segmental relaxations (such as those responsible for the glass transition) and those that are designed to probe the motion of whole polymer chains. Recent reports have provided strong evidence for the existence of a more mobile surface region at the free surface of glassy polymer films [2, 7] and the existence of a gradient in the dynamics of polymeric materials as we move away from the free surface [2]. These studies suggest that it is likely that there are polymer chains near the free surface that have segments in regions of enhanced mobility near the free surface, but that also have parts of the chains buried in glassy regions of the film. These combined experiments suggest that the enhanced surface dynamics that have been reported in recent nanoparticle embedding [7, 6] and surface relaxation studies [8] (that probe only the first few nanometers close to the surface of the films) may not be inconsistent with measurements of polymer chain diffusion coefficients that are lower than those observed in the bulk polymer [9]. If this gradient in dynamics exists, then the characteristic relaxation times of the polymer close to the free surface would be expected to vary by orders of magnitudes on length scales that are comparable to the dimensions of a single polymer molecule. These effects are likely to be further complicated by the presence of a substrate. These factors are likely to result in complicated dynamics and the decoupling of segmental and whole chain motion in ultrathin polymer films.

A simple way of testing whether or not free polymer surfaces are responsible for the reduced T_g in thin polymer films, is to try to manipulate the free surface and to determine the resulting effect upon the measured thickness dependence of the T_g. Previous attempts to achieve this have produced mixed results. The measured T_g values for SiO_x coated polystyrene (PS) films were found to be essentially the same

as those for supported films with one free surface [10]. This result was confirmed in dielectric studies of Al coated PS which also showed T_g behaviour the same as that of supported films [11]. The comparison between these results and the T_g values measured in free standing films results in an apparent and striking inconsistency. If the free surface is important in causing reduced T_g values in thin films then eliminating the free surface *must* have an influence on the measured T_g values. The fact that this does not seem to be the case has proven to be a major obstacle in understanding thin film glass transitions. More recent results have suggested that the structure of the polymer/metal interfaces produced by evaporating different metals on to polymers can play a vital role in determining whether or not the free surface effects are removed [6]. These studies also showed that PS films that are evaporatively capped with Al display a thickness dependent T_g. However, when almost identical Al capped PS films were prepared in such a way that great care was taken to ensure that the free polymer surface was removed, the thickness dependence of the T_g was suppressed.

In the studies of the glass transition in ultrathin polymer films, some efforts had been made to study ultrathin poly(tert-butyl methacryalte) (PtBMA) films. The capability of PtBMA to form both spincast films and Langmuir-Blodgett (LB) films is of particular interest to researchers. The thickness dependence of T_g in PtBMA spincast films, as a comparison to that in PtBMA LB films, helps to address the relationship between the nano-scale structure in ultrathin polymer films and their physical properties. However, despite all the efforts put into this area, some contradictory observations remain even in the most basic features. For example, Hsiung et al. and Mabuchi et al. [12, 13, 14]reported that the measured T_g in ultrathin polymer LB films was similar to the values obtained from the bulk samples, but See et al. [15] showed that significantly reduced T_g exist in ultrathin LB films.

In the present work we describe an experimental study of the glass transition in

ultrathin spin cast films of poly (tert-butyl methacrylate) (PtBMA) supported on Aluminium (Al) substrates. Ellipsometry was used to measure the thickness dependence of the T_g in PtBMA films with thickness values in the range 6-415 nm. Experiments were performed on uncapped PtBMA films, as well as films that were capped with thermally evaporated Al layers and Al capped films that were manufactured using the previously developed $2(h/2)$ sample preparation procedure [5]. We show that uncapped and evaporatively capped PtBMA films display T_g depressions of ~ 28 K relative to the bulk polymer for films as thin as 6 nm. However, Al capped films that were prepared using the $2(h/2)$ technique display bulk like T_g's for all the thickness values studied. These experiments confirm that evaporating metal capping layers on to thin PtBMA films does not necessarily remove the effects of the free surface. They also show that it is possible to remove the memory of the free surface using the $2(h/2)$ sample preparation procedure and that preparing the samples in this way results in bulk-like properties in all measured quantities for films as thin as 6 nm. This study provides strong evidence that free polymer surfaces play a significant role in determining the physical properties of nanoscale polymer samples.

4.2 Sample preparation

To demonstrate the effects of the free surface and the capping layers, samples were prepared using different methods. Five sets of PtBMA samples were prepared and measured in this study. All of these sample sets cover a wide range of PtBMA film thicknesses (6-415 nm).

For all samples sets, 1.2cm $\times$ 1.2cm single crystal silicon wafers were used as substrates. In the first sample set, these bare silicon wafers were used as supplied and PtBMA films were spin-coated on the top of the bare silicon surface. In the remaining

sample sets, the Si wafers were coated with a 300nm thick 99.999% alumium (Al) layer before being spin-coated. The Al layers were thermally evaporated onto the silicon wafers. The evaporation rate was 5.0nm/s and the pressure used in the evaporation chamber was below 1×10^{-5} torr. A type T thermocouple, i.e. a thermocouple with copper anode and constantan cathode, was hung close to these silicon wafers during evaporating so that the temperature of the substrates during evaporation could be monitored. The highest temperature of the substrates during evaporation was 310K. The thickness of Al layer was monitored by a film thickness monitor (IL100, intellemetrics Inc.), which had been calibrated by an AFM beforehand. To calibrate the film thickness monitor, scratches were made across Al evaporated layers on silicon wafers, these were then imaged with an AFM to obtain the thickness values of the Al layers. and calibrate the monitor with these values. Fig. 4.1 is an AFM image of a scratch in Al layers and the cross section view of the scratch..

For all sample sets, polymer films were formed by spin coating PtBMA (syn., $M_w =$ 275KDa, $M_w/M_n = 1.30$, Polymer Source Inc.) solutions in toluene with a spin speed of 3000 RPM. Spin-cast films were then routinely checked under an optical microscope and AFM to make sure they were dust free, flawless and uniform. Fig.4.2 shows a microscope image and two AFM images of a good spincast film. The uniform color in the optical microscope image (which varies for films of different thicknesses) indicates the uniform thickness throughout the film. AFM and optical microscopy were used to make sure that the film was flat (rms roughness < 0.5nm), flawless, and that no dewetting (the rupture of a thin film and the formation of droplets) occurs. Thin spincast polymer films (< 40nm) were found to dewet at high temperatures when being annealed in air. Fig. 4.3 shows an AFM image of a dewetted film, which couldn't be used in the experiment. A de-wetted sample can be recognized by eyes because it looks cloudy.

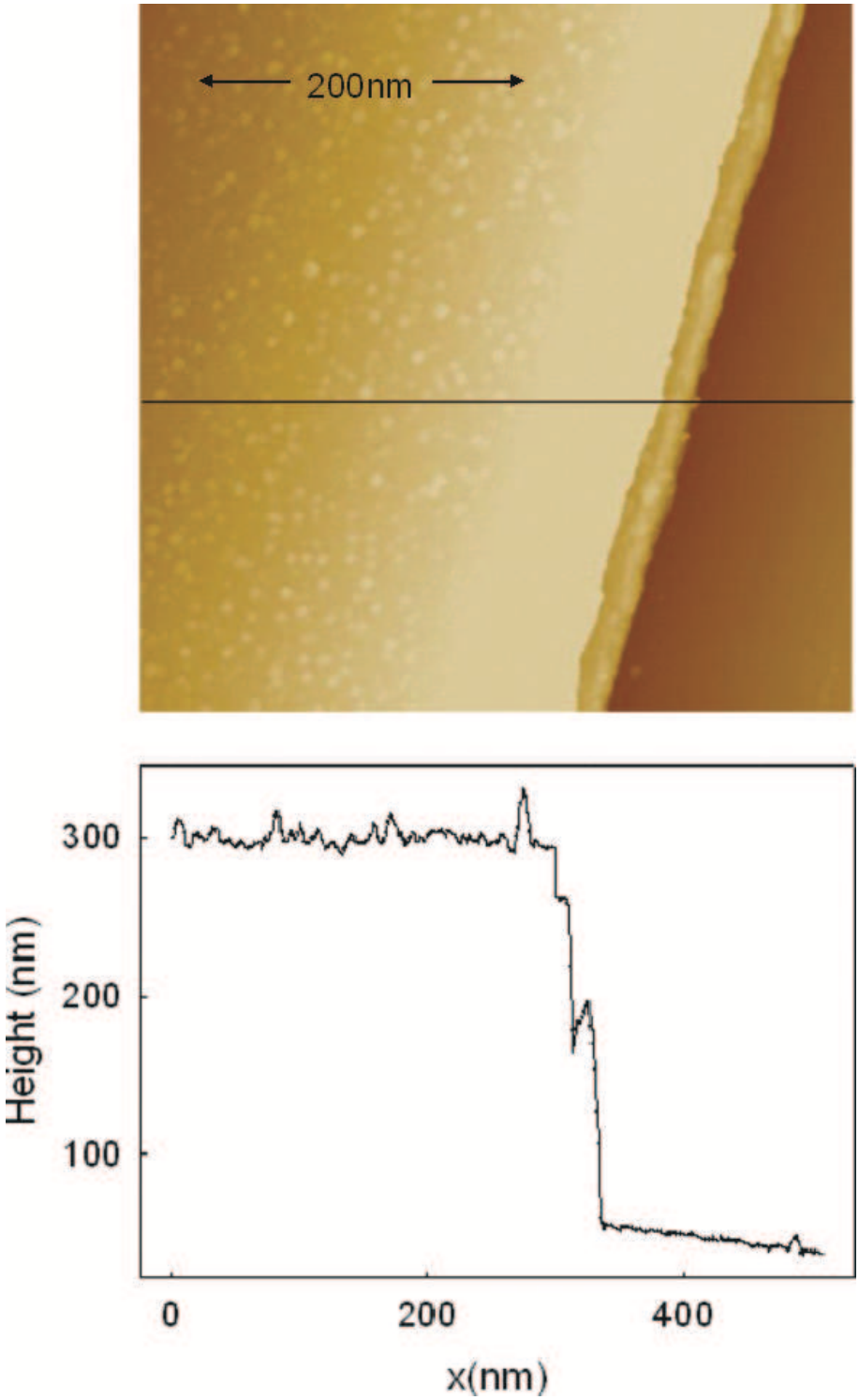

Figure 4.1: *The upper figure is an AFM image of a scratch across an Al layer on a silicon wafer. The lower figure is the cross section view of the scratch at the position of the black line which is drawn in the upper figure.*

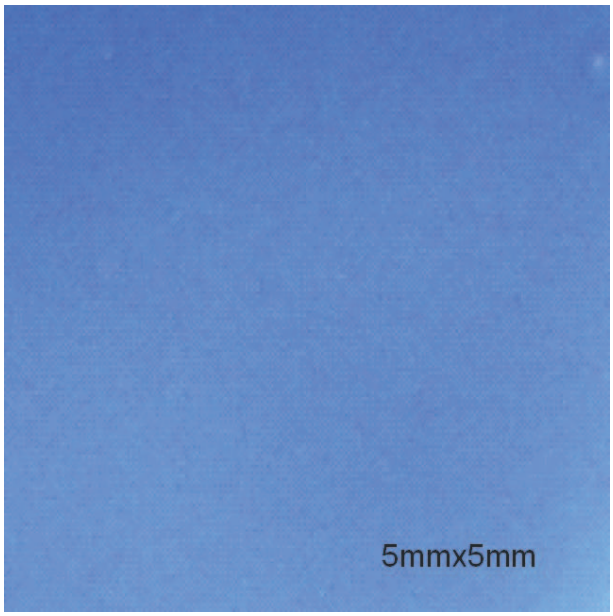

(a) Optical microscope image

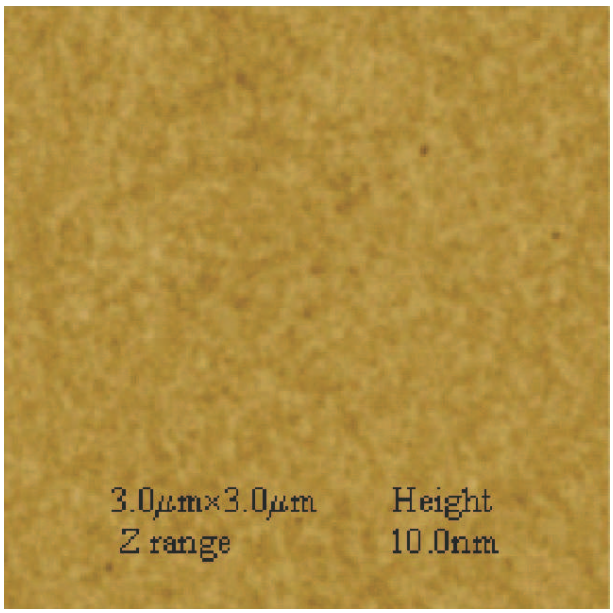

(b) AFM height image

Figure 4.2: *Images of a flawless, uniform and non-dewetted spincast PtBMA film. The top panel shows an optical microscopic image of the film showing large-scale (5mm×5mm) properties. The bottom panel shows an AFM image of a small-scale* ($3\mu\text{m} \times 3\mu\text{m}$) *properties.*

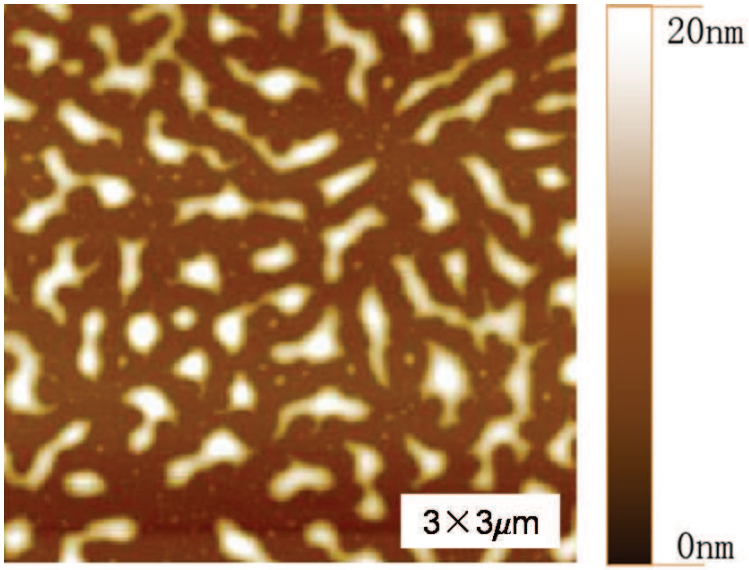

Figure 4.3: *An AFM image of a dewetted PtBMA film.*

The thickness of the spin cast polymer films was controlled by varying the concentration of the polymer solutions. The film thickness was determined by both ellipsometry and AFM. To determine film thickness using ellipsometry, the measured P and A values (the angles of the polarizer and the analyzer referring to the incident plane when the reflected laser is extinguished) are fitted to the theoretical curves to obtain the film thickness. The blue line in Fig.4.4 is the theoretical curve where P is plotted against A. It is shown that as the film thickness increases, the theoretical curve in Fig.4.4 evolves counterclockwise and finally becomes a repeating loop. For each pair of P and A values measured from the experiments, there are more than one points on the theoretical loop that fit it best. The film thickness can be determined only when we know the thickness range of the film. That's one of the reasons why AFM is used as a complementary technology in determining the film thickness. To determine the film thickness with AFM, the film surfaces were scratched with a sharp knife, and the cross section view of the AFM images of those scratches will tell a precise film

thickness. It was shown that larger concentration produces thicker films. Table 4.1 gives thickness-concentration pairs for PtBMA spin-cast films measured by ellipsometry, and the error bars are all ±1nm.

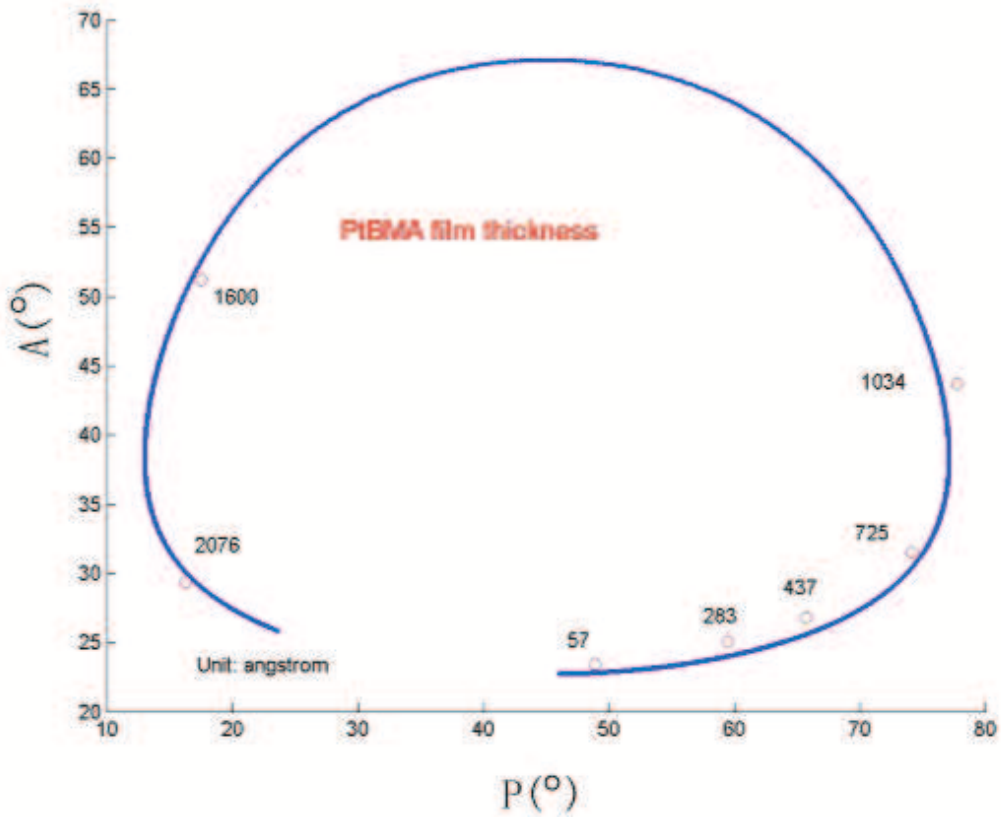

Figure 4.4: *P and A loop as a result of growing PtBMA film thickness*

The first set of samples are spincast PtBMA films on bare silicon wafers, and the second set of samples are spincast PtBMA films on bare Al substrates. The Al substrates were produced by evaporating a 300nm Al layer on top of silicon wafers as described above. Both sample sets were then annealed in vacuum at 413 K (Bulk T_g 384 ± 1K) for 10 hours to remove the solvent residue and any stresses introduced into

the films during the spin coating procedure.

The third and fourth sample sets consist of PtBMA films sandwiched between two Al layers and supported by silicon wafers, as illustrated in Fig. 4.5. The preparation procedure of the third set of samples is to prepare one more the second sample set, and then thermally evaporate 5 nm thick Al layers on the top surfaces (using the same deposition parameters described above). The fourth set of samples was prepared in a similar way except that the order of annealing and evaporation of the top Al layer were reversed. These two sets of samples were prepared to determine whether changing the sample preparation procedure has any effect on the film properties. The 5nm Al capping layer on top is expected to provide a solid boundary to remove the effect of the free surface. It is semi-transparent which will allow a laser to penetrate inside the polymer films so that these samples can be used in ellipsometry measurements. As described above, during the evaporation of the Al capping layers, a thermocouple was placed close to the samples and the temperature was monitored during evaporation. It was found that the temperature of the samples did not exceed 310 K, which is well below the bulk T_g of PtBMA ($\sim 383K$)) during evaporation. Therefore it's reasonable to believe the PtBMA films are not damaged in the evaporation. The 5nm thick Al layers are stable as is proved by both microscopy and AFM.

The fifth set of samples, named $2(h/2)$ samples, are designed to remove the effect

Table 4.1: Concentrations of the PtBMA solutions in Toluene and the corresponding spincast film thicknesses

Concentration of the PtBMA solutions (W%)	0.25	0.5	1.0	1.5	2.0	3.0	4.0
Film thickness (nm) ±1nm	6	28	44	73	103	160	207

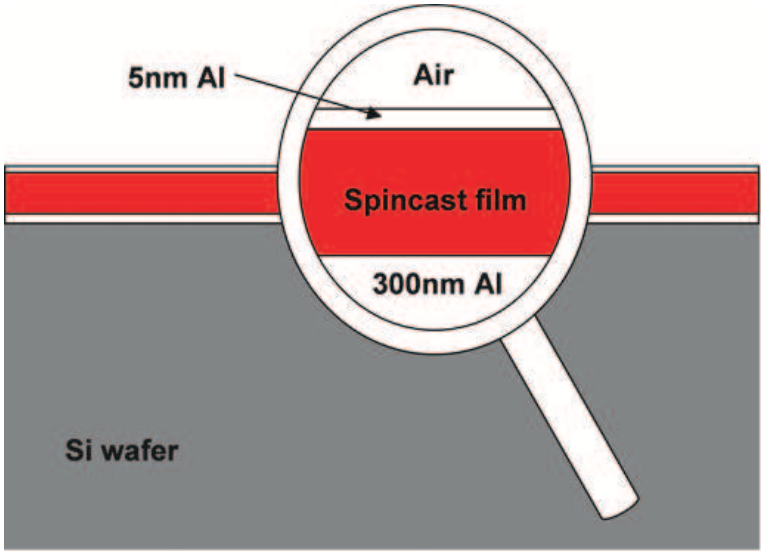

Figure 4.5: *PtBMA spincast film sandwiched between two Al layers*

of the free surface using Al capping layer with a procedure different from thermal evaporation. Previous efforts at trying to remove the effect of the free surface by covering the film surface with a solid layer usually use evaporated Al layers, which may not contact the film surface well (as discussed in chapter 2). It has been shown [6] that in the $2(h/2)$ samples the free surface effect can be successfully removed. The preparation procedure of a $2(h/2)$ sample is illustrated in Fig. 4.6. 5nm Al capping layers were thermally evaporated on top of NaCl windows, and the deposition conditions are exactly the same as described previously. PtBMA solutions were then spin coated onto the surfaces of these 5nm Al layers, and also onto Al coated silicon substrates that were prepared using a procedure similar to that described at the beginning of this section. Two samples of the same PtBMA film thickness supported on salt window and silicon wafer were then put face to face together, and a drop of deionised water (Milli-Q) was placed at the edge of the interface. The water was found to wet the NaCl/Al interface and to cause the PtBMA films and the thin Al layers to be detached from the NaCl window. The two PtBMA films were then pulled into intimate contact by surface forces. At this stage two PtBMA films of thickness

$h/2$ form a single uniform film of thickness h. These samples were then rinsed in deionised water to remove any residual NaCl and annealed in vacuum at 413 K for 10 hours.

Prior to the formation of the thinnest (6 nm thick) $2(h/2)$ composite films, an Asylum Research MFP 3D atomic force microscope was used to image the surface of the two separate (3nm thick) films that were used to manufacture the samples. This was done to ensure that films of this thickness did not dewet and break up to form droplets during spin coating. These images revealed the surface of the 3nm thick film to be uniform with a peak to peak roughness of less than 1 nm. This confirms that the films formed by spin coating PtBMA on to Al substrates were stable and did not break up prior to formation of the composite $2(h/2)$ samples.

4.3 Measurement of T_g in thin PtBMA films

A Linkam THMS600 Hot stage was mounted on the sample stage of the ellipsometer. Samples were held on the top surface of the heater in the hot stage using a clip, and were kept in good thermal contact with the heater throughout the experiment. A type T thermocouple (copper-constantan) was glued on a small Si wafer (using OMEGABOND 200 resin from OMEGA corporation) of similar size to these used as sample substrates, and placed close to the sample to ensure the temperature of the sample surface and the temperature measured by the thermocouple are similar. Nitrogen gas was purged through the sample chamber in the hot stage, so that during measurement the samples wouldn't be disturbed by water or oxygen.

In the T_g measurements, each sample was heated up to 413K (30K above the bulk T_g) and kept at this temperature for 20 minutes to erase any thermal history. The

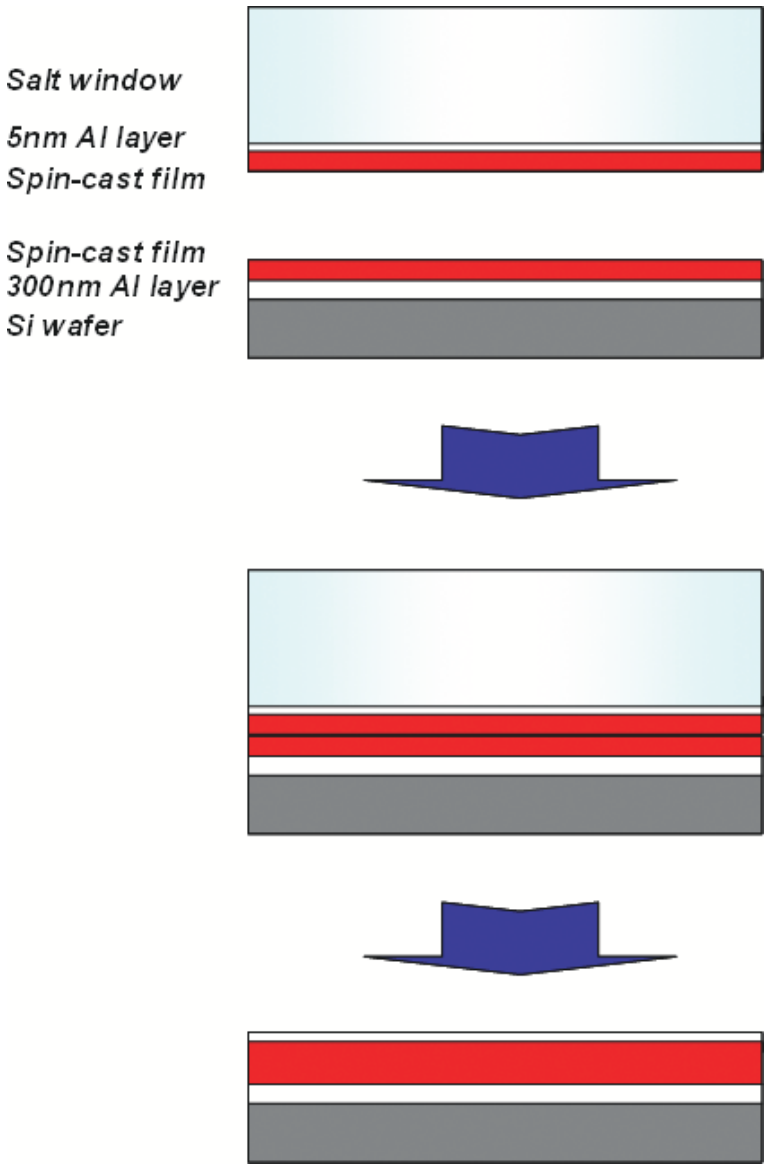

Figure 4.6: *The procedure to prepare 2(h/2) samples. Two spincast PtBMA films of the same thickness are supported on a salt window and a silicon wafer. Prior to the spin coating, a 5nm Al layer was evaporated onto the salt window and a 300nm Al layer was evaporated onto the silicon wafer. These two samples were then put face to face together, and a drop of deionised water was used to remove the NaCl window. The two PtBMA films were then pulled into intimate contact by surface forces. At this stage two PtBMA films of thickness $h/2$ form a single uniform film of thickness h.*

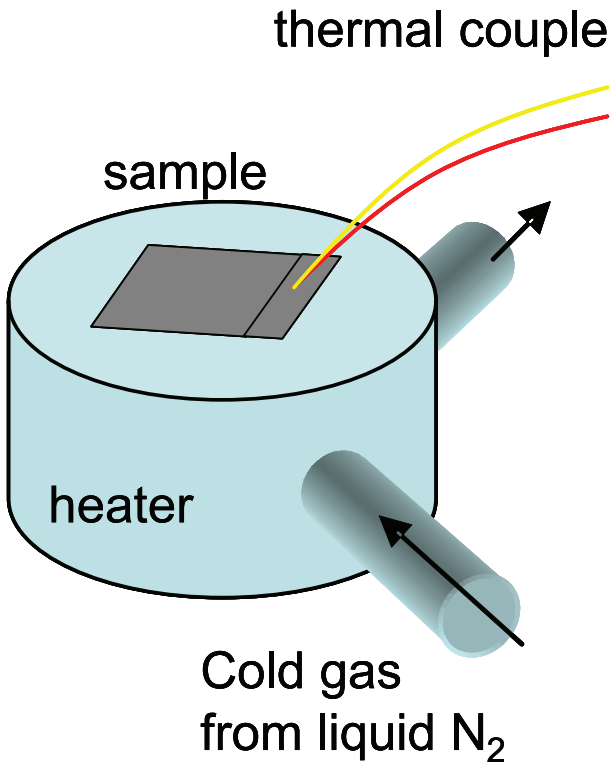

Figure 4.7: *A sample and a thermocouple are mounted on the heater*

samples were then cooled down slowly at a rate of 10K/min, and during the cooling process the angles of the two polarizers (P and A) on the ellipsometer were varied to obtain a null signal. P and A were values obtained at null recorded every 10 seconds (every 1.67K). Some other studies measured T_g by heating polymers up from glass state to melt state, but performing these measurements on cooling (as described above) eliminates the effect of thermal history and ensures that the samples are initially in equilibrium.

4.4 Results and discussion

The changes in film thickness and refractive index that are measured by the ellipsometer during the thermal contraction of thin PtBMA films are very small, so P and A values change linearly in both melt and glass states with response to changes in film thickness, and plotting P vs T or A vs T is just like plotting h vs T (or volume vs T). As illustrated in Fig. 4.8, the expansion coefficient α of a PtBMA films has different values at glass and melt state. For each set of data the regions below 350K and above 390K are fitted with a linear function and the T_g of a given film is defined as the temperature where the two linear fits intersect. Fig. 4.8 shows the polarizer angle P as a function of temperature for 6 nm and 270nm thick PtBMA films that were sandwiched between 5nm evaporated Al capping layer and 300nm Al substrates. Both these samples had been annealed after evaporation of the Al capping layers. Fig. 4.9 shows similar data for 6 nm and 270nm thick 2(h/2) samples. The 270nm thick PtBMA films with evaporated Al capping layer and the 270nm thick 2(h/2) PtBMA film, which are expected to show bulk-like behavior, and exhibit the same T_g value ($\sim 383 \pm 1$K), which is consistent with previous results [12, 13, 14, 15, 16]. The T_g of the 6nm PtBMA films with evaporated Al capping layer is $\sim$ 28$\pm$1K smaller than the bulk T_g, and this result agrees with Prucker et al.'s data [16]. This agreement is quite

encouraging because Prucker et al.'s study used a different measurement technique (Optical waveguide spectroscopy). The T_g of the 6nm thick 2(h/2) PtBMA film is equal to the bulk T_g, which suggest that the free surface effect in $2(h/2)$ samples has been successfully removed. These data also show the two 207nm thick samples have similar expansion coefficients in both liquid state and glassy state, but the two 6nm thick sample have the same expansion coefficients only in liquid state. The expansion coefficients of the 6nm thick PtBMA sample with evaporated Al capping layer is much smaller than that of the 6nm $2(h/2)$ PtBMA sample. These observations will be discussed in subsection 4.4.3 in detail.

Figure 4.10 shows the combined results of thin film glass transition studies performed on uncapped and capped PtBMA films. For all sample sets, the bulk T_g values (thick films) obtained from all 5 data sets are 383 ± 1K within the limit of experimental uncertainty. The uncapped films and the films evaporatively capped with 5nm Al layers display T_g reductions as large as 28±1 K for films as thin as 6 nm, and the T_g reductions occur in films thinner than $\sim$ 40-50 nm. The thickness dependence of T_g for all sample sets with reduced T_g in thinner films (<40nm) is the same within error.

4.4.1 Thickness dependence of T_g in uncapped and evaporatively capped PtBMA films

The uncapped PtBMA films on both Si and Al substrates displayed essentially the same thickness dependence of T_g (See inset, figure 4.10), which suggests that the effects of both Si and Al substrates on the films are similar. The $\sim$ 25K reduction

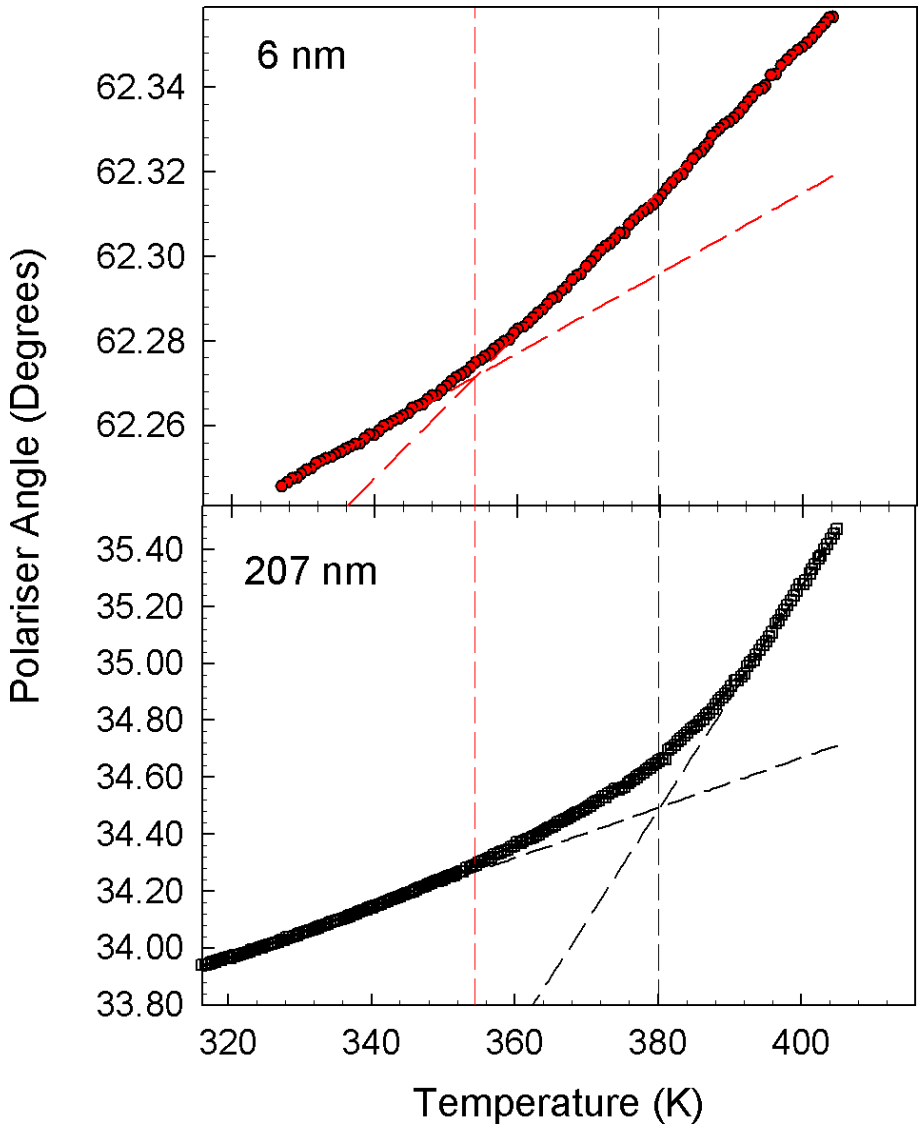

Figure 4.8: *The polariser angle (P) as a function of temperature for 6 nm thick (top panel) and 207 nm thick (bottom panel) PtBMA films that were annealed after being evaporatively coated with a 5 nm thick Al capping layer. The two dashed lines represent the fits to the melt and glass regions, and the vertical dashed lines mark the position of the* T_g

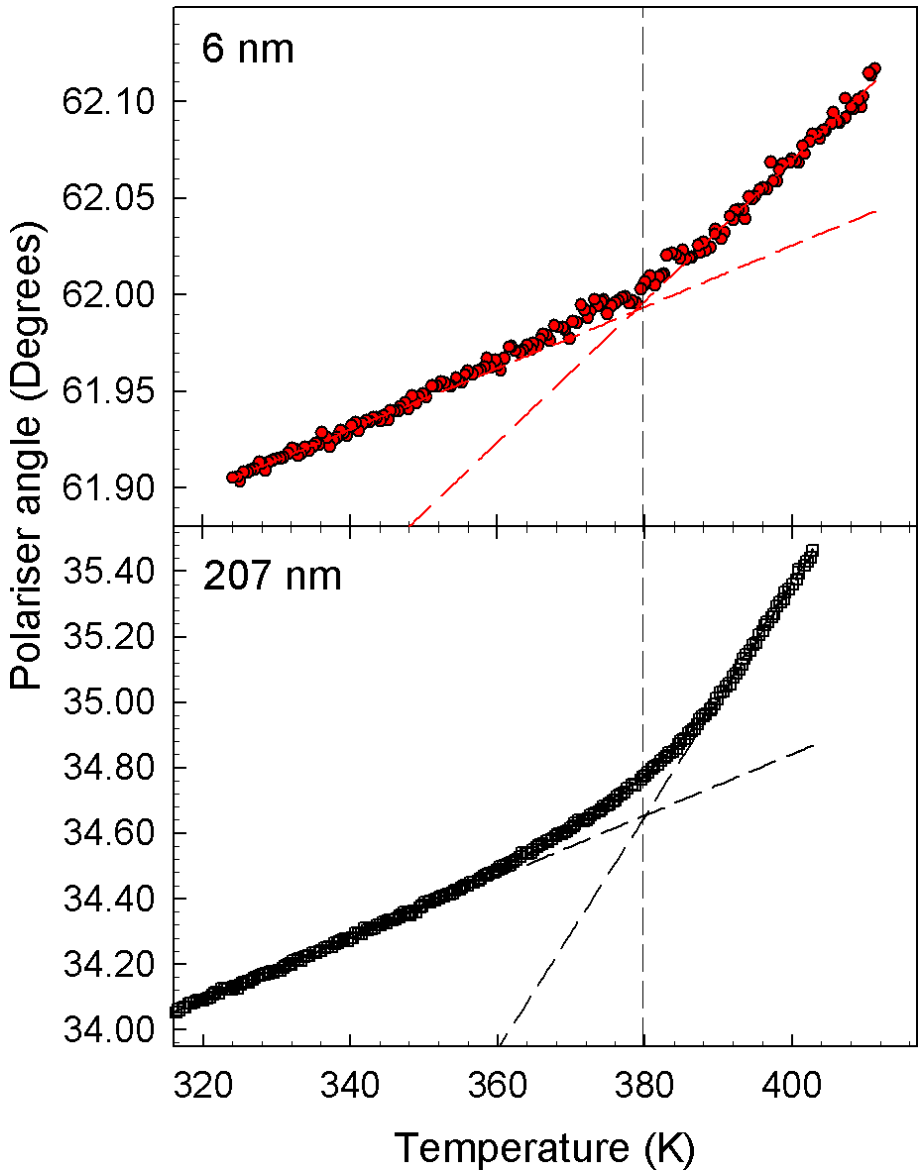

Figure 4.9: *The polariser angle (P) as a function of temperature for 6 nm thick (top panel) and 207 nm thick (bottom panel) 2(h/2) PtBMA films. The two dashed lines represent the fits to the melt and glass regions, and the vertical dashed lines mark the position of the* T_g

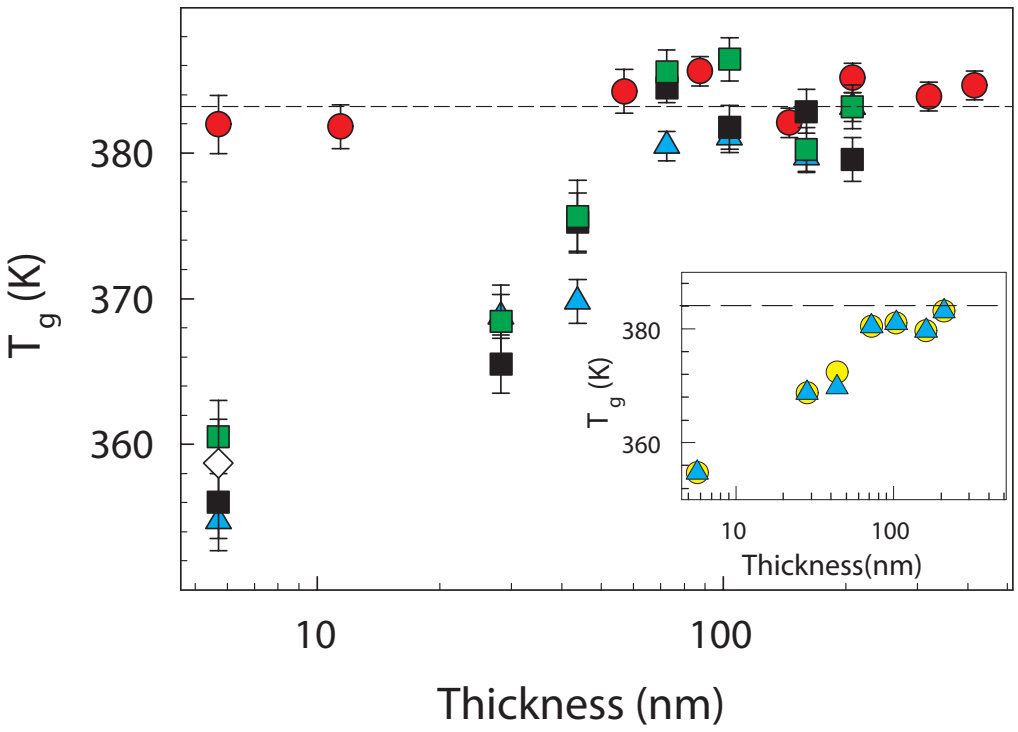

Figure 4.10: *Thickness dependence of the T_g for capped and uncapped PtBMA samples. Data are shown for uncapped films (blue △) and films capped with 5nm thick evaporated Al layers that had been annealed before (green □) and after (black ■) the evaporation. Data are also shown for $2(h/2)$ PtBMA samples (red ◯). Empty ◇ shows the data for the 6 nm thick $2(h/2)$ film after the removal of the capping layer with 0.1M NaOH. The inset shows the thickness dependence of T_g in uncapped PtBMA films on Al (blue △) and Si (yellow •) substrates.*

of T_g observed on 6nm uncapped PtBMA films is smaller than the ∼60 K shifts reported by See and coworkers [15] for silicon (Si) substrate supported PtBMA films of a similar thickness range and molecular weight. The reason for the discrepancy between our results and those of See et al.'s is not clear. One possible explanation could be related to the different substrates used in the two experiments. In the present work, we used Si wafers with the native oxide coating, while in the study be See and coworkers, the coating was removed prior to deposition of the films. The differences in the surface chemistry of the Si substrates used in the two studies could result in different polymer/substrate interactions and may explain the measured differences in the magnitude of the observed T_g reductions.

Both uncapped and evaporatively capped films display T_g reductions in thinner PtBMA films, and the thickness dependence of T_g in these two sets of samples are the same within limits of experimental uncertainty . This appears to contradict the idea that liquid like surface layers are responsible for the T_g reductions in thinner polymer films, because capping the films with a rigid metal layer is expected to suppress the enhanced mobility at the free surface and result in bulk like dynamics in even the thinnest PtBMA films. Dielectric relaxation studies [11] performed on polymer films sandwiched between metal electrodes have also observed the thickness dependence of T_g which was consistent with that reported for uncapped polymer films. This contradiction could be explained by some observations [5, 6, 17] which suggest that Al evaporated capping layer doesn't actually remove the effect of free surfaces. These studies showed that to evaporate metal layers using relatively reactive metals such as Al on to polymers will form a sharp interface between the metal layer and the polymer film, and using less reactive metals such as gold (Au) will produce a much broader interface. This explanation was confirmed by the measurements of the thickness dependence of the T_g on PS films with evaporated Al and Au capping layers,

which showed that the thickness dependence of the T_g was suppressed for the Au capped films but not for the Al capped films [5, 6]. These observations suggest that the structure of the interface between the polymer film and the metal layer has a significant effect upon the molecular dynamics in thin polymer films.

The data shown in Fig. 4.10 indicates that the T_g of thin PtBMA films capped with 5nm thick evaporated Al layer is not influenced by the order of annealing and evaporation. These results are consistent with those observed in studies of other polymers[18, 5].

4.4.2 Thickness dependence of T_g in 2(h/2) PtBMA films

To show that removing the effect of the free surface by capping layers is possible, we used an alternative method (the $2(h/2)$ sample preparation procedure) to cover the PtBMA films with a solid layer trying to manipulate the free surface properties of these samples. An advantage of this method of sample preparation is to ensure that the polymer- metal interface is sharp and that there are no metal atoms in the PtBMA films. Besides, it ensures that the top surface of the $2(h/2)$ samples has been in intimate contact with the capping layer during the spin coating, and putting free surfaces together enables interpenetration of polymer chains so that density defects can be annealed out. This should result in bulk-like polymer properties throughout the entire thickness of the samples [5]. The thickness dependence of the T_g for the $2(h/2)$ PtBMA films is shown in Fig. 4.10. The data in this figure shows that these samples display bulk-like T_g values for films as thin as 6 nm.

4.4.3 Thickness dependence of expansion coefficients in PtBMA films

Comparison of the ratio of the slopes, corresponding to the melt and glassy expansion coefficients (α_{melt} and α_{glass} respectively, obtained from the data shown in figures 4.8 and 4.9) also provides further evidence that the $2(h/2)$ PtBMA films display bulk-like properties. As illustrated in Fig. 4.11, the data shown for the evaporatively capped films and those obtained for uncapped PtBMA films have a ratio of the slopes for the 207nm thick films of $r = \alpha_{melt}/\alpha_{glass} = 3.9 \pm 0.4$, while that for the 6 nm thick films is $r = 1.8 \pm 0.6$. Previous studies have interpreted the reduction of this ratio with decreasing film thickness as being due to the presence of a liquid-like layer at the surface of the glassy polymer films [19]. The larger surface-to-volume ratio in thin films is expected to result in an increased contribution from the near surface region with enhanced dynamics. This is manifested as an increase in the effective glassy thermal expansion coefficient of the thin films and a corresponding reduction in the ratio, r. The ratio of the slopes for the $2(h/2)$ PtBMA films obtained from Fig. 4.11 give values of r =3.5 $\pm$ 0.4 for bulk-like films and r =2.7 $\pm$ 0.4 for the thin (6nm thick) film. These are similar within the limits of experimental uncertainty, indicating that the thinnest $2(h/2)$ films have bulk-like thermal expansion properties.

4.4.4 Removing the capping layer results in the restoration of a thickness dependent T_g in PtBMA films

Our next experiment gives further proof that the suppression of the thickness dependence of the T_g is due to the removal of the free surface, and not due to other aspects of the procedure used to prepare the $2(h/2)$ samples. The Al capping layer on the thinnest $2(h/2)$ sample was removed by immersing the $2(h/2)$ films in a 0.1M solution of NaOH for a few seconds, and then was rinsed in deionised water. The

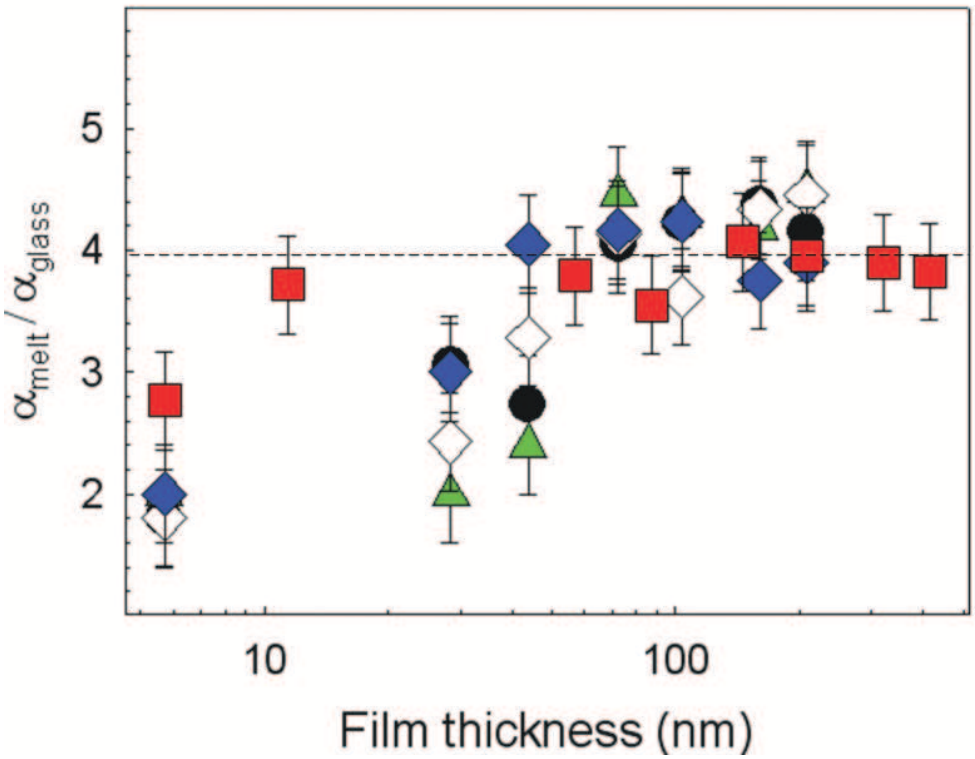

Figure 4.11: *Thickness dependence of the ratio between α_{melt} and α_{glass} for all the samples studied. Black • represents the data obtained from the uncapped PtBMA film supported on silicon wafers; green △ represents the data obtained from the uncapped PtBMA film supported on Al coated silicon wafers; white ◊ and blue ♦ represent the data obtained from the PtBMA films sandwiched between Al coated silicon wafers and evaporated Al capping layers, with the history of evaporating then annealing (white ◊) and annealing then evaporating (blue ♦); red □ represents the data obtained from the $2(h/2)$ samples. The dashed line represents the bulk value of $\alpha_{melt}/\alpha_{glass}$*

sample was then annealed at 413 K under vacuum (1×10^{-3} torr) for 10 hours, and then the T_g of this sample was measured using ellipsometry. Removing the capping layer and restoring the free surface in this way should result in the restoration of the free surface and the subsequent recovery of the thickness-dependent Tg that is observed in uncapped PtBMA films. The T_g value obtained is shown as the diamonds in Fig. 4.10, and it is found to be comparable to that of an uncapped PtBMA film of the same thickness. Hence restoring the free surface results in the recovery of the thickness dependent T_g in ultrathin PtBMA films.

To make sure that the chemical treatment used to remove the capping layer was not responsible for changing the properties of the thin polymer film. A 6 nm thick uncapped PtBMA film on Al substrate was immersed in 0.1M NaOH for the same period of time as that for the 6 nm thick $2(h/2)$ sample described above. This sample was then rinsed in deionised water, annealed under the same conditions and its T_g measured using ellipsometry. The T_g obtained from this sample (shown as the ∇ in Fig. 4.12) is identical to that obtained from an uncapped PtBMA films of the same thickness. Another 6 nm thick film was also treated in a similar way except that it had been immersed in saturated NaCl solutions, and it also displayed a T_g value ($\circ$) similar to the untreated film of the same thickness. Hereby it's reasonable to say that the chemicals used to prepare $2(h/2)$ samples and to remove the capping layers in the $2(h/2)$ samples don't change the properties of the polymer films. This indicates that any changes in the thickness dependence of the T_g of the PtBMA films must be due to the manipulation of the free surfaces.

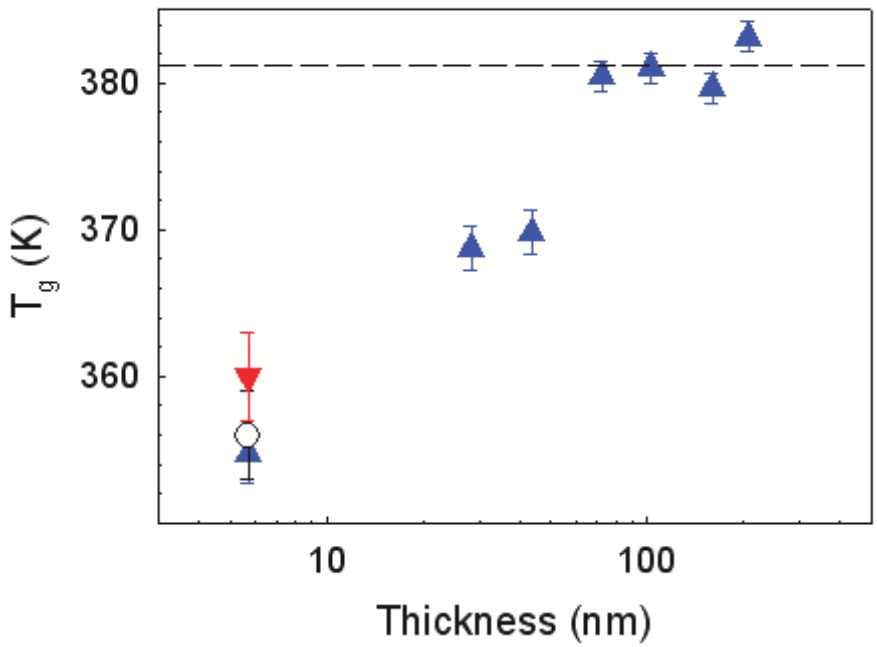

Figure 4.12: *Thickness dependence of the T_g for the uncapped PtBMA films supported by Al coated substrates (blue $\triangle$). Red ∇ represents a 6 nm PtBMA film supported by a Al coated substrate which was immersed in 0.1M NaOH, and $\circ$ represents a 6nm PtBMA film supported by a Al coated substrate which was immersed in saturated NaCl solution. The dashed line represents the bulk T_g value of the PtBMA films*

4.4.5 The width of the glass transition in ultra-thin PtBMA films

The width of the glass transition in thin polymer films can also be determined by extracting the temperatures T_+ and T_- at which the linear fits to the melt and glassy slopes deviate from the P vs T data respectively. Fig. 4.13 shows the thickness dependence of T_+ and T_- for the PtBMA films on Al substrates. This figure shows that in all of the PtBMA films studied the value of T_+ remains constant over much of the film thickness range studied. There is some evidence that the value of T_+ starts to decrease for the thinnest films studied, however, this is difficult to determine within the limits of experimental scatter and uncertainty. The values of T_- shown for the uncapped and evaporatively capped PtBMA films in Fig. 4.13 have a stronger film thickness dependence than the values of T_+. The reductions in T_- with decreasing film thickness indicate that the glass transition in these samples experiences a broadening to lower temperatures as the film thickness is decreased. These results are consistent with previous reports of the thickness dependence of the width of the transition in other polymers [19]. The T_- values obtained for the $2(h/2)$ PtBMA films remain constant over much of the range of film thickness values studied with some possible evidence of a slight increase in T_- for the thinnest films studied. This analysis reveals that the width of the transition in the thinnest $2(h/2)$ films is the same as that in the thickest (bulk-like) polymer films studied. This provides further evidence for the bulk-like nature of the thinnest $2(h/2)$ PtBMA samples.

4.5 Conclusion

The experiments described above show that uncapped PtBMA films and PtBMA films with evaporated Al capping layers displayed T_g reductions in thinner films. The

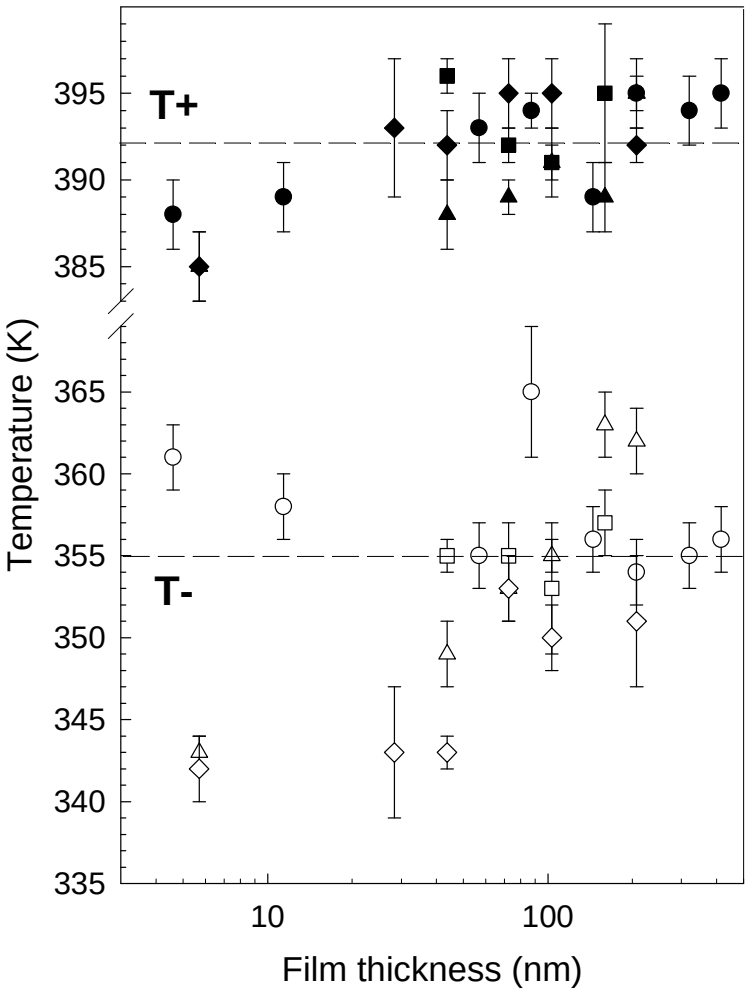

Figure 4.13: *Thickness dependence of T_+ and T_- in PtBMA films. Data are shown for uncapped PtBMA films ($\triangle$) and films capped with evaporated Al layers that have been annealed before ($\diamond$) and after ($\bigcirc$) capping. Data are also shown for $2(h/2)$ films ($\bigcirc$). The solid symbols mark the position of T_+ and the hollow symbols mark the position of T_-.*

smallest thickness values to display bulk T_g is of $\sim$ 40-50 nm and the largest T_g reduction found is 28 $\pm$ 1 K for a 6 nm thick film. The $2(h/2)$ samples whose upper polymer-Al interfaces were formed by spin-coating rather than evaporation showed no T_g reduction and displayed bulk-like physical properties in all measured quantities for films as thin as 6 nm. Removal of the Al capping layers in $2(h/2)$ samples was shown to result in the recovery of thickness dependence of the T_g in these samples. Samples that were prepared by placing two substrate supported films with their free surfaces in contact showed no T_g reductions for films as thin as 6 nm. This indicates that the $2(h/2)$ sample preparation procedure that was used to prepare these films is capable of removing the effects of the free surface, resulting in bulk-like physical properties in nanoscale polymer samples. These results suggest that great care has to be taken when interpreting the results obtained from evaporatively capped polymer films.

Bibliography

[1] H. Yang and J. S. Sharp. *Macromolecules*, **41**:4811, 2008.

[2] C. J. Ellison and J. M. Torkelson. *Nature Materials*, **2(10)**:695, 2003.

[3] J. R. Dalno. *Phys. Rev. E*, **59(2)**:2153, 1999.

[4] K. Dalnoki-Veress, J. A. Forrest, C. Murray, C. Gigault, and J. R. Dutcher. *Phys. Rev. E*, **63**:031801, 2001.

[5] J. S. Sharp and J. A. Forrest. *Phys. Rev. Lett.*, **91**:235701, 2003.

[6] J. H. Teichroeb J. S. Sharp and J. A. Forrest. *Eur. Phys. J. E*, **15**:473, 2004.

[7] J. H. Teichroeb and J.A. Forrest. *Phys. Rev. Lett.*, **91**:016104, 2003.

[8] Z. Fakhraai and J. A. Forrest. *Science*, **319**:600, 2008.

[9] S. Ge, Y. Pu, W. Zhang, M. Rafailovich, J. Sokolov, C. Buenviaje, R. Buckmaster, and R.M. Overney. *Phys. Rev. Lett*, **85**:2340, 2000.

[10] J. A. Forrest, K. Dalnoki-Veress, and J. R. Dutcher. *Phys. Rev. E*, **56**:5705, 1997.

[11] K. Fukao, S. Uno, Y. Miyamoto, A. Hoshino, and H. Miyaji. *Phys. Rev. E*, **64**:051807, 2001.

[12] H. Hsiung, K. Beckerbauer, and J. M. Rodriguezparada. *Langmuir*, **9**:1971, 1993.

[13] M. Mabuchi, K. Kawano, S. Ito, and M. Yamamoto. *Macromolecules*, **31**:6077, 1998.

[14] M. Mabuchi, K. Kawano, S. Ito, M. Yamamoto, M. Takahashi, and T. Masuda. *Macromolecules*, **31**:6083, 1998.

[15] Y. K. See, J. Cha, T. Chang, and M. Ree. *Langmuir*, **16**:2351, 2000.

[16] O. Prucker, S. Christian, H. Bock, J. Rühe, C. W. Frank, and W. Knoll. *Macromol. Chem. Phys.*, **199**:1435, 1998.

[17] F. Faupel, R. Willecke, and A. Thran. *Mater. Sci. Eng. Rep.*, **22**:1, 1998.

[18] J. A. Forrest and K. Dalnoki-Veress. *Adv. Coll. Int. Sci.*, **94**:167, 2001.

[19] S. Kawana and R. A. L. Jones. *Phys. Rev. E*, **63**:021501, 2001.

Chapter 5

Frequency Dependence of the Dynamics in Ultra-thin PVAc Films

5.1 Introduction

As discussed in Chapter 2, Keddie et al's study [1] on ultra-thin (<100nm) polystyrene films triggered the interest of researchers and numerous efforts were put on the study on the molecular dynamics in ultrathin polymer films. These studies have come to an agreement that ultra-thin polymer films exhibit thickness dependence of molecular dynamics as a result of interfacial effects (polymer-air interface or polymer-substrate interface) or molecular confinement. However, a number of controversial reports have been made relating to discrepancies found between the dilatometric techniques that are often used to measure the T_g of thin film polymer samples and other probes of the dynamics such as nanocalorimetry [2, 3] and dielectric studies [4]. One example of this is the observation of $\sim$ 10 K reductions in the T_g of isotactic-PMMA for films thinner than $40nm$ (when measured at cooling rates of 1 Kmin^{-1} using ellipsometry) and no apparent film thickness dependence in the position of the temperature dependent alpha relaxation for similar samples measured at frequencies of 1 KHz using dielectric techniques [4]. Similarly, no T_g reductions have been observed in ultrafast

and AC calorimetry studies of thin polymer films measured at frequencies of $\sim$ 10 Hz and above [2, 3]. Aside from differences in the polymer/substrate interactions (which have largely been accounted for in these studies), a key difference between the dilatometric studies of thin polymer films and these other techniques that is often overlooked, lies in the range of frequencies that are used to probe the material properties of the samples. Dilatometric measurements of the T_g of thin film polymer samples are usually performed at cooling rates of $\sim 0.1 - 100$ Kmin^{-1}. As will be shown in this chapter these correspond to effective measurement frequencies of less than 0.01 Hz. However, comparisons between dilatometric and other techniques mentioned above are often performed at measurement frequencies greater than 1 Hz [2, 3, 4]. The fact that complementary techniques such as these can be used to probe dynamics in thin polymer film samples and give strikingly different results is worrying. This either points to a severe lack in our understanding of the dynamic processes that occur in these samples, or it suggests that interfacial and confinement effects in thin film polymer samples have an intrinsic frequency dependence. This issue was raised recently by Fakhraai et al [5], who used ellipsometry to show that the thickness dependence of the T_g in thin polystyrene films has an intrinsic cooling rate dependence. However, to resolve the issues related to the observed discrepancies between different measurement techniques, a comparative study of the role of measurement frequency still needs to be performed.

To determine whether the frequency of the measurement probe used is important in determining the measured thickness dependence of the T_g/T_α, a study of the frequency dependence of ultrathin film confinement effects was performed on thin films of poly(vinyl acetate) (PVAc). PVAc was used in these experiments because it has a low bulk T_g value ($\sim$ 313 K), so that the dielectric spectroscopy can work in low temperature ranges during the measurements, and the noise due to contamination of the spectra from ambient water vapor can be suppressed at low temperatures.

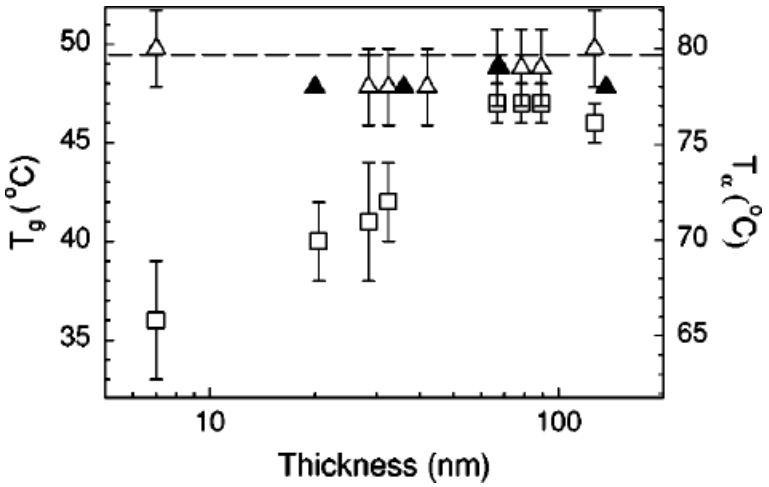

Figure 5.1: *Thickness dependence of T_g measured by ellipsometry and T_α measured by dielectric spectroscopy. The □ represents T_g measured by ellipsometry and △ and ▲ represent by dielectric spectroscopy measured at 1KHz, The plot is taken from reference [4], and the data ▲ is from reference [6]*

Polymers with even lower T_g values were not used because they are in liquid state at room temperature and can not form spincast films. PVAc was used also because it has large dipole moments and hence displays a large α dielectric relaxation peak. Direct comparisons are made between ellipsometry measurements of the thickness dependence of the T_g and broadband dielectric spectroscopy studies of the same samples. These studies reveal that the thickness dependence of the dynamics in ultra thin films of PVAc are frequency dependent and that comparisons between the data can only be made when the dielectric measurements are performed at frequencies of less than $10Hz$. To our knowledge, these are the first experiments where the results of low frequency dielectric studies have been compared directly to dilatometric measurements on thin film polymer samples. These experiments help to understand the role of measurement frequency in the observation of thin film effects in polymeric glass forming materials, and show that the frequency of the measurement probe being used must be taken into consideration when making comparisons between the results from different measurement techniques.

5.2 Sample preparation

The sample preparation procedure is shown in Fig. 5.2. Glass slides were cut into $1.3cm \times 1.3cm$ square pieces to serve as supporting substrates. These glass squares were then blown in N_2 gas to remove dust generated during the cutting procedure. They were cleaned with methanol in an ultrasonic bath for 20 minutes, then with acetone for another 20 minutes. This was done to degrease the glass slides and to remove any further contaminates.

200nm Al (Advent, U.K., 99.999%) electrodes were thermally evaporated onto these glass squares. The evaporation rate used was 5.0nm/s and the pressure inside the chamber was below 2×10^{-5} torr. A type T thermocouple was hung close to those glass substrates during evaporation so that the temperature could be monitored during the evaporation. The highest temperature measured during the evaporation was 310K. The thickness of the Al layers was measured using a film thickness monitor (IL100, Intellemetrics Inc.), which had been calibrated using an AFM beforehand (as described in chapter 4). A metal mask was used during the evaporation to make three 0.75mm wide stripe-like Al electrodes. A 10 mm diameter circle of Al was also evaporated on to the glass slides at a different position on the sample.

Thin films of poly(vinyl acetate) (PVAc, $M_w = 184.1$K, $M_w/M_n = 2.99$, Scientific Polymer Product Inc., U.S.) were spin coated from toluene on to these Al coated glass squares. The film thickness was controlled by varying the concentration of the polymer in solution. PVAc films with thicknesses in the range $9 - 486$ nm were prepared in this way. The samples were then annealed at 333 K (bulk $T_g(PVAc) \sim 312 \pm 2$ K, as determined using ellipsometry) under vacuum for 5 hours.

The samples were then removed from the oven and three further stripe-like Al electrodes were thermally evaporated on top of the PVAc films using the same evaporation condition given above. These top electrodes were perpendicular to the bottom ones, and the thickness of the top electrodes was also 200 nm. This resulted in the formation of nine individually addressable capacitors that could be used in broadband dielectric studies. A second 5 nm thick, 10 mm diameter Al circle was also evaporated on top of the PVAc films above the circle that was evaporated on the substrate. This capping layer is semitransparent and make ellipsometry measurements possible. The conditions used during the evaporation were the same as those described above. The final geometric configuration of the samples is illustrated in Fig. 5.2.

Thicknesses of the PVAc films was pre-determined both by ellipsometry and AFM, as discussed in chapter 4, and the results are shown in Table 5.1.

Table 5.1: Concentrations of the PVAc solutions in toluene and the corresponding spincast film thicknesses

Concentration of the PVAc solutions (W%)	0.5	1.0	2.0	3.0	4.0	8.0
Film thickness (nm) ($\pm$1 nm)	20	35	77	117	177	486

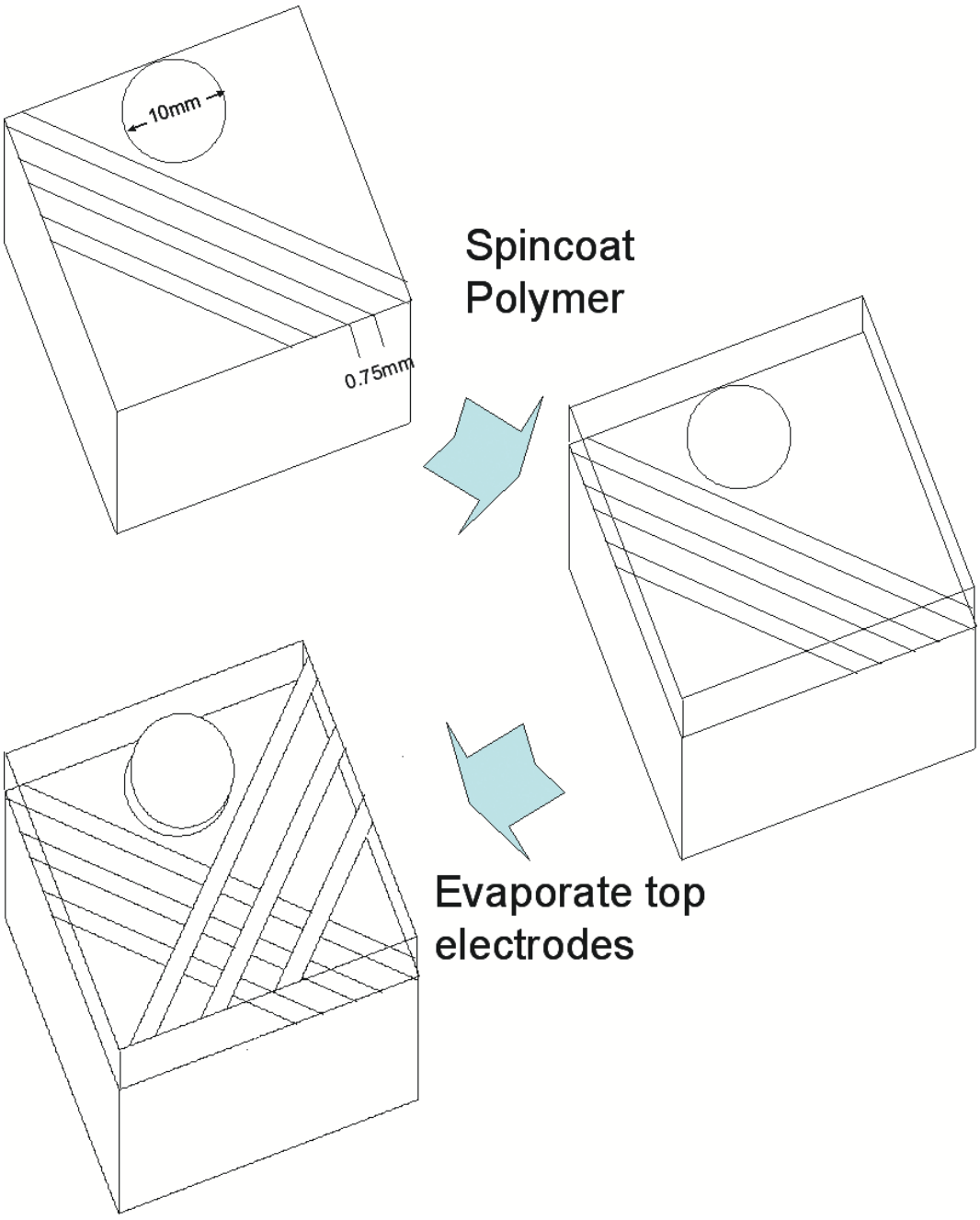

Figure 5.2: *The preparation procedure of a PVAC sample for both ellipsometry and dielectric measurements. Three 0.75mm wide 200nm thick stripe-like Al electrodes and a* 10 *mm diameter circle of Al (200nm thick) were evaporated onto the glass substrates. PVAC films were spin coated from toluene on to these Al coated glass squares. Three 0.75mm wide 200nm thick stripe-like Al electrodes and a* 10 *mm diameter circle of Al (5nm thick) were evaporated onto the spin cast films. The top electrodes were perpendicular to the bottom ones, and this resulted in the formation of nine individually addressable capacitors that could be used in broadband dielectric studies. The top Al circle was evaporated above the bottom one and the circular area is for ellipsometry measurements. The lower plot shows the cross section view of a sample.*

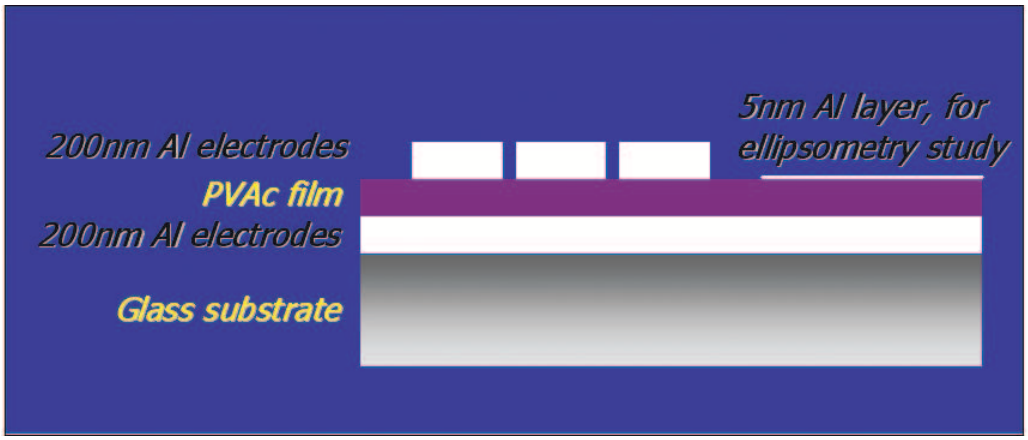

Figure 5.3: *The cross section view of a sample for both ellipsometry and dielectric measurements.*

5.3 Measurement of dielectric relaxation in ultra-thin PVAc films

After sample preparation, the PVAc film samples were transferred immediately to the sample chamber of a TA Instruments DEA 2970 dielectric analyser, where they were purged using dry nitrogen gas. These samples were then heated up from 300K at a constant heating rate of 0.5K/min, and during the heating process a sinusoidal voltage was applied and the current through the system was monitored. The heating rate is slow enough that for all the frequencies studied, there is enough time for more than one measurement cycles to be recorded and analyzed per 1K increase in temperature. The use of such a slow cooling rate ensures that the measurements are not convoluting with a changing sample temperature profile. After each measurement, the sample chamber was cooled down to 300K at a rate of 1K/min under the control of water circulation, and then the sample was heated and measured again at a new frequency. For all the films studied, dielectric measurements of the temperature dependent alpha relaxation were performed at frequencies of 0.01 Hz, 1 Hz, 10 Hz and 100 Hz over a range of temperatures between 300 K and 340 K (see Fig. 5.5).

After dielectric measurement the samples were taken out and transferred immediately to a Linkam Hotstage mounted on a home-built self nulling ellipsometer, where the samples were purged with dry nitrogen gas. The samples were then heated to a temperature of 348 K which is above the bulk T_g of the material, and were kept at this temperature for 10 mins to establish equilibrium. The samples were then cooled to $272K$ at rates of $9Kmin^{-1}$ and $90Kmin^{-1}$ and the angles P and A were recorded to monitor changes in the thickness of the samples.

Each ellipsometry measurement was repeated twice and the results were proved to be reproducible. Each dielectric spectroscopy measurement was also repeated once and the data also show high reproducibility. This is illustrated in Fig. 5.4. The measurements therefore don't result in large error bars for the measured T_g and T_α. Their error bars mainly come from the fitting procedures.

5.4 Results and discussion

Fig. 5.5 shows the temperature dependence of the dielectric loss factor ϵ'' in ultrathin PVAc films. Data are shown for the value of the dielectric loss factor (ϵ'') normalized by its peak value (ϵ''_{max}) for measurement frequencies of $0.01Hz$ ($\bullet$), $1Hz$ ($\triangle$), $10Hz$ ($\square$) and $100Hz$ ($\circ$). The data shown are for a $9nm$ (top panel) and $117nm$ thick sample (bottom panel) respectively. The vertical dashed lines mark the positions of the temperature dependent alpha relaxation, T_α.

Fig. 5.6 shows typical plots of the variation in the Polarizer angle, P, as a function of temperature. The T_g of the polymer was defined as the temperature at which the fits to the two linear regions (corresponding to the melt and glassy slopes) intersect, as described in chapter 4.

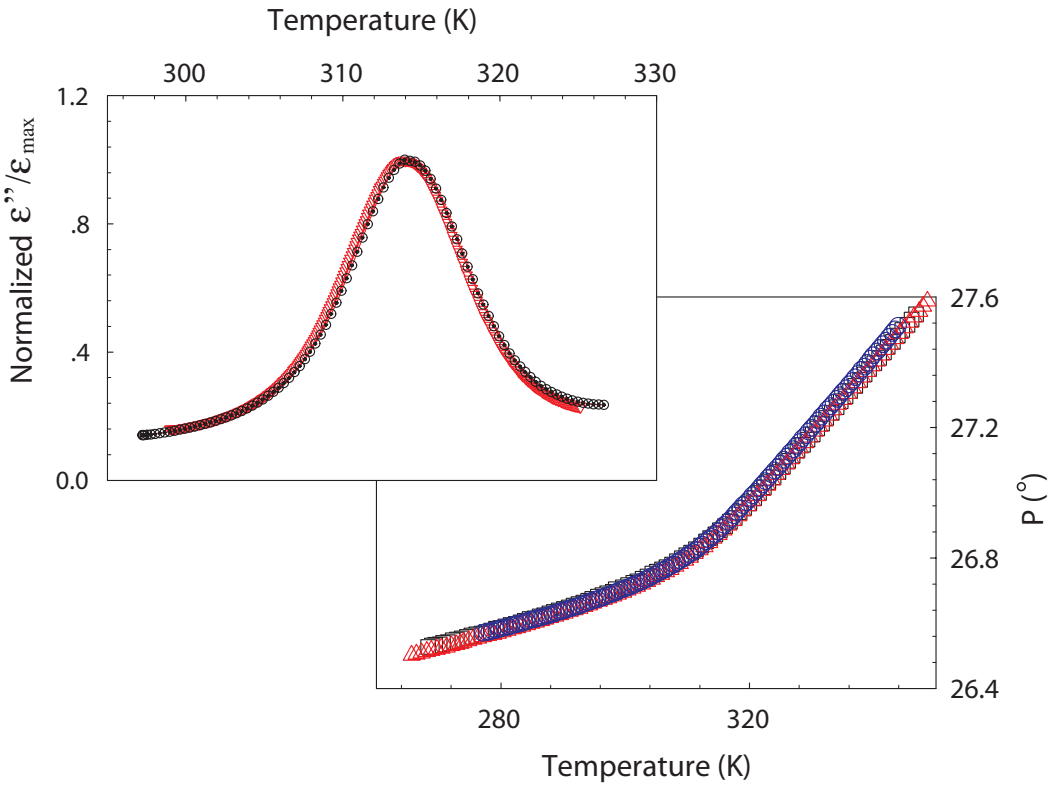

Figure 5.4: *The reproducibility of the raw data. The upper plot shows the two sets of dielectric spectroscopy data (symbolized by black ∘ and red ∇) measured on the 20nm PVAc film sample at the frequency of 9Hz. The lower plot shows the three sets of ellipsometry data (symbolized by black □ blue ∘ and red △) measured on the 117nm PVAc film sample at the cooling rate of 9K/min.*

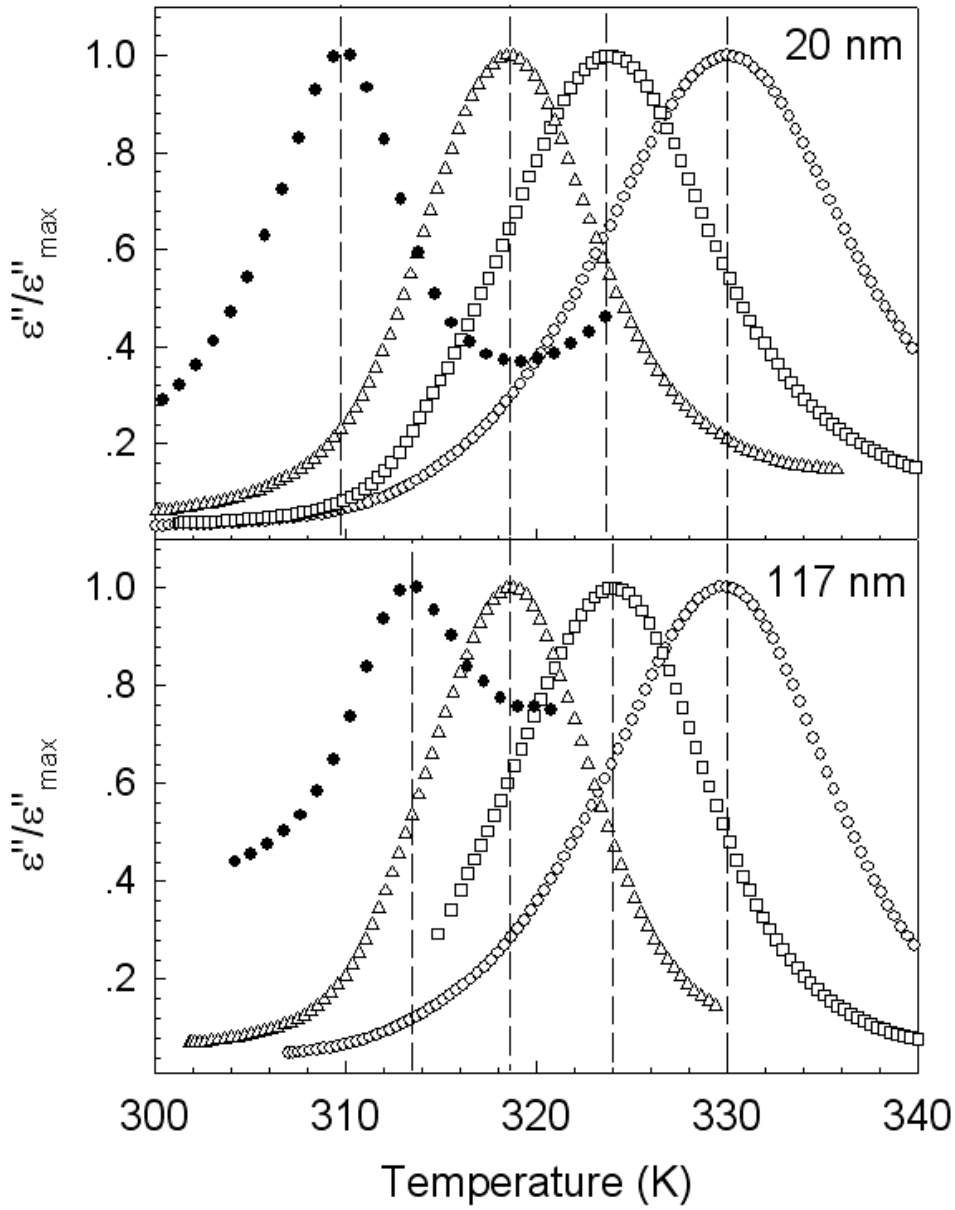

Figure 5.5: *Temperature dependence of the dielectric loss in ultrathin PVAc films. Data are shown for the value of the dielectric loss factor (ϵ'') normalized by its peak value (ϵ''_{max}), for measurement frequencies of* $0.01Hz$ (•), $1Hz$ (△), $10Hz$ (□) *and* $100Hz$ (○). *The data shown are for a* $9nm$ *(top panel) and* $117nm$ *thick sample (bottom panel) respectively. The vertical dashed lines mark the positions of the temperature dependent alpha relaxation,* T_α.

In the ellipsometry measurements each sample was measured at two different cooling rates, 90K/min and 9K/min. Fig. 5.7 shows the data obtained from a 117nm sample for the two cooling rates.

The thickness dependencies of T_g and T_α are shown in Fig. 5.8 for all the cooling rates and frequencies studied. As shown in the bottom panel of Fig. 5.8, the dilatometric T_g of the polymer is reduced for films thinner than $\sim$ 80 nm. This occurs for the cooling rate of 9Kmin^{-1}, not for the cooling rate of 90Kmin^{-1}. The inset in this plot shows the variation of the measured T_g of the bulk polymer as a function of cooling rate.

Comparison of the T_g shifts shown in the bottom panel of Fig. 5.8 with the T_α shifts shown in the top panel of the same figure reveal that the thickness dependence of the position of the alpha peak is consistent with the T_g shifts for frequencies less than $\sim$ 10Hz and cooling rates of 9Kmin^{-1}. However for frequencies of 10Hz and above the thickness dependence of the position of the alpha relaxation is suppressed over the range of film thickness values studied.

These results clearly show that consideration *must* be given to the measurement frequency used to probe the dynamic properties of ultra thin polymer samples. Previous studies have reported discrepancies between measurements that have been performed using different techniques that operate over different frequency ranges. This has resulted in a significant amount of recent controversy about the nature of the dynamics of polymeric materials in thin films. However, the simple experiments presented in the present study highlight the need to consider the role of the measurement/probe frequency and they indicate that great care must be taken to compare only low frequency ($<$ 10Hz) measurements of the dynamics with the T_g measurements that have

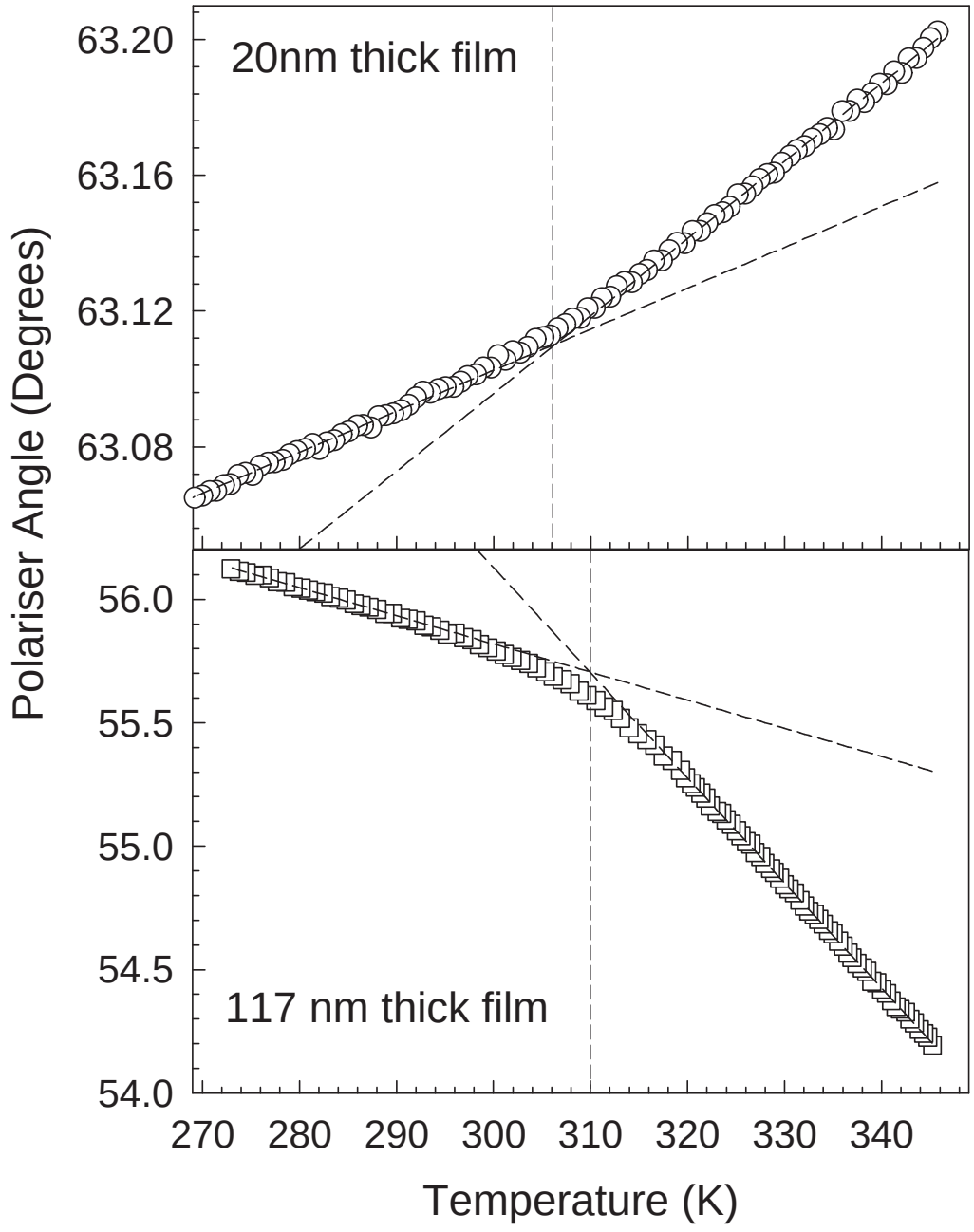

Figure 5.6: *Ellipsometry measurements of the T_g of thin PVAc films. Data are shown for the variation in the analyzer angle (A), as a function of temperature for 20 nm thick (top panel) and 117 nm thick (bottom panel) PVAc films. Both data sets were obtained using a cooling rate of $90Kmin^{-1}$. The dashed lines represent fits to the melt and glassy slopes of the curves respectively and the vertical dashed lines mark the position of the T_g for each film.*

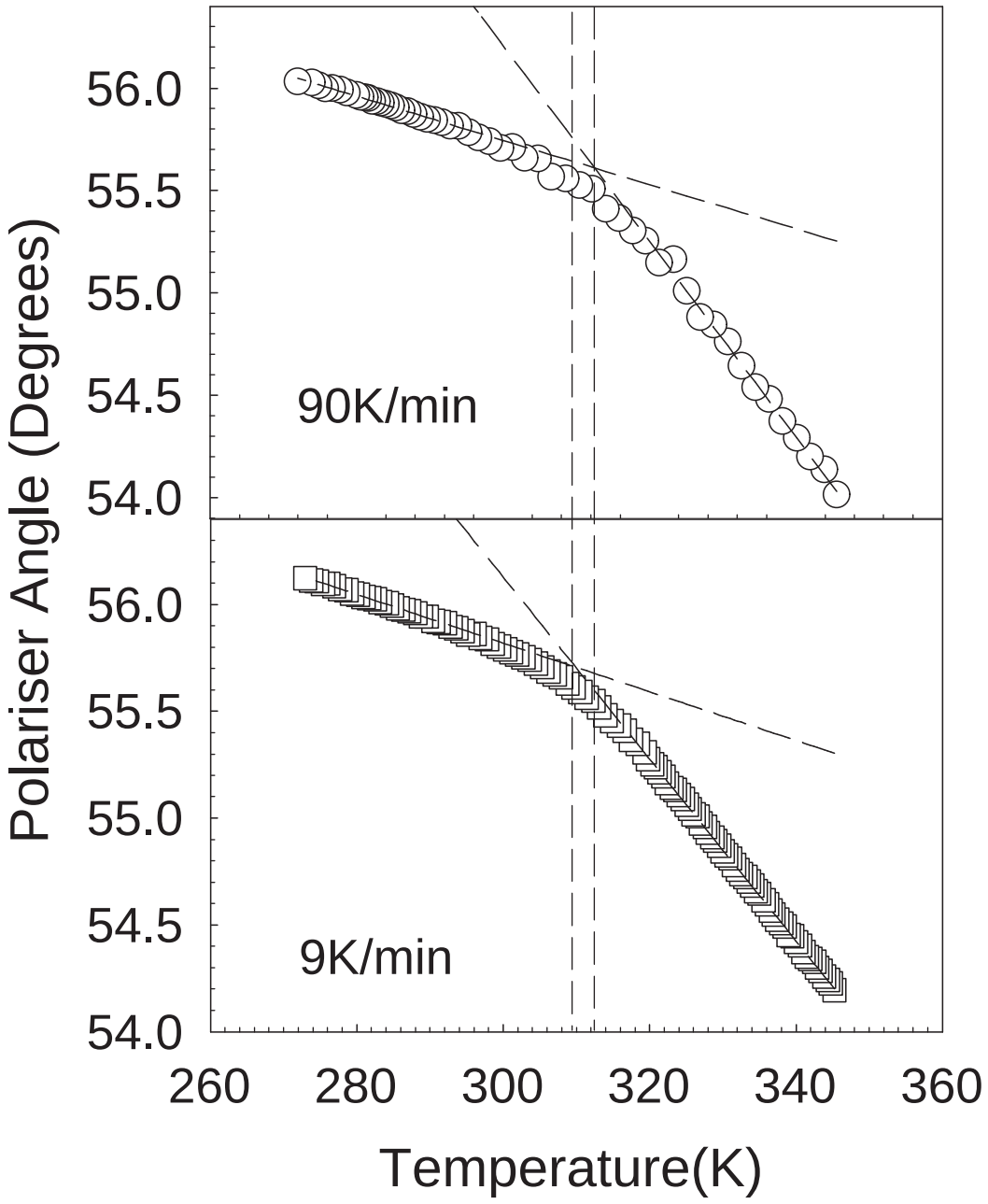

Figure 5.7: *The data of Ellipsometry measurement obtained from a 117nm PVAc film for cooling rates of 90K/min (•) and 9K/min (□). Data are shown for the variation in the polarizer angle (P), as a function of temperature. The vertical lines mark the position of the T_g for each cooling rate.*

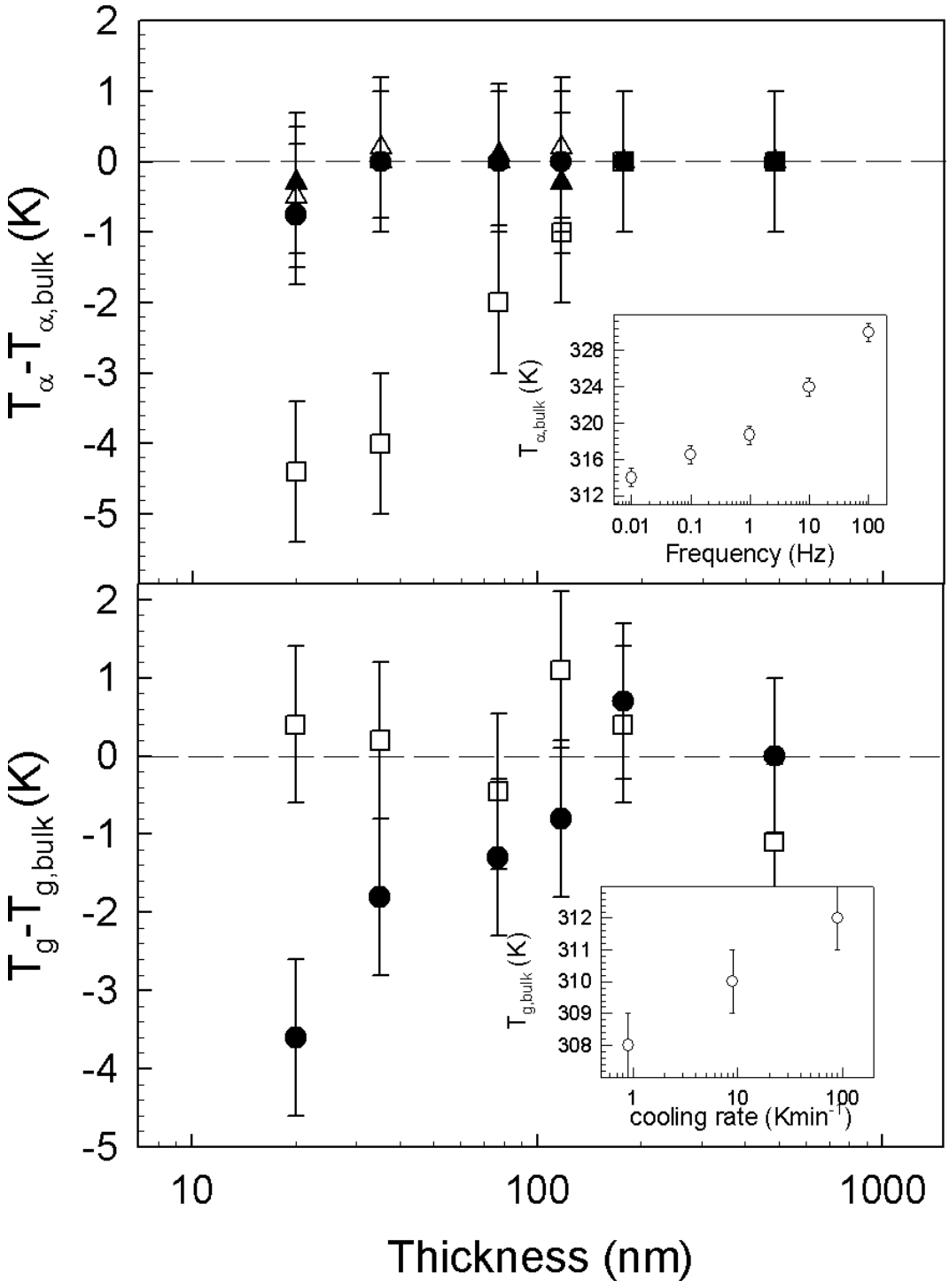

Figure 5.8: *Film thickness dependence of the shifts in T_g and T_α for PVAc. The top panel shows the thickness dependence of T_α determined at measurement frequencies of $0.01Hz$ (□), $1Hz$ (▲), $10Hz$ (•) and $100Hz$ (△). The bottom panel shows the variation in T_g with film thickness for cooling rates of $9Kmin^{-1}$ (•) and $90Kmin^{-1}$ (□). The insets show the variation of the bulk values of T_α and T_g with frequency and cooling rate respectively.*

been widely reported for thin polymer films samples. Only then can the thickness dependencies of T_α and T_g be compared directly.

Assuming that the thickness dependence of T_α can be correlated with the corresponding thickness dependence of the T_g in these samples, a comparison of the frequency and cooling rate dependencies for the bulk polymer should enable us to determine an equivalence between the cooling rates and measurement frequencies used in the two techniques. A consideration of the insets shown in Fig. 5.8 indicates that a cooling rate of 90Kmin^{-1} gives a T_g value that is approximately the same (but slightly lower) than the T_α value obtained for bulk PVAc at a measurement frequency of $\sim 0.01Hz$. This result is similar to that used by Fakhraai and coworkers in thin film studies of cooling rate effects in polystyrene [5].

A comparison of the thickness dependence of T_α and T_g at this frequency and cooling rate reveals that the observed shifts are the same within the limits of experimental uncertainty. This gives us some confidence in our interpretation of the results and the equivalence of the frequency and cooling rates used. However, it is worth noting that this simple method of analyzing the results does not take into account differences in the shapes of the distributions of molecular relaxation times that can be inferred from the dielectric spectra. Changes in the symmetry of the peaks shown in Fig. 5.5 would also indicate a change in the distribution of molecular relaxation times in the material. Such a change in this distribution would be expected to affect the global dynamics in the films and would influence the comparisons being made between T_g and T_α. It is worth noting however that the high level of symmetry in the dielectric peaks shown in Fig. 5.5 is retained as the film thickness and measurement frequency are changed. This would seem to indicate that the simple analysis performed above is valid for this particular polymer. We note that a previous study by Serghei and coworkers has reported changes in the peak shapes of BDS spectra for PVAc [7], but

no apparent changes were observed in the present study. The reason for these differences isn't clear.

One possible interpretation of the observed frequency dependence of thin film dynamics in PVAc could be related to the existence of cooperative dynamics in glass forming materials. As discussed by Fakhraai et al. [5] and others [4, 8, 9], there is expected to be a characteristic length scale (ξ) associated with the cooperative motions of segments in the bulk polymer, as is shown in Fig. 5.9. At higher temperatures and measurement frequencies, the number of polymer segments that are required for the material to relax would be expected to decrease [4, 8, 9, 10]. This would result in a corresponding reduction in ξ. The onset of film thickness effects in these materials are expected to occur when the film thickness starts to approach the characteristic length scale associated with these cooperative relaxation mechanisms. Therefore as the measurement frequency is increased we might expect that the onset of film thickness dependent dynamics and confinement effects would be shifted to lower film thickness values.

In principle, a study that determines the onset film thickness at which the effects of free surfaces or molecular confinement occurs for different frequencies may provide further insights into how the size of these regions of heterogenous dynamics scale with temperature and probe frequency. However, these experiments are currently beyond the scope of the present work.

5.5 Conclusion

In summary, we have shown that great care must be taken when comparing the results of different techniques that are being used to probe dynamics in thin polymer films.

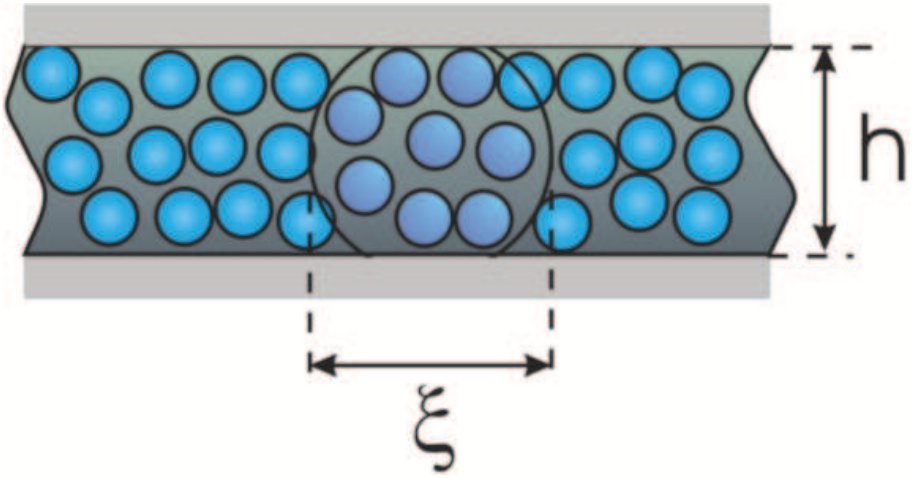

Figure 5.9: *Characteristic length scale (ξ) associated with the cooperative motions of segments in the bulk polymer. ξ is expected to be a function of temperature and measurement frequency.*

Combined ellipsometry and broadband dielectric studies have been used to show that thin film effects in glass forming polymers such as poly(vinyl acetate) have an intrinsic frequency dependence. These experiments address the existing controversial reports about the apparent discrepancies between what should be highly complementary methods of measuring the dynamics in thin film polymer samples. They highlight the necessity to ensure that the appropriate range of measurement/probe frequencies are used when comparing different methods of probing the dynamics in thin film polymer samples.

Bibliography

[1] J. L. Keddie, R. A. L. Jones, and R. A. Cory. *Europhys. Lett.*, **27**:59, 1994.

[2] M. Y. Efremov, E. A. Olson, M. Zhang, Z. Zhang, and L. H. Allen. *Phys. Rev. Lett.*, **91(8)**:085703, 2003.

[3] H. Huth, A. A. Minakov, A. Serghei, F. Kremer, and C. Schick. *Eur. Phys. J.-Special Topics*, **141**:151, 2007.

[4] J. S. Sharp and J. A. Forrest. *Phys. Rev. E.*, **67**:031805, 2003.

[5] Z. Fakhraai and J. A. Forrest. *Phys. Rev. Lett*, **95**:025701, 2005.

[6] L. Hartmann, J. Gorbatschow, J. Hauwede, and F. Kremer. *Eur. Phys. J. E*, **145**:8, 2002.

[7] A. Serghei, M. Tress, and F. Kremer. *Macromolecules*, **39**:9385, 2006.

[8] M. Arndt, R. Stannarius, H. Groothues, E. Hempel, and F. Kremer. *Phys. Rev. Lett.*, **79(11)**:2077, 1997.

[9] S. H. Anastasiadis, K. Karatasos, G. Vlachos, E. Manias, and E.P. Giannelis. *Phys. Rev. Lett.*, **84(5)**:915, 2000.

[10] J. S. Sharp and J. A. Forrest. *Phys. Rev. Lett.*, **91**:235701, 2003.

Chapter 6

Studies of the Dynamics in Ultra-thin Polyvinylacetate (PVAc) Films by Dielectric Spectroscopy

6.1 Introduction

Dielectric spectroscopy is widely used to probe the molecular dynamics in polymer samples. Dielectric spectroscopy can be described in the frequency domain (i.e. described by $\varepsilon'(\omega)$, $\varepsilon''(\omega)$, or $\tan\delta(\omega)$, where ε', ε'', $\tan\delta$ and ω in turn represent dielectric permittivity, dielectric loss, $\frac{\varepsilon''}{\varepsilon'}$ and angular frequency) or described in the temperature domain (i.e. described by $\varepsilon'(T)$, $\varepsilon''(T)$, or $\tan\delta(T)$, where T represents temperature), and both are used in these studies. The relaxation processes (α relaxation and secondary relaxations) can be characterized by the presence of resonance peaks in $\varepsilon''(\omega)$ or $\varepsilon''(T)$. The shape parameters of the resonance peaks in $\varepsilon''(\omega)$ or $\varepsilon''(T)$ provide useful information about the molecular dynamics in polymer samples. For example, the widening of the α relaxation peaks in $\varepsilon''(\omega)$ obtained from a polymer sample may suggest the widening of the distribution of the molecular relaxation times. However, although many efforts have been put into the study of the shape parameters of the relaxation peaks in $\varepsilon''(\omega)$, only a few reports [1] are related to the

study of the shape parameters of the relaxation peaks in $\varepsilon''(T)$.

As to the dielectric spectroscopy of $\varepsilon''(T)$ obtained from polymer samples, the α relaxation peaks of many polymers are close to symmetric [2, 3, 4, 5]. In contrast it is widely accepted that in the $\varepsilon''(\omega)$ obtained from some of these samples the α relaxation peaks are not symmetric (The high frequency ends of these peaks are usually wider). The symmetry is more striking when the large discrepancy among the constituents of those polymers is taken into consideration. In the present work we relate the shape parameters of the α relaxation peaks in $\varepsilon''(\omega)$ to the observed symmetry of the α relaxation peaks in $\varepsilon''(T)$. We show that this effort can lead to fruitful results.

In the present work we also investigated the measurement frequency effect on the the thickness dependence of the shape parameters using ultra-thin (9nm-486nm) PVAc films.

6.2 Experiment

Glass slides were cut into $1.3cm \times 1.3cm$ square pieces to serve as supporting substrates. These glass squares were then blown in N_2 gas to remove dusts generated during the cutting procedure. They were cleaned with methanol in an ultrasonic bath for 20 minutes, then with acetone for another 20 minutes. This was done to degrease the glass slides and to remove any further contaminant.

200nm Al (Advent, U.K., 99.999%) electrodes were thermally evaporated onto these glass squares. The evaporation rate was 5.0nm/s and the air pressure was below 2×10^{-5} torr. A type T thermocouple was hung close to those glass substrates during evaporating so that the temperature could be monitored during the evaporation.

The highest temperature measured during the evaporation was proved to be below 310K. The thickness of Al layer was monitored by a film thickness monitor (IL100, Intellemetrics Inc.), which had been calibrated by an AFM beforehand, as described in chapter 4. A metal mask was used in the evaporation to make three stripe-like Al electrodes.

Thin films of poly(vinyl acetate) (PVAc, $M_w = 184.1$K, $M_w/M_n = 2.99$, Scientific Polymer Product inc., U.S.) were spin coated from toluene on to these Al coated glass squares. The film thickness was controlled by varying the concentration of the polymer in solution. PVAc films with thicknesses in the range $9 - 486$ nm were prepared in this way. The samples were then annealed at 333 K ($T_g(PVAc) \sim 312 \pm 2$ K, as determined using ellipsometry) under vacuum for 5 hours.

The samples were then removed from the oven and three further stripe-like Al electrodes were thermally evaporated on top of the PVAc films using the same evaporation condition given above. These top electrodes were perpendicular to the bottom ones, and the thickness of the top electrodes was also 200 nm. This resulted in the formation of nine individually addressable capacitors that could be used in broadband dielectric studies.

The thickness of the PVAc films was pre-determined both by ellipsometry and AFM, as discussed in chapter 4, and the result is shown in Table 6.1.

After sample preparation, the PVAc film samples were then transferred immediately to the sample chamber of a TA Instruments DEA 2970 dielectric analyser, where they were purged using dry nitrogen gas. The measurement procedures are the same as those in Chapter 5, except that a broader (10^{-2}Hz $- 10^5$Hz) measurement frequency range was used.

6.3 Results and discussion

Fig. 6.1 shows the normalized dielectric spectroscopy measured from the 35nm thick PVAc film. We tried several functions to fit these data to and found that the best fitting function for these data is

$$\varepsilon'' = \varepsilon''_{\infty} + \frac{\varepsilon''_{\max}}{1 + (\frac{T - T_c}{w})^2} \tag{6.3.1}$$

where $\varepsilon''_{\max}$ represents the maximum/peak value of ε'' and T_c represents the temperature where $\varepsilon'' = \varepsilon''_{\max}$. ε''_{∞} represents the value of ε'' when $T = \infty$. w is a parameter which characterize the width of the α relaxation peaks. Since Eqn. 6.3.1 describes a symmetric relaxation peak, the good fitting of the data to Eqn. 6.3.1 suggests the measured resonance peaks in Fig. 6.1 are symmetric. The data measured at 0.01Hz is the overlap of the contribution from a relaxation peak and a background which increases with increasing temperature. The background is due to the low frequency conductivity [6] and it can be fitted to a simple exponential function. The background was then removed from the dielectric spectroscopy before this set of data was fitted to Eqn. 6.3.1.

Table 6.1: Concentrations of the PVAc solutions in Toluene and the corresponding spincast film thicknesses

Concentration of the PVAc solutions (W%)	0.5	1.0	2.0	3.0	4.0	8.0
Film thickness (nm) (±1 nm)	20	35	77	117	177	486

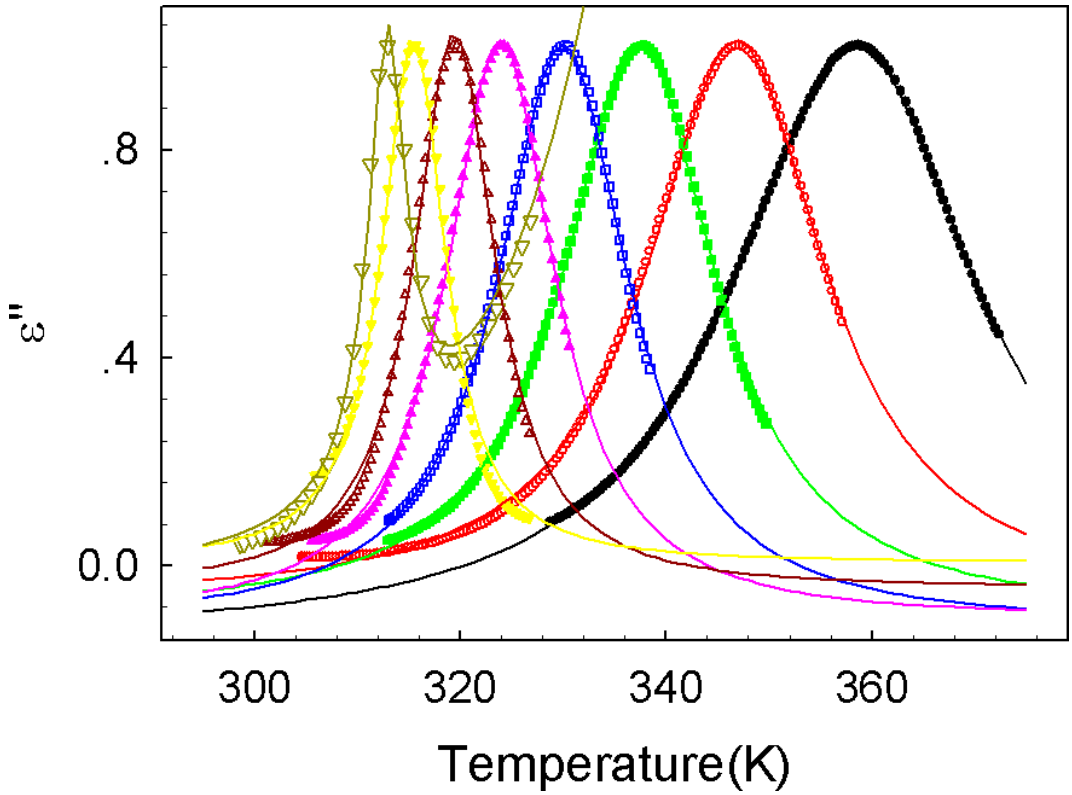

Figure 6.1: *Normalized dielectric spectroscopy in the temperature domain measured from a 35nm spin-cast PVAc film. The measurement frequencies are 100KHz (●), 10KHz (○), 1KHz (■), 100Hz (□), 10Hz (▲), 1Hz (△), 0.1Hz (▼) and 0.01Hz (▽). The solid lines are the fitting results of the data to empirical functions. The data measured at 0.01Hz is the overlap of the contribution from a relaxation peak and a background which increases with increasing temperature. The background is due to the low frequency conductivity [6]. It was fitted to a simple exponential function and then removed from the data before fitting the data to Eqn. 6.3.1. Other data were fitted directly to Eqn. 6.3.1.*

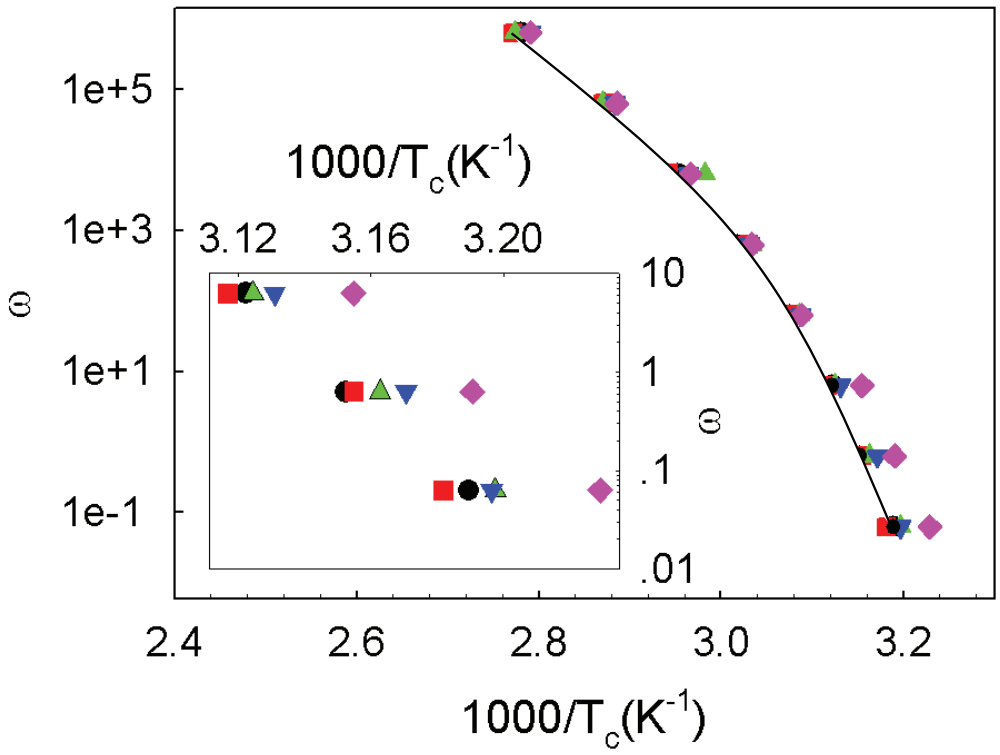

Figure 6.2: *Measurement frequencies as a function of* $1000/T_c$ *measured from 486nm (●), 177nm (■), 117nm (▲), 35nm (▼) and 9nm (♦) thick PVAc films. The black line represents the fitting of the data from the 35nm thick sample to the VFT function. For a better view, The inset zooms in the data points in the low frequency region.*

The relationship between the α relaxation rate and the sample temperature is usually determined by keeping polymer samples at constant temperature and measuring the dielectric spectroscopy in the frequency domain. In this experiment this relationship is determined by keeping the measurement frequency at a constant value and measuring the dielectric spectroscopy in the temperature domain. The temperatures where ϵ is at maximum (represented by T_c) are plotted against the measurement angular frequency, as shown in Fig. 6.2. In the high frequency region, the data from PVAc films of different thickness values are indistinguishable, which suggests that at high

measurement frequencies ($>\sim$ 10Hz) the polymer molecular dynamics doesn't exhibit a thickness dependence. In the low frequency region T_c is significantly dependent on film thickness and the thinner films have smaller T_c values, which suggests that thinner films have faster molecular dynamics. The inset shows T_c vs film thickness h when the samples being measured at 0.01 Hz. The frequency effect on thickness dependence of molecular dynamics have been extensively discussed in Chapter 5.

The data in Fig. 6.2 can be fitted to the Vogel-Fulcher-Tammann (VFT) function [7, 8, 9]:

$$\tau = \tau_0 \exp \frac{B}{T - T_0} \tag{6.3.2}$$

where τ equals $1/\omega$. τ_0 is the characteristic time of α relaxation at a very high temperature, and is usually set to be 10^{-13}s. B is a constant. T_0 is a temperature below T_g, and at T_0 the α relaxation time is expected to become infinite. The fitting result for the 35nm thick sample is $B = 1568 \pm 20$K and $T_0 = 265 \pm 1$K.

After the relationship between ω (or $1/\tau$) and the sample temperature is determined, the data shown in Fig. 6.2 can be plotted against $\ln \tau$ instead of against T, as shown in Fig. 6.3. After this transformation the α relaxation peaks all become asymmetric. The right halves of the peaks are significantly wider than the left halves. The asymmetry is better illustrated in Fig. 6.4. The data used in Fig. 6.4 is the set of data used in Fig. 6.3 which is measured at 1Hz. The dashed line represents a symmetric relaxation peak. Its left half reproduces the experimental data but its right half is narrower than the experimental data. This plot shows the significant distortion of the α relaxation peaks when they are plotted against $\ln \tau$. We also noticed a common observation that the α relaxation peaks plotted in $\epsilon''(T)$ are nearly symmetric for many polymers but when they are plotted against the measurement frequencies they

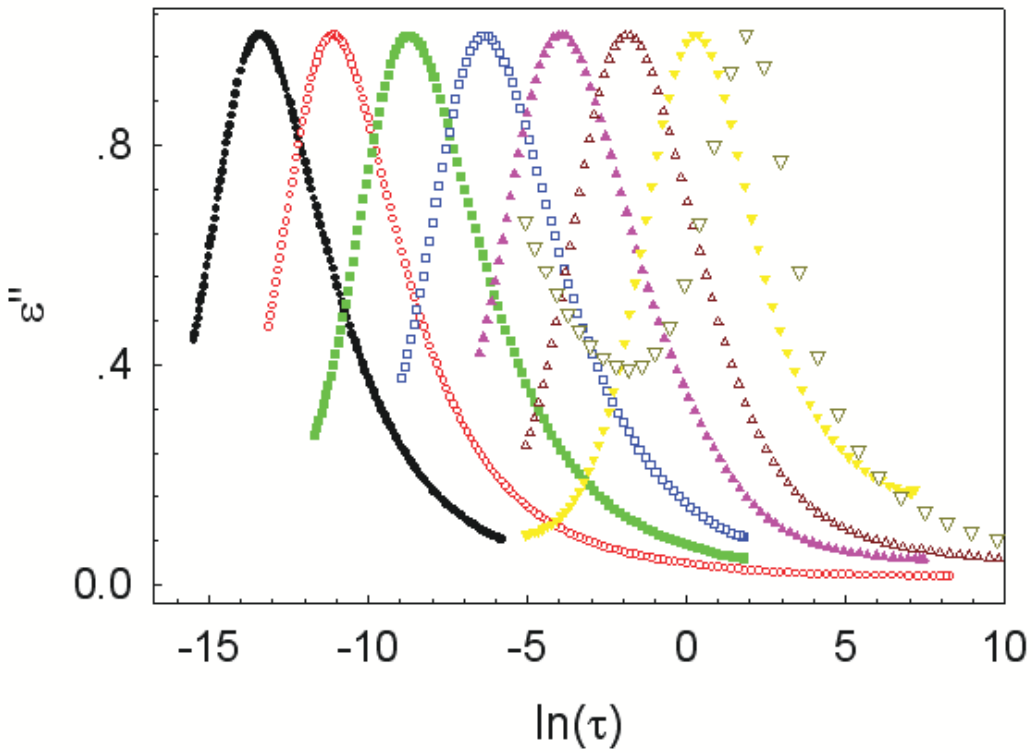

Figure 6.3: *Normalized dielectric spectroscopy ($\epsilon''(\ln\tau)$) obtained from a 35nm spin-cast PVAc film. The measurement frequencies are 100KHz (●), 10KHz (○), 1KHz (■), 100Hz (□), 10Hz (▲), 1Hz (△), 0.1Hz (▼) and 0.01Hz (▽).*

become asymmetric [2, 3, 4, 5]. To help to understand this, we firstly make a few definitions, which are illustrated in Fig. 6.4.

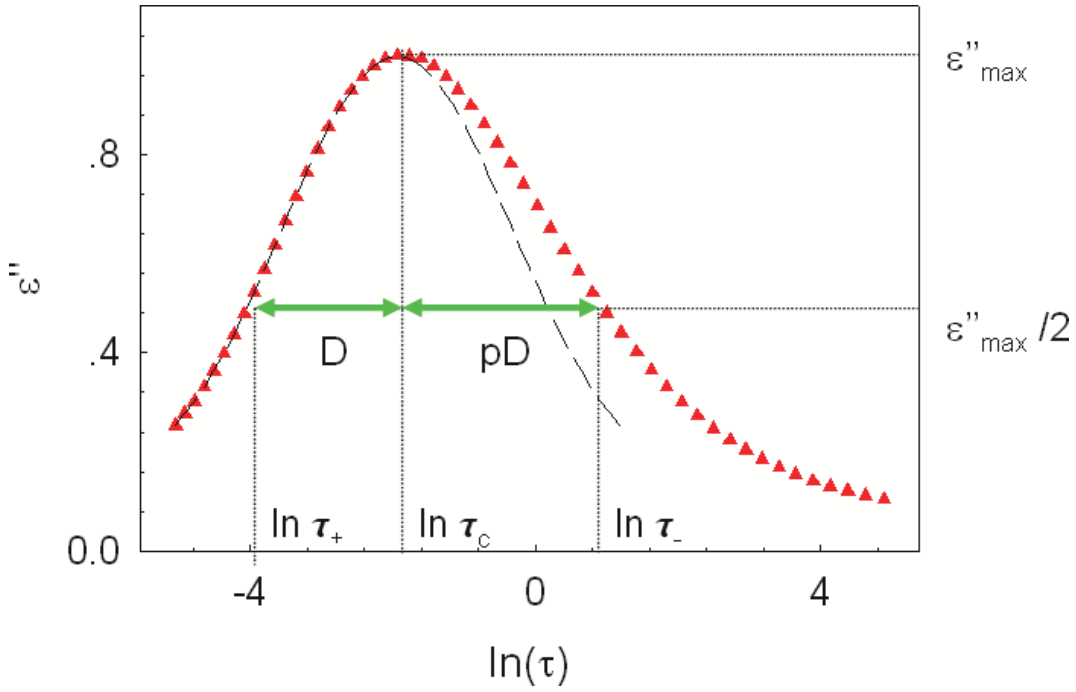

Figure 6.4: *Normalized dielectric spectroscopy obtained from a 35nm spin-cast PVAc film at a measurement frequency of 1Hz (△). The dashed line represents a symmetric relaxation peak. Its left half reproduces the experimental data and its right half is narrower than the experimental data. This plot also illustrates some definitions used in the present work.* $\epsilon''_{\max}$ *is the maximum value of* ϵ''. τ_c *represents the relaxation time where* $\epsilon'' = \epsilon''_{\max}$. τ_+ *and* τ_- *represent the relaxation time where* $\epsilon'' = \epsilon''_{\max}/2$. $(\tau_- > \tau_+)$. $\ln\tau_- - ln\tau_c = pD$ *and* $ln\tau_c - ln\tau_+ = D$, *therefore the factor p quantitatively describes the distortion of the* α *relaxation peaks.*

τ_c represents the relaxation time where $\epsilon'' = \epsilon''_{\max}$. It equals to $1/\omega_c$ where ω_c is the measurement frequency. τ_+ and τ_- represent the relaxation time where $\epsilon'' = \epsilon''_{\max}/2$ $(\tau_+ < \tau_-)$. Two shape parameters p and D which describe the α relaxation peaks in $\epsilon''(\ln\tau)$ are defined by

$$\ln\tau_- - ln\tau_c = pD \qquad \text{and} \qquad \ln\tau_c - ln\tau_+ = D. \tag{6.3.3}$$

The factor p quantitatively describes the distortion of the α relaxation peaks. If and only if $p = 1$ the α relaxation peak in $\epsilon''(\ln\tau)$ is symmetric. For all the data sets in Fig. 6.3, these two parameters were found to be the same within error ($D = 2.0 \pm 0.2$ and $p = 1.38 \pm 0.03$.).

We further define T_c to be the temperature where $\epsilon'' = \epsilon''_{\max}$, and define T_+, T_- to be the temperatures where $\tau = \tau_+$ and $\tau = \tau_-$. The values of $T_+ - T_c$ and $T_c - T_-$ can be obtained by replacing T_+, T_- and T_c with τ_+, τ_- and τ_c, which leads to

$$T_+ - T_c = \frac{B \times D}{\ln(\omega_c\tau_0)(\ln(\omega_c\tau_0) + D)} \tag{6.3.4}$$

$$T_c - T_- = \frac{B \times pD}{\ln(\omega_c\tau_0)(\ln(\omega_c\tau_0) - pD)} \tag{6.3.5}$$

Combining Eqn. 6.3.4 and Eqn. 6.3.5 we get

$$\frac{T_+ - T_c}{T_c - T_-} = \frac{\frac{1}{p}\ln(\omega_c\tau_0) - D}{\ln(\omega_c\tau_0) + D} = C \tag{6.3.6}$$

where B is the parameter in a VFT equation, and C describes how close the α relaxation peaks in $\epsilon''(T)$ are to strict symmetry. The α relaxation peaks are strictly symmetric if and only if $C = 1$. The value of C is calculated using Eqn. 6.3.6 (suppose $D = 2.0$ and $p = 1.38$.), and is plotted against the measurement frequency f in Fig. 6.5. It is found that the C values for all measurement frequencies are less than (but close to) 1, which suggests that the α relaxation peaks in $\epsilon''(T)$ obtained in this experiment are not strictly (but close to) symmetric. According to the solid line in Fig. 6.5, the α relaxation peaks measured at higher frequencies are closer to strict symmetry than those measured at lower frequencies, and at a certain measurement frequency (4.9×10^6Hz) the α relaxation peaks are strictly symmetric. The solid line

also suggests at even higher measurement frequencies the α relaxation peaks become asymmetric again. However, these predictions assume that D and p don't rely on measurement frequencies. Although D and p are quite constant in this experiment, the assumption may not be true in a wider measurement frequency range.

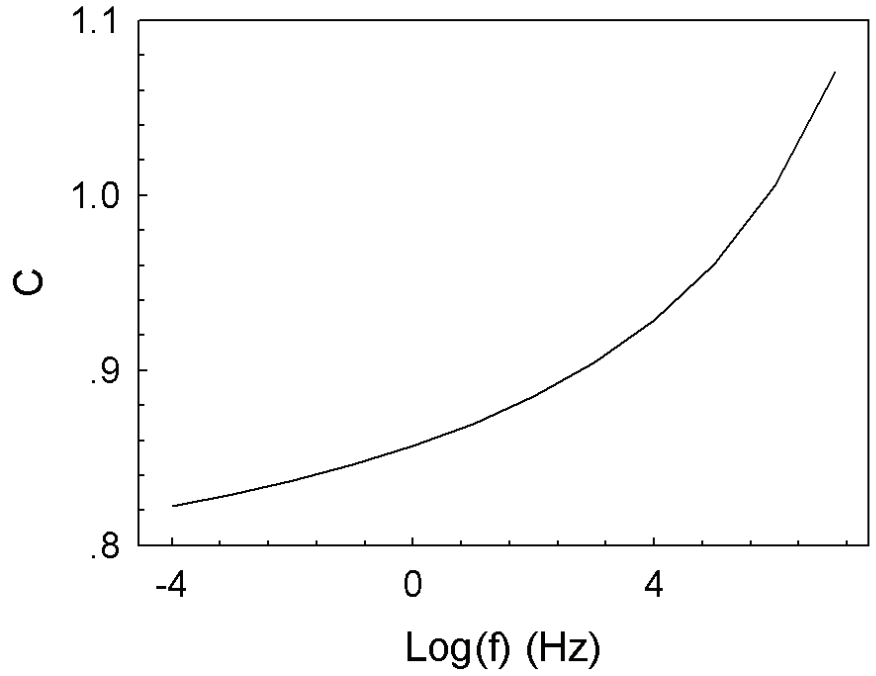

Figure 6.5: *The value of C is calculated using Eqn. 6.3.6 (suppose $D = 2.0$ and $p = 1.38$.), and is plotted against the measurement frequency f*

Another notable observation is the widening of the α relaxation peaks in Fig. 6.1 with increasing measurement frequency. To help to understand this, we add Eqn. 6.3.4 and Eqn. 6.3.5 together and get

$$\frac{B \times D(p+1)}{T_+ - T_-} = \ln^2(\omega_c \tau_0) + D(1-p)\ln(\omega_c \tau_0) - pD^2 \qquad (6.3.7)$$

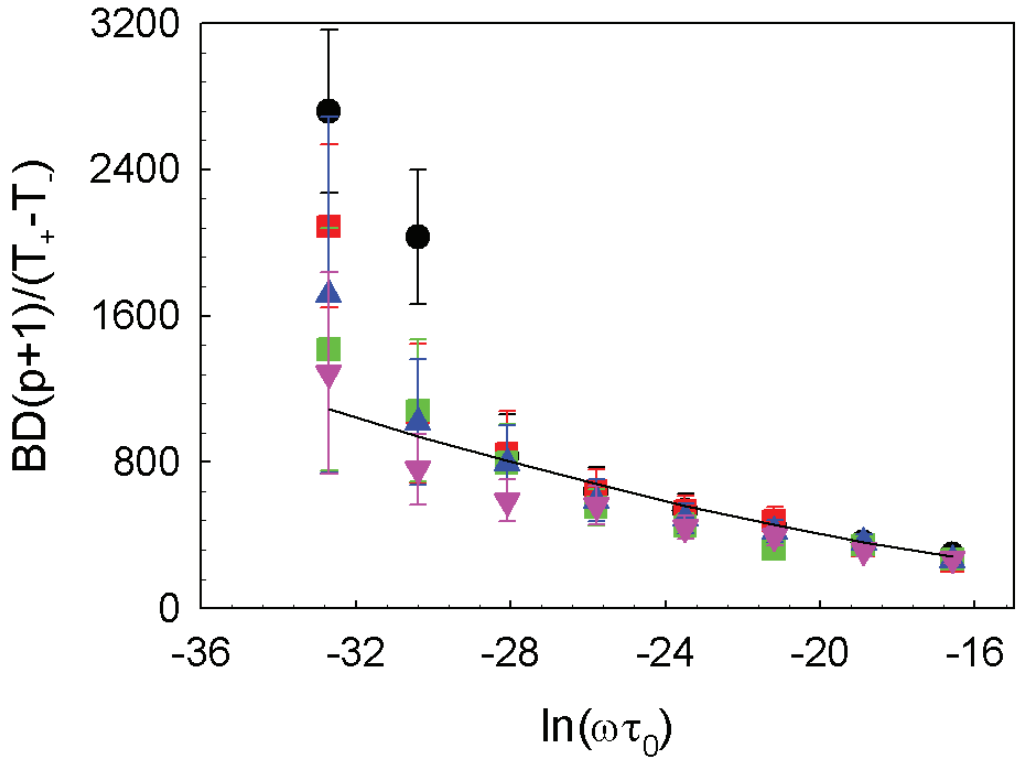

Figure 6.6: *The relationship between the width the α relaxation peaks and the measurement frequency. Data are shown for PVAc films of 486nm (black •), 177nm (red ■), 117nm (green ■), 35nm (blue ▲) and 9nm (pink ▼) thickness. The solid line is a theoretical prediction which supposes $D = 2.0$ and $p = 1.38$.*

This equation suggests that if D and p are constants for all measurement frequencies, the width of the α relaxation peaks increases with increasing measurement frequency. This explanation is confirmed by Fig. 6.3 where $B/(T_+ - T_-)$ is plotted against $\ln(\omega_c \tau_0)$. The solid line represents the theoretical prediction made by Eqn. 6.3.7 which supposes $D = 2.0 \pm 0.2$ and $p = 1.38 \pm 0.03$, and the data measured from the 35nm thick sample reproduce the theoretical prediction.

Fig. 6.3 further shows that while in the higher frequency region ($>$ 1Hz), the data measured from films of different thicknesses reproduce each other, in the lower frequency region ($< 1Hz$) the data obtained from thinner films have wider α relaxation peaks than those obtained from thicker ones. This observation is consistent with Fukao et al's results [10]. The thickness dependence of the the width of the α relaxation peaks can also be explained by the existence of the liquid like surface layer. The enhanced molecular mobility in the liquid like surface layer is supposed to bring in a wider distribution of relaxation times. While in thick films the effect of the liquid like surface layer is too small and can be neglected, in ultra-thin ($<$ 100nm) films the effect of liquid like surface layer becomes significant. Thin films therefore have broader distribution of relaxation times and wider α relaxation peaks. The α relaxation peaks obtained from the thin films with broader distribution of relaxation times are supposed to broaden to low temperatures due to the faster dynamics in these films. However, the data measured at low frequencies has pronounced background of low frequency conductivity, which makes it not possible to determine this. The reason why in the higher frequency region ($>$ 1Hz) there doesn't exist the thickness dependence of the widthes of the α relaxation peaks can be explained with the discussion given in Chapter 5, where we showed that only probes with slow measurement time scales ($<$1Hz) are able to detect the thickness dependence of the cooperative molecular dynamics. That's why only in the lower frequency range ($<$1Hz) could the

thickness dependence of the width of the α relaxation peaks be observed.

6.4 Conclusion

Dielectric spectroscopy in the temperature domain $\epsilon''(T)$ was measured on thin (<486nm) PVAc films. The data were plotted against $\ln\tau$ and the parameters describing the widening and distortion of the α relaxation peaks are constant for all measurement frequencies. The observed symmetry of the α relaxation peaks in $\epsilon''(T)$ were related to the constant shape parameters of the asymmetric α relaxation peaks in $\epsilon''(\ln\tau)$. An explanation is given for the observed widening of the α relaxation peaks with increasing measurement frequency in $\epsilon''(T)$. At a lower measurement frequency (<1Hz), the data obtained from thinner PVAc films showed wider α relaxation peaks (in $\epsilon''(T)$) than the data obtained from thicker films, and at a higher frequency (>1Hz) this thickness dependence doesn't exist . This was explained using the existence of the liquid-like surface layer with enhanced molecular mobility, and using the measurement frequency effects.

Bibliography

[1] A. Serghei, M. Tress, and F. Kremer. *Macromolecules*, **39**:9385, 2006.

[2] E. Donth, H. Huth, and M. Beiner. *J. Phys.: Condens. Matter*, **13**:L451, 2001.

[3] C. Alvarez, V. Lorenzo, and E. Riande. *J. Chem. Phys.*, **122**:194905, 2005.

[4] A. Linares and J. L. Acosta. *Die Angewandte Makromolekulare Chemie*, **257**:23, 1998.

[5] E. Dantras, A. M. Caminade, J-P Majoral, and C. Lacabanne. *J. Phys. D.: Appl. Phys.*, **35**:5, 2002.

[6] Y. Miyamoto. *Polymer*, **25**:63, 1984.

[7] H. Vogel. *Phys. Z.*, **22**:645, 1921.

[8] G. S. Fulcher. *J. Am. Ceram. Soc.*, **6**:339, 1925.

[9] G. Tammann and G. Hesse. *Z. Anorg. Allg. Chem.*, **156**:245, 1926.

[10] K. Fukao, S. Uno, Y. Miyamoto, A. Hoshino, and H. Miyaji. *Phys. Rev. E*, **64**:051807, 2001.

Chapter 7

Investigation of physical aging process in thin polystyrene films

Extensive studies have been performed to investigate the physical aging process in bulk polymer samples, but only a small number of experiments were dedicated to the study of the physical aging process in thin polymer films. As was discussed in previous chapters, the observed deviation in other physical processes in ultra-thin polymer films (usually <100nm) reminds us of the possibility that physical aging processes in ultra-thin polymer films may be also different from those in bulk polymer samples. This is proved by the observations [1, 2, 3, 4, 5, 6] that several kinds of ultra-thin polymer films exhibited accelerated physical aging processes. Reports also exist [7] about the slower physical aging rates near the film surface and the faster physical aging rates in the central part of a film. More complex physical aging processes in ultra-thin polymer films were reported by Ellison et al. [8], as has been discussed in chapter 2.

However, compared to the number of the studies of the glass transition in ultra-thin polymer films, much less effort has been put into the study of the physical aging process in these samples, and there remain many questions that need to be answered. For example, why do the free-surface and substrate effects penetrate inside the central

part of the films to such a long distance (usually >100nm) [1, 2, 9]. As a comparison, in the studies of glass transition in ultra-thin polymer films, the free surface effect can be neglected in films thicker than ∼100nm. And, how do the free surface and substrate affect the physical aging processes in ultra-thin polymers? Ellison et al. and Priestley et al. suggested that the origin of the deviation is the enhanced mobility of the molecule segments near the free surface of the films. But Huang et al. [9, 1, 2] suggested that in thin polymer films, it's easier for the free volume to dissipate from the central part to the surface during physical aging, and that's the origin of the accelerated physical aging rate observed in ultra-thin polymer films. However, 'there is no direct confirmation of this hypothesis' [2]. To answer these questions, detailed and systematic studies need to be performed to investigate physical aging process in ultra-thin polymer films.

In the present work isothermal physical aging process in thin polystyrene (PS) films were studied with ellipsometry. The effect of aging temperature and films thickness on the aging process are reported. We also propose an explanation for these observations.

7.1 Sample preparation

Polystyrene (PS) films were formed by spin coating PS (syn., $M_w = 600$KDa, $M_w/M_n = 1.07$, Polymer Source Inc.) solutions in toluene with a spin speed of 3000 RPM onto 1.2cm × 1.2cm single crystal silicon wafers. The film thickness was controlled by varying the concentration of the solutions, and the thickness values of the spin-cast PS films were measured using ellipsometry and AFM (the measurement procedure is described in Chapter 4). Fig. 7.1 and Table 7.1 show thickness-concentration pairs

for PS spin-cast films. After spin-coating all samples were annealed at 393K in vacuum for 10 hours to remove solvent residue and any stress/strain introduced into the films during the spin coating procedure.

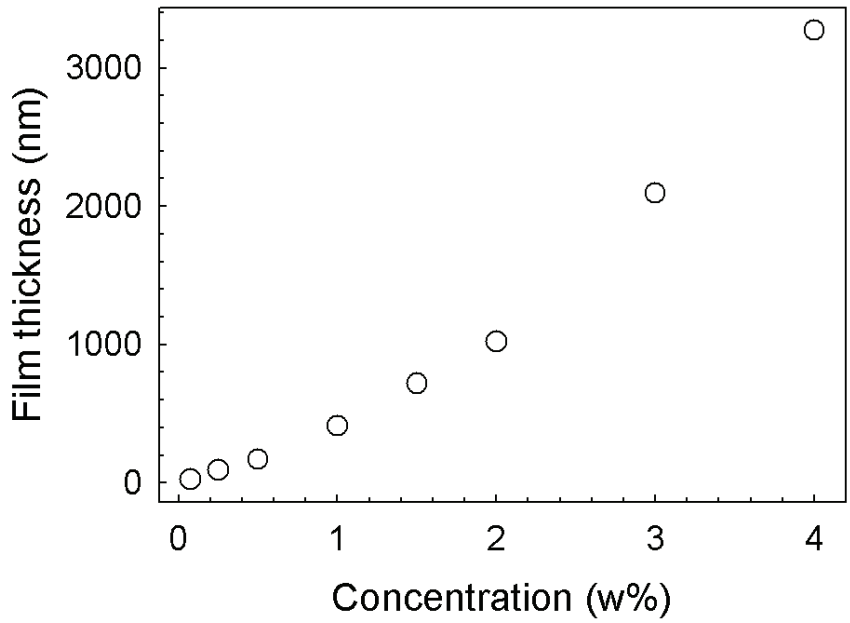

Figure 7.1: *The thickness of spin-cast PS films vs the concentration of the solutions. In this experiment, the spin speed is* 3000 *RPM and the solvent is toluene.*

Table 7.1: PS film thicknesses determined by concentration of the solution

Concentration of the PS solutions (W%)	0.25	0.5	1.0	1.5	2.0	3.0	4.0
Film thickness (nm) (±1nm)	9	17	41	72	102	209	327

7.2 Measurement of physical aging rates in thin PS films

After being annealed the samples were transferred immediately to the sample stage on the ellipsometer, where the samples were purged with N_2 so that during measurement the samples wouldn't be influenced by water or oxygen. A type T thermocouple was glued on a small Si wafer (using OMEGABOND 200 resin from OMEGA corporation) of similar size to these used as sample substrates, and placed close to the sample to ensure the temperature of the sample surface and the temperature measured by the thermocouple are similar. Nitrogen gas was purged through the sample chamber in the hot stage, so that during measurement the samples wouldn't be disturbed by water or oxygen.

Then the T_g's of the PS samples were measured using the ellipsometer. Each sample was heated up to 400K (the T_g of a bulk PS sample is 369K$\pm$1K) and kept at this temperature for 20 minutes to erase any thermal history. The samples were then cooled down slowly at a rate of 10K/min, and during the cooling process the angles of the two polarizers (P and A) on the ellipsometer were varied to obtain a null signal. P and A were values obtained at null recorded every 10 seconds (every 1.67K).

To measure the physical aging process of these samples, each sample was then heated up to 383K (14K larger than the bulk T_g) and kept at that temperature for 10mins. The samples were expected to be in equilibrium at this stage. They were then cooled down at 30K/min down to the aging temperatures while the angles of the two polarizers on the ellipsometer were varied to obtain null signals. This system was capable of measuring 1 P and A data point in less than 1 second. A type T thermocouple (copper-constantan) was glued on a small Si wafer (using OMEGABOND 200 resin from OMEGA corporation), and placed close to the sample to ensure the temperature

of the sample surface and the temperature measured by the thermocouple are equal. Since in these experiments the variation of the film thickness and the refractive index is very small, the changing of both P and A is proportional to the changing of the film thicknesses and the refractive index. The evolution of P and A was therefore used directly to characterize the physical aging process of the thin film samples, and the calculation of film thickness and the refractive index were not necessary.

7.3 Results and discussion

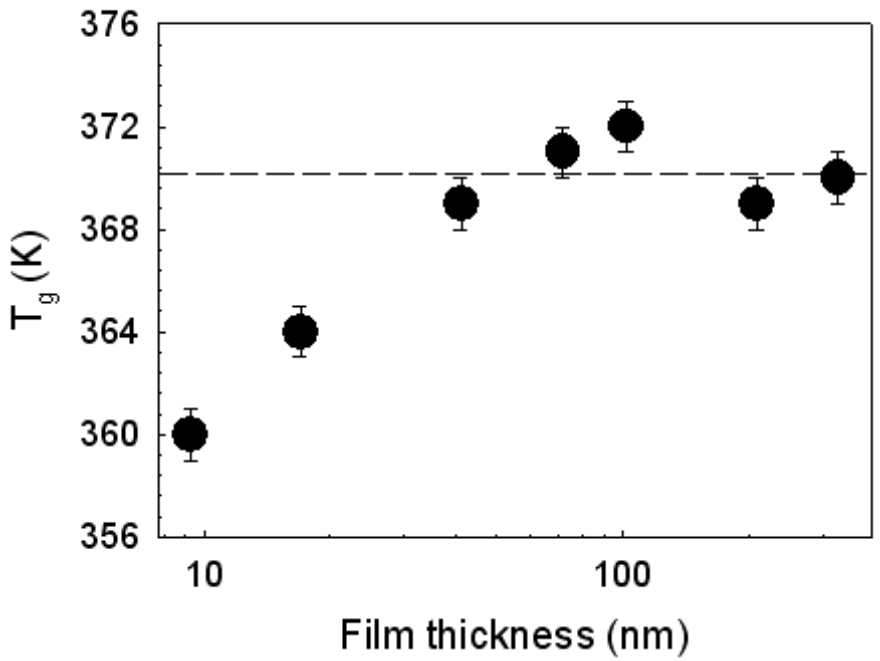

Figure 7.2: *Thickness dependence of the T_g for PS film samples. Data are shown for uncapped films. The dashed line represents the bulk T_g value for PS samples*

The thickness dependence of T_g for PS film samples is shown in Fig. 7.2. The T_g values of the uncapped PS films thicker than $\sim$ 40nm are 370K$\pm$1K. The T_g values

of the uncapped PS films thinner than $\sim$ 40nm are smaller than the bulk T_g, and the maximum depression of T_g (10 ± 1K) is found on the thinnest film (the 9nm thick one). These observations agree well with previous studies [10, 11, 12, 13, 14] where the thickness dependence of thin PS films were measured.

Fig. 7.3 shows the the variation of $\Delta P/\Delta P_\infty$ (ΔP_∞ represents the total change of P after an infinite time) as a function of time obtained from 17nm and 323nm uncapped PS samples on silicon wafers. The data are are measured at aging temperatures of 368K, 363K, 357K and 353K. The dashed line represents where the data saturate. The changing of $\Delta P/\Delta P_\infty$ is fast at the beginning and slows down fast as time goes on, which is consistent with the self retarding relaxation process described by Struik et. al. [15] (see chapter 1). The saturation of $\Delta P/\Delta P_\infty$ measured at high aging temperatures occurs much earlier, which indicates that the aging rates at high temperatures are much faster. For the 17nm sample, at aging temperatures of 368K and 363K, there is no slow relaxation and the data is a fast jump instead. This can be explained by low T_g (360$\pm$1K) of this sample. At the same aging temperature, the aging rate of the 323nm sample is much slower than that of the 17nm sample, which suggests the dependence of the aging rate on film thickness. This is better demonstrated in Fig. 7.4. Fig. 7.4 shows the variation of $\Delta P/\Delta P_\infty$ as a function of time obtained from the uncapped PS films on silicon wafers. The dashed line represents where the data saturate. The aging temperatures for all the data in this plot are the same (363K), and the thick films exhibited much longer physical aging processes than the thin films.

To determine the aging rates, $\ln(1 - \Delta P/\Delta P_\infty)$ vs time was plotted against time, as is illustrated in Fig. 7.5. Although physical aging isn't an exponential relaxation

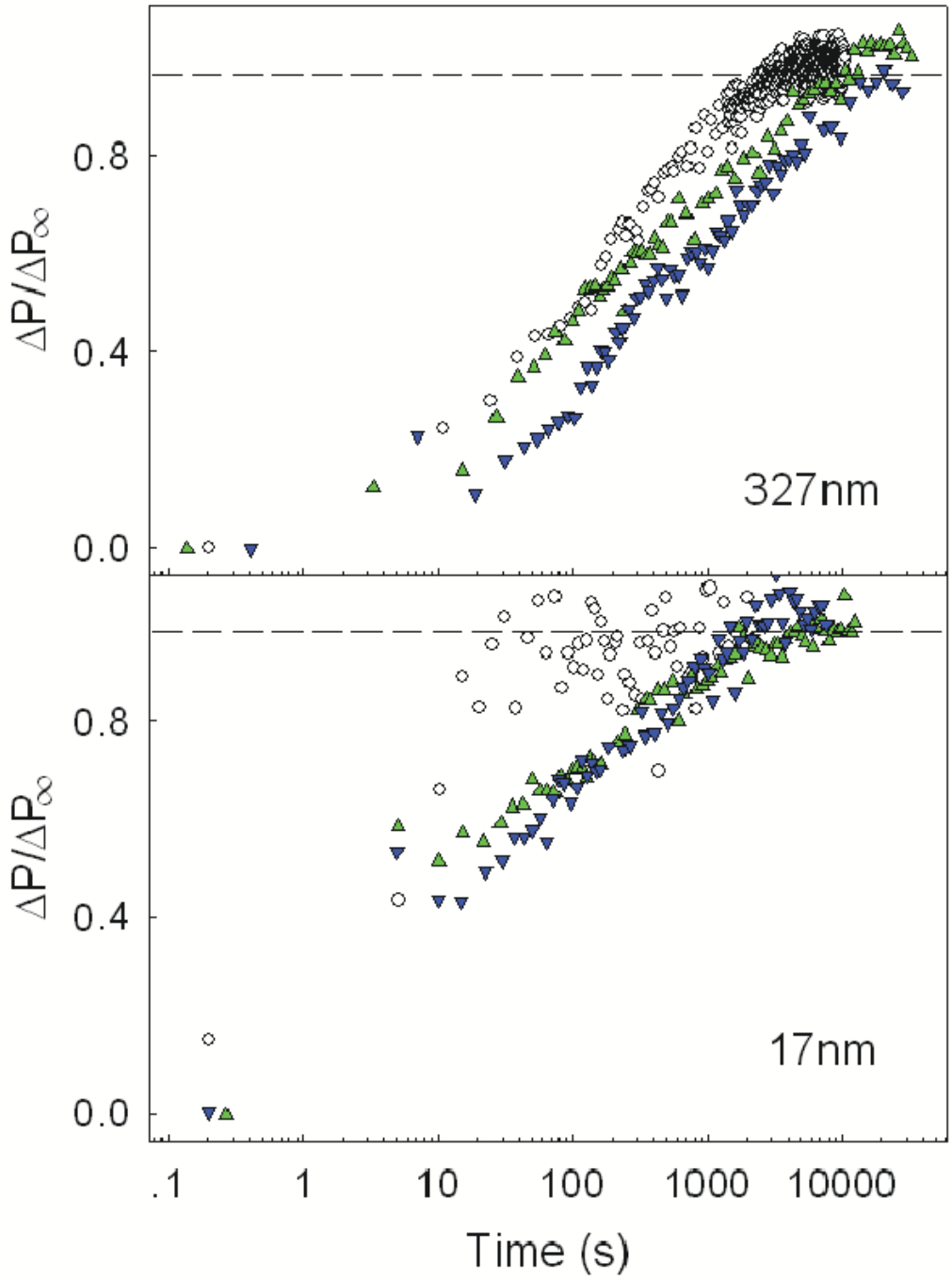

Figure 7.3: *the variation of $\Delta P/\Delta P_\infty$ as a function of time measured at aging temperatures of 368K (◯), 357K (▲) and 353K (▼). The data are obtained from the uncapped 17nm (upper plot) and 323nm (lower plot) PS films on silicon wafers. The dashed line shows the saturated value of $\Delta P/\Delta P_\infty$.*

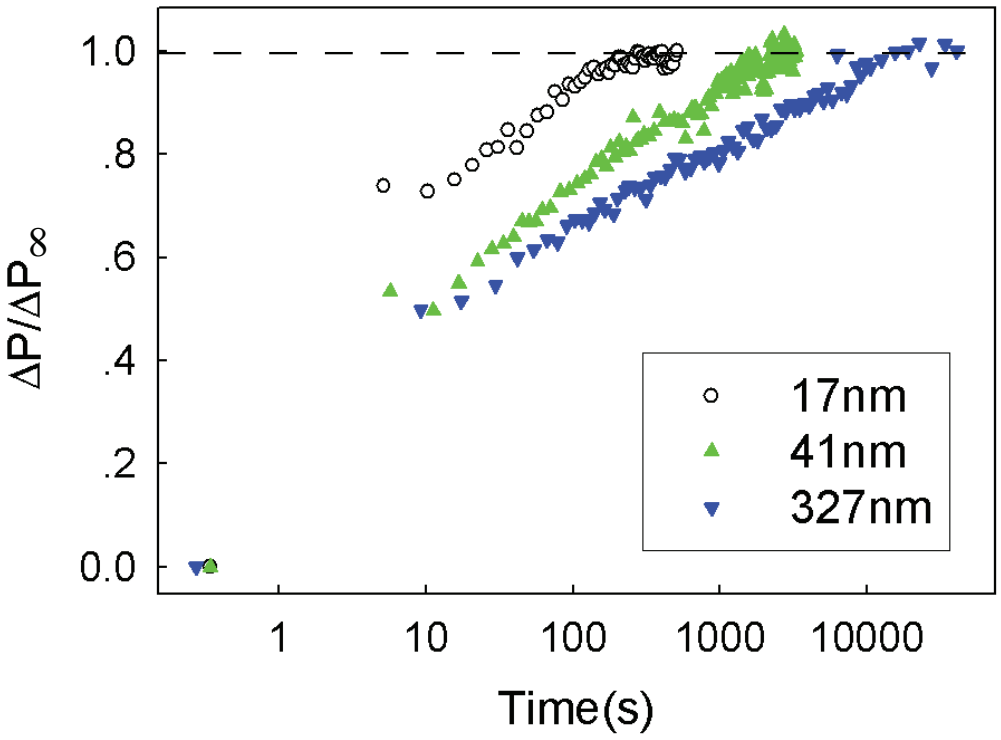

Figure 7.4: *The variation of $\Delta P/\Delta P_\infty$ as a function of time obtained from the uncapped PS films on silicon wafers. The aging temperature for the data in this plot is 363K. The dashed line represents where the data saturate.*

process and that data of $\ln(1 - \Delta P/\Delta P_\infty)$ vs time cannot be exactly fitted to linear functions (as was discussed by Struik et. al. [15]), It was found the major part of the data can be fitted well by linear functions. The slopes of the linear fits to this part are defined as the physical aging rate in the present work, and the reciprocals of the aging rates are defined to be the characteristic time τ of the physical aging.

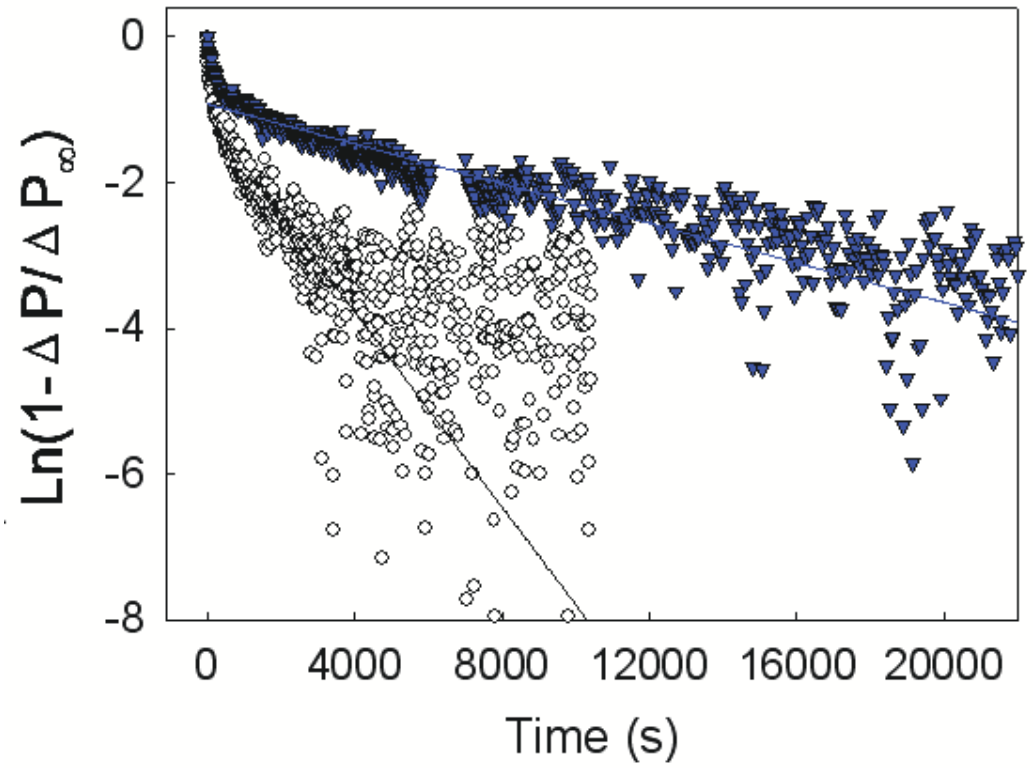

Figure 7.5: *Isothermal aging data plotted as* $\ln(1 - \Delta P/\Delta P_\infty)$ *vs time. The data is obtained from a 323nm PS sample and the aging temperatures are 368K (Black data) and 353K (blue data). It is found that except the very beginning of the data and the saturated data, the data can be fitted well by linear functions. The fitting results are shown as the straight lines.*

The upper plot in Fig. 7.6 shows Relaxation time as a function of $T - T_{g,\text{bulk}}$, and to

make a comparison with the thickness dependence of T_g, these data are also plotted against $T - T_{g,film}$ (the lower plot). The data are obtained from the 17nm (▼), 41nm (▲), 250nm (■) and 323nm (●) thick samples.

In Fig. 7.6, the physical aging rate measured from the 323nm and 250nm thick samples decreases with decreasing aging temperature. Hereby we use the explanation proposed by Priestley et al. [7]. That is, the rate of an isothermal physical aging can be determined by two factors, i.e., the distance to equilibrium and the aging temperature. As the aging temperature decreases, the distance to equilibrium, which serves as the driving force of the physical aging, becomes larger and acts to increase the physical aging rate. However, the reduction in temperature causes a slowing down of the dynamics and the physical aging rate. In polystyrene films, the factor of the aging temperature is dominant, and that's why aging rate decreases with decreasing aging temperature. A linear relationship between τ and T is found on the data obtained from these samples. The reason to the linearity isn't clear yet. The data measured from the 41nm thick samples have more complex behavior. While it shows the trend of the increasing aging time with decreasing aging temperature, there doesn't exist the linear relationship between the $\log \tau^{-1}$ and $1000/T$. A maximum physical aging rate appears when the aging temperature is $\sim$ 17K below $T_{g,\mathrm{film}}$. Such an aging rate maximum also exists in PMMA films, and a 500nm thick PMMA film exhibits an aging rate maximum $\sim 73 - 88$K below bulk T_g [7]. This can be explained by the competition between the driving force and the molecular dynamics, as was discussed in Chapter 2 (see Fig. 2.13). The aging rate becomes much faster when the aging temperature is very close to T_g, and this is confirmed by the data measured on the 41nm PS sample at 1K below the film T_g, which is much ($\sim$1 degree of magnitude) faster than those measured at more than 2K below the film T_g.

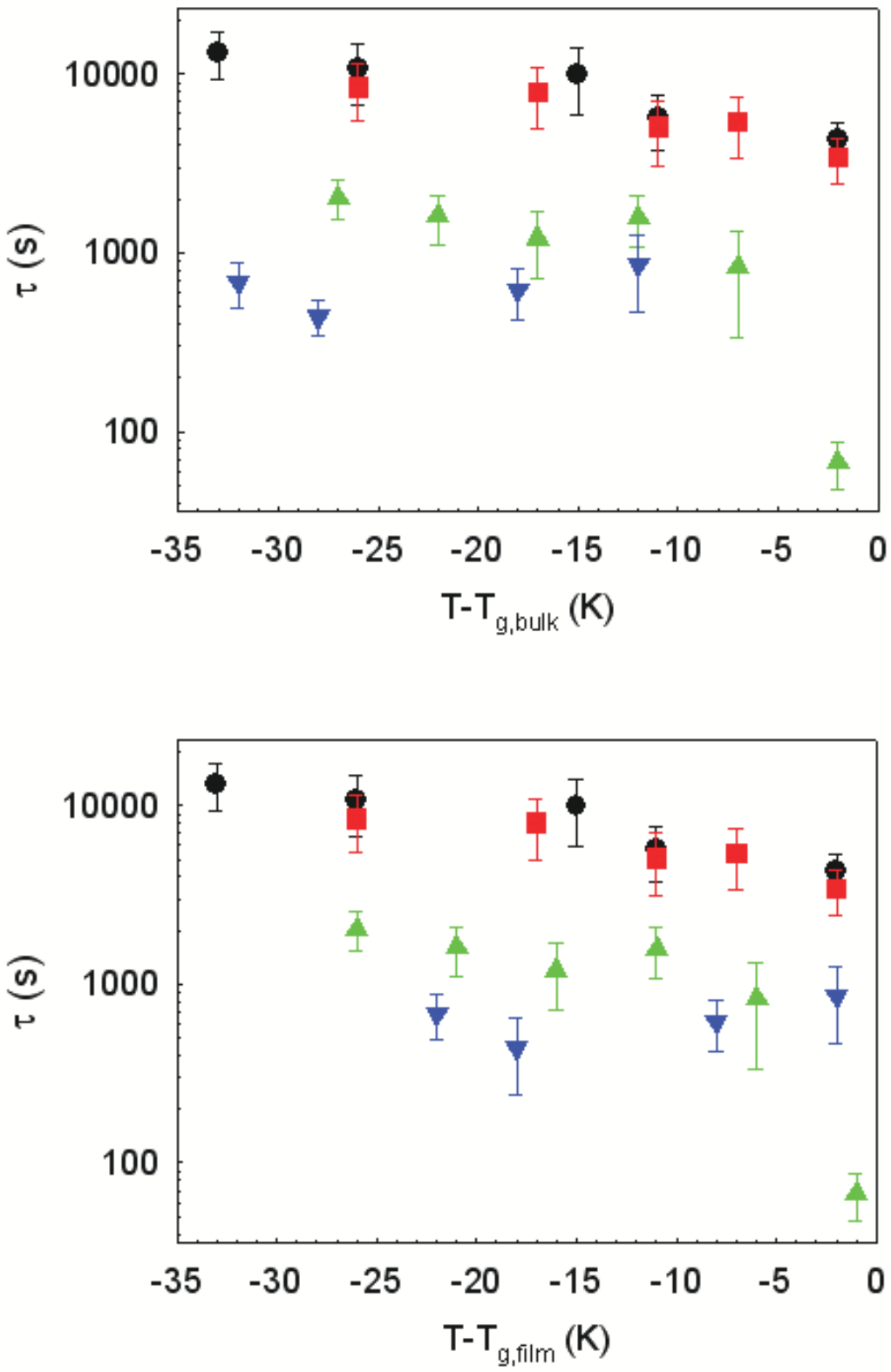

Figure 7.6: *Relaxation time as a function of* $T - T_{g,\mathrm{bulk}}$ *(the upper plot) and* $T - T_{g,\mathrm{film}}$ *(the lower plot). The data are obtained from the 17nm (blue ▼), 41nm (green ▲), 250nm (red ■) and 323nm (black ●) thick samples.*

Fig. 7.6 shows the thickness dependence of aging time in PS films. The data obtained from the 323nm thick and the 250nm thick films reproduce each other within the limits of experiment uncertainties. This suggests that the thickness dependence of aging rate isn't significant in PS films if the films are thick enough (for example, >250nm). The 41nm thick film and the even thinner ones exhibit faster molecular dynamics than the bulk samples. An explanation of the observed faster dynamics is the enhanced relaxation rates near the free surfaces which have much stronger effect on films thinner than a threshold value. However, there are several reasons to claim that the thickness dependence of aging time doesn't share totally the same origin with the thickness dependence of T_g. Firstly, if τ is plotted against $T - T_{\mathrm{g,film}}$ (shown in the lower plot in Fig. 7.6), the data obtained from films of different thicknesses don't reproduce each other. Secondly, the 41nm thick PS sample which has a bulk-like T_g value exhibits faster aging rates than bulk samples. We propose that, the faster aging rates observed in the thinner PS films (e.g., h <41nm) is due to the enhanced dynamics near the free surfaces, but the aging time τ as a probe of molecular dynamics is more sensitive than T_g. Consider a molecular layer near the free surface which has faster dynamics than the bulk material, its T_g may be tens of degrees smaller than bulk values, while its aging rate could be many decades' faster. The T_g and the aging rate of a polymer film thinner than the threshold values are determined by the averaged dynamics of all layers, therefore it could show a T_g depressed by, approximately 10K, while showing an aging rate of orders of magnitude faster, or, it doesn't exhibit significant depression of T_g, but still shows an accelerated physical aging. This scenario helps the understanding of the origin of this high sensitivity and our observations can be better understood in this framework. The molecular dynamics in the 41nm PS sample is faster than that in bulk samples due to the free surface effect, but this can only be shown in $\tau(h)$ and can not be shown in $T_g(h)$ due to the different sensitivity of these two probes.

The thickness dependence of physical aging rate is better illustrated in Fig. 7.7, where τ is plotted against film thickness. Films thinner than ∼100nm show significant depression of aging time, while in contrast is in the study of the thickness dependence of T_g with PS films, where only films thinner than ∼40nm exhibit depression of T_g. This comparison confirms our idea that the aging rate serves as a more sensitive probe than T_g does in the study of the thickness dependence of polymer molecular dynamics.

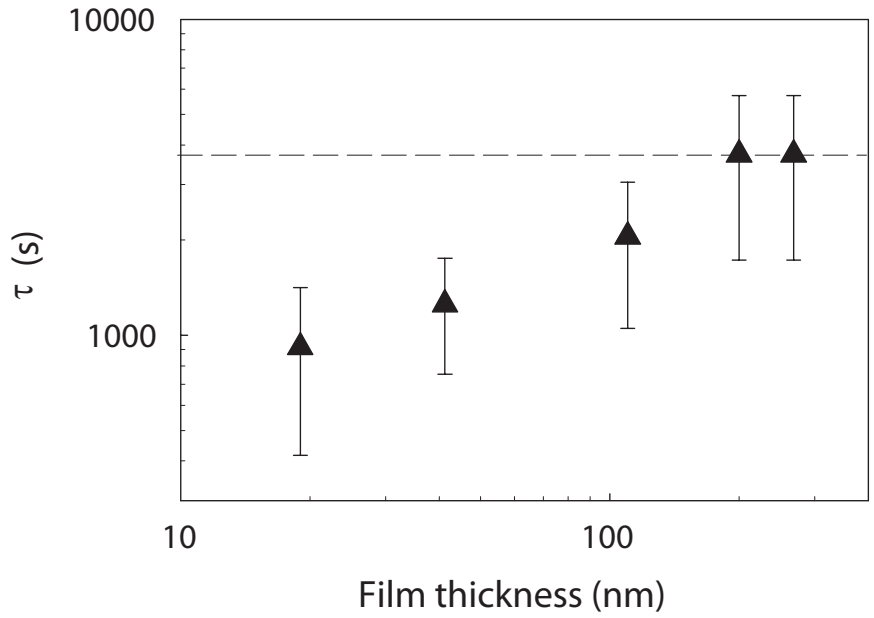

Figure 7.7: *Characteristic time τ of the physical aging process as a function of the film thickness. The data is measured at the aging temperature of 358K.*

7.4 Conclusion

Aging temperature and film thickness dependence of physical aging has been studied using PS films. A trend of decreasing of aging rate with decreasing aging temperature

is found for all samples. In ultra-thin PS films (<41nm thick) a maximum aging rate at ∼17K below $T_{g,\mathrm{film}}$ is found. These observations were explained using the competition of the factors that affect the aging, that is, the distance to the equilibrium and the fraction of the free volume. A comparison between the thickness dependence of aging rate and the thickness dependence of T_g suggests that the aging rate serves as a more sensitive probe in the study of polymer molecular dynamics than T_g does.

Bibliography

[1] Y. Huang and D. R. Paul. *Polymer*, **45**:8377, 2004.

[2] Y. Huang and D. R. Paul. *Macromolecules*, **39**:1554, 2006.

[3] P. G. Debenedetti and F. H. Stillinger. *Nature*, **410**:259, 2001.

[4] C. A. Angell. *Science*, **267**:1924, 1995.

[5] V. N. Novikov and A. P. Sokolov. *Nature*, **431**:961, 2004.

[6] P. G. de Gennes. *Eur. Phys. J. E*, **2**:201, 2000.

[7] R. D. Priestley, L. J. Broadbelt, and J. M. Tokelson. *Macromolecules*, **38**:654, 2005.

[8] C. J. Ellison, M. K. Mundra, and J. M. Torkelson. *Macromolecules*, **38**:1767, 2005.

[9] R. D. Priestley et al. *Science*, **309**:456, 2005.

[10] J. S. Sharp and J. A. Forrest. *Phys. Rev. Lett.*, **91**:235701, 2003.

[11] J. S. Sharp, J. H. Teichroeb, and J. A. Forrest. *Eur. Phys. J. E*, **8**:473, 2004.

[12] H. Yang and J. S. Sharp. *Macromolecules*, **41**:4811, 2008.

[13] J. L. Keddie, R. A. L. Jones, and R. A. Cory. *Europhys. Lett.*, **27**:59, 1994.

[14] J. A. Forrest, K. Dalnoki-Veress, and J. R. Dutcher. *Phys. Rev. E*, **56**:5705, 1997.

[15] L. C. E. Struik. *Physical Ageing in Amorphous Polymers and Other Materials*. Elsevier, New York, 1978.

Chapter 8

Conclusion and Plan of future work

8.1 Conclusion

There are two reasons to study the molecular dynamics in ultra-thin polymer films (<100nm). The first reason is that the development of science and technology are placing increasing importance on the study of smaller and smaller material systems and this trend tends toward nanometer scale. As discussed in previous chapters, material systems at this scale exhibit features which differ from their bulk properties, and of particular interest are the role played by interfacial effects in determining the physical properties in ultra-thin polymer films. Complete understanding of these differences is required. The second reason is that the molecular dynamics in polymer samples remains not totally understood. The CRR theory suggests that there is a characteristic length scale related to the relaxation processes in polymer samples, which is around several nanometers. Ultra-thin polymer films provide an excellent model system for the study of this length scale. This work provided a detailed study of relaxation processes (such as the glass transition, physical aging and dielectric relaxation) in thin polymer films and discussed the origin of the anomalous dynamics in these samples.

A general observation in this project is the accelerated molecular dynamics in polymer

films thinner than threshold values. These threshold values are listed in Table 8.1, and they depend on the polymers used and the processes being measured. Polymer films thinner than these values showed smaller T_g's, larger aging rates and faster dielectric relaxation processes. These observations are consistent with the proposition that the molecular layer near the free surfaces has faster dynamics than the bulk.

Processes / polymers	glass transition	physical aging	dielectric relaxation
PtBMA	∼40nm	NA	NA
PVAc	∼80nm	NA	∼80nm
PS	∼40nm	∼100nm	NA

Table 8.1: Threshold thickness values

An experiment was performed to test whether it's the free surface effects that account for the observed fast dynamics in these thin films. The free surfaces were covered with solid capping layers and then these films were measured again to see whether the free surface effects were removed. Al capping layers were prepared using different procedures (evaporation and the '$2(h/2)$' procedure). The thickness dependence of the glass transition temperature ($T_g(h)$) was essentially the same as that of the uncapped films if the samples are covered by evaporated Al capping layers, but there is no significant change in $T_g(h)$ from the bulk value in the samples capped using the '$2(h/2)$' procedure. These observations suggest that the effects of free surfaces are responsible for the diverted dynamics in thin polymer films, but not all capping layers can remove the free surface effect. Great care has to be taken in any attempt to remove the free surface effects by solid capping layers.

We also showed that in these experiments great care has to be taken when comparing results measured with different techniques. That is, discrepancies may exist if these results are measured using different frequency/time scales. An experiment in this project investigated the frequency dependence on the thickness dependence of α relaxation temperature ($T_\alpha(h)$), and it was performed on ultra-thin PVAc films using dielectric spectroscopy. The results showed that only when being measured at a low frequency (in this experiment, $\sim$10Hz) will the samples exhibit a thickness dependence of the dynamics. Another experiment was done to investigate the cooling rate dependence of the $T_g(h)$ using the same samples, and the thickness dependence of $T_\alpha(h)$ is stronger at a lower cooling rate. The comparison of these two experiments demonstrated the measurement frequency/time scale effects on the diversion of physical properties observed in thin polymer films, and the results help to address the existing controversial reports about the apparent discrepancies observed between measurements that are performed using different techniques.

We further performed theoretical analysis of the shape parameters of the dielectric spectroscopy measured on these PVAc films. The data were plotted against $\ln\tau$ and the parameters describing the widening and distortion of the α relaxation peaks are constant for all measurement frequencies. The observed symmetry of the α relaxation peaks in $\epsilon''(T)$ were related to the constant shape parameters of the asymmetric α relaxation peaks in $\epsilon''(\ln\tau)$. An explanation is given for the observed widening of the α relaxation peaks with increasing measurement frequency in $\epsilon''(T)$. At a lower measurement frequency (<1Hz), the data obtained from thinner PVAc films showed wider α relaxation peaks (in $\epsilon''(T)$) than the data obtained from thicker films, and at a higher frequency (>1Hz) this thickness dependence doesn't exist . This was explained using the existence of the liquid-like surface layer with enhanced molecular mobility, and the measurement frequency effects.

The physical aging process in thin PS samples was investigated using ellipsometry and we reported a couple of observations. Firstly while a trend of decreasing of aging rate with decreasing aging temperature is found for all samples, in ultra-thin PS films (<100nm thick) there exists a maximum aging rate at ∼15-20K below the film glass transition temperature. The aging rate as a function of aging temperature were explained using the competition of the two factors that affect the aging, that is, the distance to the equilibrium and the fraction of the free volume. Secondly, a comparison between the thickness dependence of the aging rate and the thickness dependence of T_g suggests that the aging rate serves as a more sensitive probe in the study of polymer molecular dynamics than T_g does.

8.2 Plan of future work

1. In the present work the physical process of glass transition, dielectric relaxation and physical aging process in thin (< 100nm) polymer films were investigated. Accelerated molecular dynamics were observed in the samples thinner than threshold thicknesses. These observations were explained by the effect of the free surface with enhanced molecular dynamics. an intimately arising question is: how to describe the thickness dependence of these physical processes in thin polymer films? That is to say, what's the functions of $T_g(h)$ and $\tau(h)$ are like (h represents the film thickness, τ represents the relaxation time)? Till now, all we have got is the empirical descriptions [1] and computer simulation results [2]. Theoretical models based on polymer molecular dynamics are required.

   To address the above problems, the effect of the free surface on the molecular dynamics has to be determined first. one approach is to suppose a semi-infinite

polymer sample, and determine the form of $\tau(x)$ in this sample, where x represents the distance to the free surface and τ is the local relaxation time. Given the knowledge of $\tau(x)$, many theoretical questions about the thin polymer films can be clear. For example, the mean relaxation time of a film h can be estimated by

$$\frac{1}{h}\int_0^h \tau(x)\mathrm{d}\, x \tag{8.2.1}$$

2. The free surfaces of thin polymer films have both faster (in PS, PtBMA and PVAc samples) and slower (in PMMA samples) molecular dynamics than the glassy region. While there is a general agreement that the enhanced molecular dynamics near to the free surfaces are due to the more degree of freedom of the molecular movements, the reason for the slower dynamics of the free surfaces is not very clear yet. To answer this question, one can use many different polymers and test the thickness dependence of molecular dynamics in these polymer films. It will be helpful to know which kind of polymers show faster dynamics in thin films samples and which kind of polymers show slower dynamics in thin films. This will help to find how polymer molecular structures affect the molecular dynamics in a region near to the free surfaces.

3. As is illustrated in Fig. 8.1, suppose a flat and conductive substrate with round holes of the same size (diameters $\sim$ several hundred nanometers) regularly distributed on it. A spin cast polymer film on the substrate will have regions with 1 free surface and regions with 2 free surfaces, and both of these regions are regularly distributed. Suppose that an AFM tip is scanning across the spin cast

film, the AFM tip, the small area of spin-cast film that is exactly under the AFM tip, and the conductive substrate form a capacitor. If a sinusoidal voltage is applied between the tip and the substrate, the dielectric spectroscopy of this small region can be obtained by measuring the feedback current. When the AFM tip is scanning across a polymer region with 1 free surface, we will obtain the dielectric spectroscopy of the spin cast film with 1 free surface, and when the AFM tip is scanning across a region with 2 free surfaces, we will obtain the dielectric spectroscopy of the spin cast film with 2 free surfaces. Scanning through the polymer surface we can get the map of the distribution of the dielectric relaxation process. and such a map will be a strong evidence to support the idea of free surface effects on polymer molecular dynamics. Besides, the cooperative relaxation rearrangement is supposed to be discrete in a small enough area, and this experiment is hopefully to be able to find the discrete cooperative relaxation rearrangement.

This experiment requires dealing with weak signals. Kim et al. [3] have shown that such a measurement is possible. They obtained discrete signals of the cooperative relaxation in spin cast films. Our lab has been able to produce regular porous Al substrates with electro-polishing process, and have started to do such an experiment.

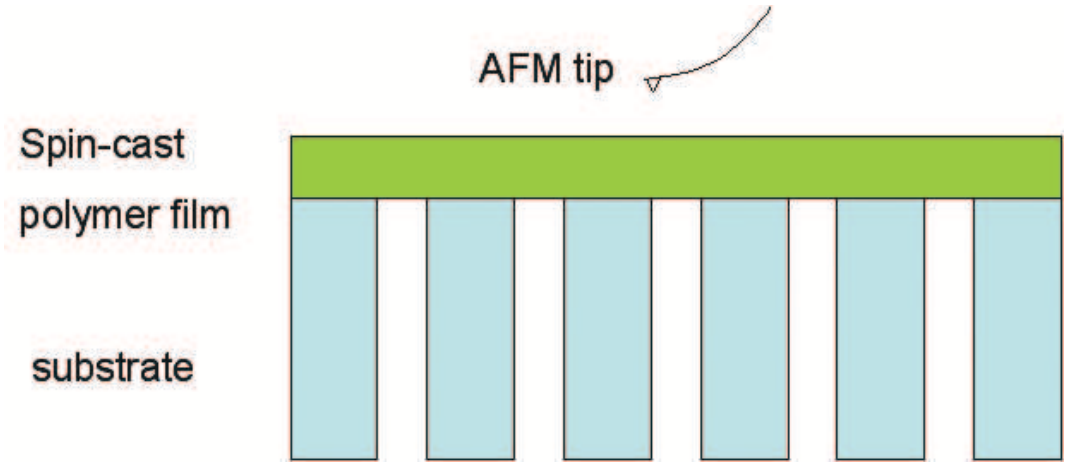

Figure 8.1: *A polymer film is supported on a porous conductive substrate. The substrate, the polymer film and the AFM tip scanning across the film form a dielectric capacitor. The polymer film has regions with 1 free surface (those regions supported exactly on top of the substrate)and regions with 2 free surfaces (those supported exactly on top of the holes). Due to the different molecular dynamics in these two kinds of regions, the dielectric spectroscopy measured at these two kinds of regions are expected to be different*

Bibliography

[1] J. L. Keddie, R. A. L. Jones, and R. A. Cory. *Europhys. Lett.*, **27**:59, 1994.

[2] I. Bitsanis and G. Hadziioannou. *J. Chem Phys*, **92**:3827, 1990.

[3] C. Kim, A. Facchetti, and T. J. Marks. *Science*, **318**:76, 2007.